

TRANSPORT OF ANTHROPOGENIC AND NATURAL SOLUTES NEAR A
PREHISTORIC NATIVE AMERICAN PUEBLO

by

Daniel C. Dolmar

Submitted in Partial Fulfillment of the Requirements
for the Attainment of the Degree

Master of Science in Hydrology

New Mexico Institute of Mining and Technology
Department of Earth and Environmental Science

Socorro, New Mexico

December, 2001

ABSTRACT

Two solute tracers of anthropogenic origin were identified near a prehistoric Native American Pueblo in central New Mexico. These anthropogenic tracers, the chloride:bromide ratio ($\text{Cl}:\text{Br}^-$) and nitrate (NO_3^-), were present in two boreholes where thick, intact midden deposit was present but absent in five other more pristine boreholes. The Cl:Br signal has traveled 140 ± 30 cm and the nitrate peak has traveled 220 ± 40 cm in the 625 ± 70 years since the time the midden was deposited.

Unconfined water was not found in any of the boreholes drilled at the site. Several lines of evidence indicate that there is upward flow from a leaky confined aquifer encountered at 800 to 2100 cm below ground surface. A conceptual model of water flow and solute transport at the pueblo site was formed that included: (1) upward flow from the leaky confined aquifer to the root zone; (2) the Cl:Br ratio and NO_3^- peaks are assumed to be man-made; (3) precipitation and evapotranspiration, which were hypothesized to be sufficient to explain the anthropogenic solute positions.

The anthropogenic solute signals were modeled with the HYDRUS-1D unsaturated water and solute transport code. Modeling results were compared to the data gathered at the field site, and it was demonstrated that the relatively simple conceptual model could be calibrated with the data from the field site. Model results indicate that the majority of the transport of the anthropogenic solutes took place very early in the time

since midden deposition, and that the anthropogenic solutes are essentially frozen in place, pending some unusually high degree of wetness that would push them farther down into the profile. In the numerical model, solute transport events take place in the winter when transpiration is zero and potential evaporation is low, and are due to an accumulation of several storm events. The HYDRUS simulations predict that the anthropogenic solutes do not move below the root zone, and therefore also predict that no recharge from precipitation is occurring at the site.

The simulated solute peak position was used as a performance measure in a sensitivity analysis of the HYDRUS model. The peak position is sensitive to the unsaturated hydraulic conductivity in the upper 120 cm of the profile, to the particulars of the top boundary condition, and to the maximum rooting depth. By contrast, the peak position is relatively insensitive to the wilting point.

The upward flow process below the root zone was also modeled with HYDRUS. This work predicts that the environmental solute peaks remain at the bottom of the root zone at ~400 cm bgs, and are held there by the upward flow coming from the underlying leaky confined aquifer and the subsequent removal of this water flow by the plant roots.

ACKNOWLEDGEMENTS

This research was funded by Sandia National Laboratories under Project Number LDRD Case 3515.090. Dr. James McCord was the primary researcher who obtained the funding, and he provided assistance and guidance through much of the field-phase of the project.

The University of New Mexico's Office of Contract Archeology performed a heroic amount of work in the field. I am grateful to the many field workers who contributed their time and elbow grease to the project. Particular persons from UNM-OCA who deserve much thanks include: Carrol Treadwell, Dr. Dick Chapman, and most exceptionally, Dr. Bill Doleman.

I am grateful for the help of Ed Bulloch of the Bureau of Indian Affairs, who helped make sense of the story that the soils had to tell.

Dr. Fred Phillips of New Mexico Tech's Hydrology Program has been contributing good ideas and fair criticism to this project since its inception. Laura Changaran (née Quemada) was the best working partner one could hope for on a project, and laid the foundation upon which all of my work rests. Dr. Rob Bowman and Dr. John Wilson have made many valuable suggestions as thesis committee members. A thousand thank-you's go to Dr. Jan Hendrickx, my advisor, whose graceful style as a boss and top-

drawer character as a human being were the best lessons of all. *De antwoorden zijn altijd al aanwezig*--hope I got that right.

To the many friends I have made during my **long** time at Tech: what path could be hard with people like you as companions?

To Roy and Virginia: this is for me, I know, but it is also for you.

TABLE OF CONTENTS

	PAGE
ABSTRACT	
ACKNOWLEDGEMENTS	ii
LIST OF TABLES	vii
LIST OF FIGURES	ix
I. INTRODUCTION	1
Previous Work On This Project	4
Field Site	5
Archaeological Study of Fernandez Pueblo	8
Hydrologic Field Investigation	9
Chloride Mass Balance	18
Soil and Water Data	22
Chloride Mass Balance, Revisited, and Upward Flow	25
Modeling the Midden Project Data	29
Outstanding Questions	29
Hypothesis of This Thesis	31

II. CONCEPTUAL MODEL AND METHODS	32
Conceptual Model	32
Soil Profile	33
Root Zone	36
Top Boundary Condition	37
Bottom Boundary, Upward Flow	41
Initial Condition	43
HYDRUS-1D Code	44
Preliminary Simulations	52
Sensitivity Analysis	57
Temporal Scale of Solute Movement	65
III. RESULTS AND DISCUSSION	67
Preliminary Simulations	67
Sensitivity Analysis	74
Temporal Scale of Solute Movement	83
IV. OTHER CONSIDERATIONS	93
Differing Positions of Cl:Br and NO ₃ ⁻	93
Reverse Osmosis	95
Two-Dimensional Stratigraphy	98
Vapor Flux	102
Anion Exclusion	103
Preferential Flow	104
Solute Diffusion	105

V. CONCLUSIONS	113
Suggestions for Future Work	116
VI. REFERENCES	119
APPENDIX A. THE DRILL FOAM ISSUE	124
APPENDIX B. PLOTS FROM THE SENSITIVITY ANALYSIS	127
APPENDIX C. TRENCH SOIL PROFILES AND FULL SOIL PROFILE	144
APPENDIX D. A FEW COMMENTS ON OBSERVING AND MODELING A RATIO OF SOLUTES	154
APPENDIX E. TWO ADDITIONAL SIMULATIONS EXPLORING THE EFFECT OF K_{sat} ON SOLUTE MOVEMENT	160
APPENDIX F. SAMPLE INPUT FILES FROM A HYDRUS SIMULATION	163

LIST OF TABLES

Table	Page
1. Test pits which had midden content within them, along with the total excavated volumes of each. Adapted from Doleman [1995].	11
2. Present-day solute signal peak depths,...	19
3. Chloride mass balance ages through 10 meters depth, in the boreholes at Fernandez Pueblo.	21
4. A comparison of trends in chloride mass (represented by CMB age), water content between the root zone and the confined aquifer below, and the surface slope.	28
5. Stratigraphic parameters used in preliminary simulations. θ_r , θ_s , α , n , K_{sat} , are van Genuchten model parameters.	53
6. Sensitivity analysis schedule, showing the design points (simulations) and the high/low status of the four parameter groups for each simulation. High variant is indicated by a +.	59
7. Stratigraphic parameters used in sensitivity analysis. θ_r , θ_s , α , n , K_{sat} , are van Genuchten model parameters.	63
8. Results of the sensitivity simulations, showing the outcome of each of the design points in terms of the solute peak depth. Maximum rooting depth in the model is provided for comparison.	75

9.	The HYDRUS model sensitivities to the four parameter groups used in the analysis, by peak depth.	82
10.	Average Cl ⁻ concentrations below the environmental solute bulge, and the Cl ⁻ concentrations just before confined water was reached. Chloride concentration in the confined aquifer water was 410 mg L ⁻¹ .	96
11.	Sensitivity analysis schedule for the diffusion investigation, showing the design points (simulations) and the high/low status of the three parameter groups for each simulation. High variant is indicated by a +.	108
12.	Results of the diffusion sensitivity analysis.	109

LIST OF FIGURES

Figure	Page
1. Location of Fernandez Pueblo site.	6
2. A sketch of Fernandez Pueblo.	7
3. Chloride, bromide, Cl:Br ratio, nitrate-N, and volumetric water contents from two of the seven boreholes from which soil samples were taken for analysis.	13
4. Present-day soil profile at Borehole 71, adapted from Quemada, [1995].	23
5. Plot showing relative elevations of the surface,...	24
6. Typical soil profile at Fernandez Pueblo site, for the time of midden deposition.	34
7. Estimated volumetric water content from boreholes 71 and 103, showing the reduced apparent water content in the bottom 2 m.	35
8. A comparison of the Bingham station annual precipitation record used in modeling the Fernandez Pueblo solutes,...	38
9. Model of water stress response function $\gamma(h)$.	48
10. HYDRUS model results, with matric potential, water content, and concentration profiles from the “wet” and “dry” scenarios.	68
11. Repeat of wet scenario plots (Figure 10), with the simulated	

	environmental solute peak included.	70
12.	Complete matric potential and water content profiles from the dry scenario.	72
13.	Pressure head, water content and concentration profile results from the sensitivity analysis, design point 1.	77
14.	Pressure head, water content and concentration profile results from the sensitivity analysis, design point 8.	78
15.	Pressure head, water content and concentration profile results from the sensitivity analysis, design point 5.	79
16.	Year-by-year simulated solute center of mass position for design point 8 of the sensitivity analysis.	84
17.	Precipitation and HYDRUS model solute center of mass at three levels of resolution in time, after 72 years of simulation in design point 8 of the sensitivity analysis.	85
18.	Precipitation and HYDRUS model solute center of mass at three levels of resolution in time, from the beginning 8 th design point simulation of the sensitivity analysis.	88
19.	Volumetric water content through time, for the first 90 days in year 85 of the design point 8 simulation, for several depths below ground surface. Points are at 5-day intervals.	90
20.	Elevation at which water was found during borehole drilling, plotted against local north-south coordinate, and against local east-west coordinate.	100

21.	Peak concentration position of the simulated anthropogenic solute from design point <i>b</i> of the sensitivity analysis.	111
22.	The solute profile from design point <i>b</i> of the diffusion sensitivity analysis, extended through 161 years.	112
A1.	Cl:Br and NO ₃ -N solute profiles from the two boreholes within the midden.	126
B1.	Plots of HYDRUS output from sensitivity analysis, design point #1.	128
B2.	Plots of HYDRUS output from sensitivity analysis, design point #2.	129
B3.	Plots of HYDRUS output from sensitivity analysis, design point #3.	130
B4.	Plots of HYDRUS output from sensitivity analysis, design point #4.	131
B5.	Plots of HYDRUS output from sensitivity analysis, design point #5.	132
B6.	Plots of HYDRUS output from sensitivity analysis, design point #6.	133
B7.	Plots of HYDRUS output from sensitivity analysis, design point #7.	134
B8.	Plots of HYDRUS output from sensitivity analysis, design point #8.	135
B9.	Plots of HYDRUS output from sensitivity analysis, design point #9.	136
B10.	Plots of HYDRUS output from sensitivity analysis, design point #10.	137
B11.	Plots of HYDRUS output from sensitivity analysis, design point #11.	138
B12.	Plots of HYDRUS output from sensitivity analysis, design point #12.	139
B13.	Plots of HYDRUS output from sensitivity analysis, design point #13.	140
B14.	Plots of HYDRUS output from sensitivity analysis, design point #14.	141
B15.	Plots of HYDRUS output from sensitivity analysis, design point #15.	142

B16.	Plots of HYDRUS output from sensitivity analysis, design point #16.	143
C1.	Soil profile at 544.5N:581.7E.	145
C2.	Soil profile at 544.5N:594E.	146
C3.	Soil profile at 544.5N:571E.	147
C4.	Soil profile at 544.5N:565E.	148
C5.	Soil profile at 580.5N:577E.	149
C6.	Soil profile at 580.5N:596.5E.	150
C7.	Soil profile at 580.5N622.5E.	151
C8.	Ortho-rectified topographic map of Fernandez Pueblo.	152
C9.	Soil profile inferred from grab samples taken during drilling of borehole 72 [605N:552E].	153
E1.	Results of the simulations 8A and 12A.	162

I. INTRODUCTION

The nuclear age has created the need for long-term interment of the waste generated by nuclear power and weapons. The suitability of a site for waste interment is mainly assessed, aside from political concerns, by addressing whether or not the waste is likely to escape before it is rendered harmless by radioactive decay. One of the main vectors for escape of a radionuclide from a geological repository is through contact with moving water and subsequent transport through the subsurface. This suggests geologic interment in an arid vadose zone where the repository will not be exposed to “transporting” quantities of subsurface water at any time in the foreseeable future. One of the main candidates for nuclear waste interment is the Yucca Mountain site in Nevada, which currently satisfies the above criteria [e.g., National Resource Council, 1995].

But the time of the required interment is quite long, on the order of 10,000 years for high-level waste, or 1,000 years for low-level waste. Therefore researchers have built many conceptual models of the natural processes in play at potential waste disposal sites, and have implemented these models in computer codes that are used to predict the fate of the waste [e.g., Wu and Pruess, 2000; Seong and Rubin, 1999]. Since the scientific community has only been seriously interested in issues of contaminant transport in arid vadose zones for only a few decades, there are no data available for model calibration on

the time frames of several hundred to several thousand years. The overall hypothesis of the present work is that archaeological sites in the American Southwestern desert can provide field data for model calibration over periods of several hundred years.

Many researchers have studied water and solute movement in arid vadose zones through field studies and modeling investigations. A large portion of the research has focused on the existence and quantification of diffuse natural recharge to desert aquifers. Hendrickx and Walker [1997], and Scanlon et al. [1997] compiled large surveys of the work to date. Stephens [1994] compiled a table of recharge estimates that focused mainly on the American Southwest that shows the diversity of recharge estimates for the region, from 2 mm yr^{-1} [Phillips et al., 1988] to 37 mm yr^{-1} [Stephens and Knowlton, 1986] in the Socorro, New Mexico area. Kearns and Hendrickx [1998] made detailed numerical simulations using one hundred years of precipitation data from semi-arid New Mexico; their model results indicated that both intense rainfall events (that are present in the actual record) and gradual accumulation could cause substantial recharge. On the other hand, Fontes et al. [1986] found a $\sim 2 \text{ mm yr}^{-1}$ net *upward* flux from a Saharan Desert phreatic aquifer at 10 m depth. Scanlon et al., [1991] reported on field work and numerical modeling of a West Texas Chihuahuan Desert site, where very low water potentials ($< -154,000 \text{ cm H}_2\text{O}$) in the root zone, and higher potentials at greater depth, indicate the potential for upward flow. Gee et al., [1994] in a nine-year study indicate that the presence of plants on a site eliminated deep drainage in the semi-arid New Mexico desert. Plummer et al., [2001] compared simulated and measured matric potentials from dry regions as diverse as Southeastern Washington State, the Nevada Test Site, West-Central New Mexico, and the Chihuahuan desert of West Texas. This study

indicated that vadose zones in all of these regions have been in a monotonic drying state (below the root zone) with net upward flux for thousands of years.

Methods of measuring water movement which are straightforward to use in humid climates, such as the mass balance and Darcy flux methods, do not work in arid environments, essentially due to the typically small, slow fluxes in the subsurface which greatly multiply measurement uncertainty [Allison et al., 1994]. Because significant or interesting transport phenomena tend to take many years to develop in arid unsaturated zones, researchers have often used tracers that have already had significant travel times within the vadose zone, such as bomb pulse radionuclides (e.g., Phillips et al., 1988; Scanlon, 1992), which have been in the subsurface since the beginning of above-ground nuclear testing in the 1940's.

Archaeological sites have been suggested as potential analogs for nuclear waste sites [e.g., Miller and Chapman, 1995]. If a suitable anthropogenic (man-made) tracer could be identified at a prehistoric site, it would have a travel time of hundreds to thousands of years, many times longer than the bomb pulse isotopes. Recently, researchers at New Mexico Tech and the Office of Contract Archaeology of the University of New Mexico have found an anthropogenic tracer in the form of the chloride/bromide ratio (Cl:Br) in the midden (waste dump) of Fernandez Pueblo, a prehistoric Native American pueblo in central New Mexico. This project is known as "The Midden Project", and will be referred to here by that name.

The Cl:Br ratio has been used as a tracer for identifying the presence of water from domestic sources in the subsurface [Davis et al., 1998]. Cl:Br has been shown to be in excess of 1500 (mass/mass) in the urine of modern humans [Sangster et al., 1983],

although of course we cannot know for certain that this is true for prehistoric Southwestern Natives. The movement of treated municipal sewage has been traced by following a spike in the Cl:Br ratio in groundwater [Davis et al., 1998].

As will be discussed in the next section, Previous Work On This Project, I noticed that a nitrate signal is strongly associated with the Cl:Br ratio signal, and is therefore likely to be anthropogenic as well. The presence and high concentration of nitrogen in human sewage is well-known. Under oxidizing conditions, nitrogen is usually converted to nitrate by bacteria in the soil (e.g., Fetter, 1993).

The remainder of this introductory chapter consists of two sections. The first section is a synopsis of the previous methods and results from the Midden Project, and the second section describes some of the unanswered questions left by the Midden Project data, and outlines the objectives of this thesis.

Previous Work On This Project

In this section I report the results that are relevant to my thesis from the archaeological study [Doleman, 1995] and the hydrologic study [Quemada, 1995] undertaken at Fernandez Pueblo. In addition, I describe my work on the site and present my interpretation of Quemada's data.

Field Site

The Fernandez Pueblo is located approximately 12 miles North of Bingham, NM, in the Chupadera Arroyo drainage basin in the northern-most reach of the Jornada del Muerto (Figure 1). A sketch of Fernandez Pueblo is included as Figure 2 (adapted from Doleman [1995], after Mera, [1940]). The pueblo site consists of four house mounds and the surrounding terrain. The local geology surrounding Fernandez Pueblo has been described by Treadwell and Garcia [1995], and by Quemada [1995].

The upper (degraded) shale member of the Dockum Formation dominates the site; this is composed of clay/mudstone with lenses of coarse to medium sandstones. The pueblo sits atop one of these sandstone beds. The Dockum was deformed during the Laramide Orogeny. Osburn [1984] mapped north-northeast trending anticline and synclines in the area. A small outcrop, ~20m west of the pueblo, dips approximately due east, indicating that the axis of the syncline is east of the pueblo. A horizontal Eocene lacustrine/playa formation, the Baca, lies unconformably over the Dockum, starting about 50m east of the pueblo. This formation contains two types of units: (1) a clay/silt unit with interbedded gypsum, and (2) a poorly-sorted medium sand. Pediment gravels were deposited across the surface during a Pliocene erosional event; these are occasionally exposed at the surface. After the pueblo occupation, colluvial sand sheets covered the region surrounding the Pueblo. These sands have also buried most of the pueblo structure so that only small ($<1 \text{ m}^2$) areas of masonry are still exposed.

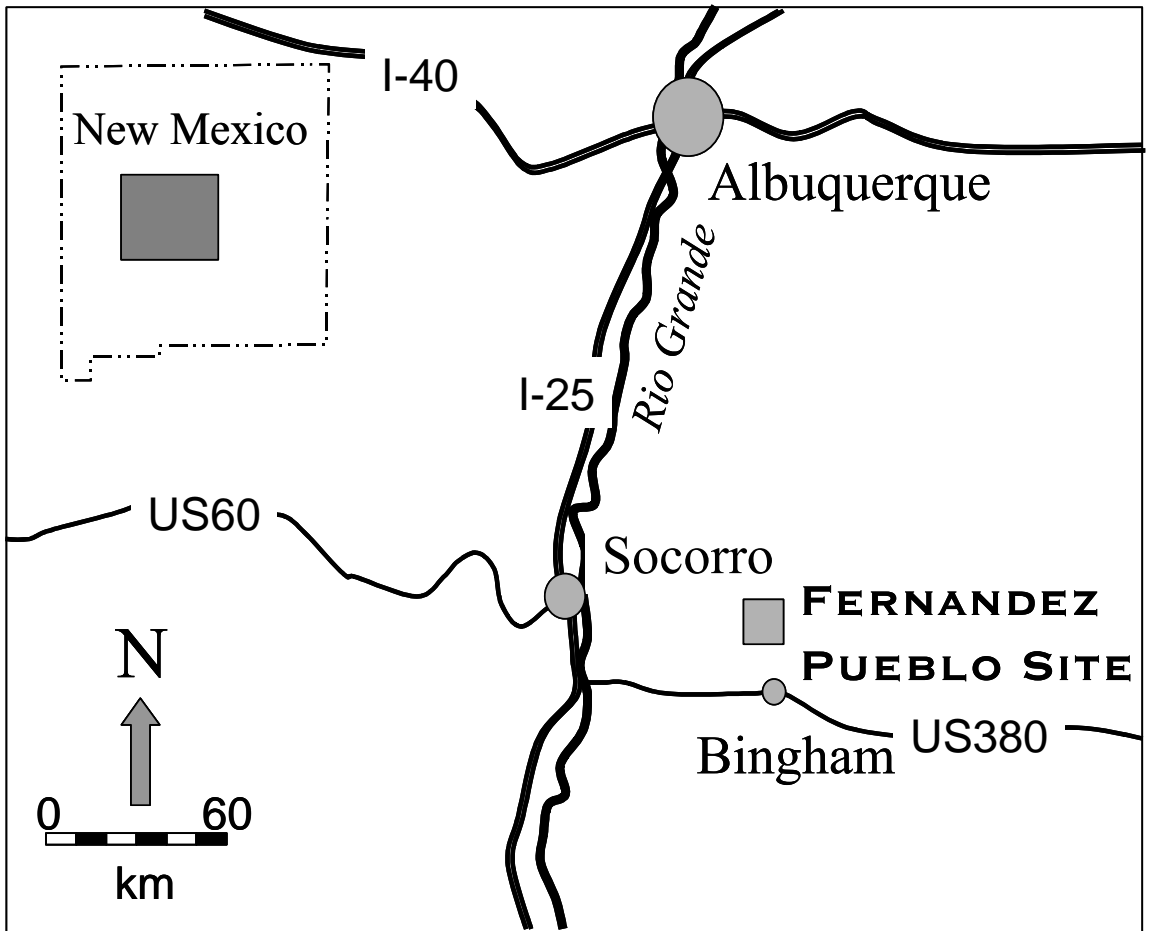


Figure 1. Location of Fernandez Pueblo site.

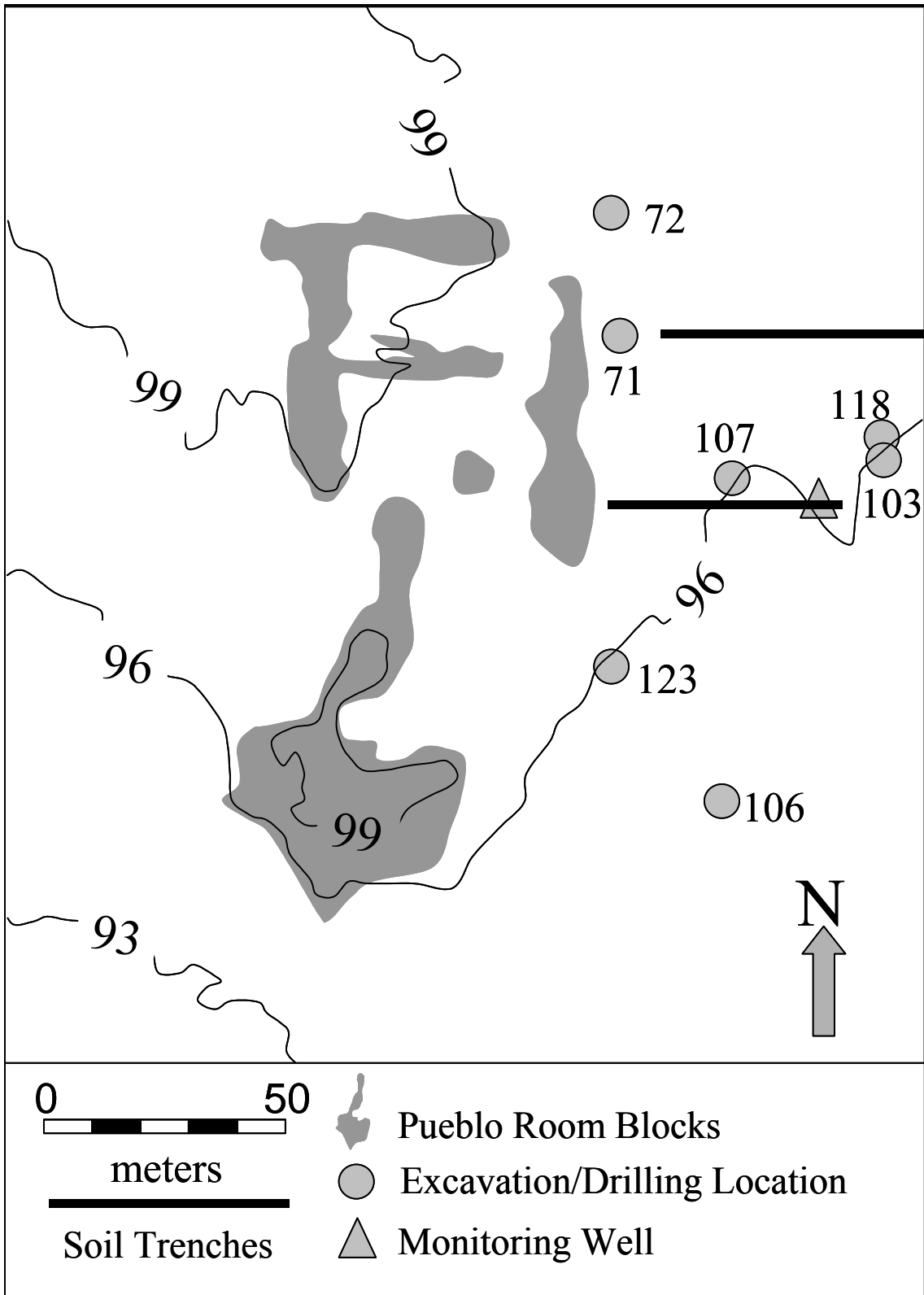


Figure 2. A sketch of Fernandez Pueblo. The contours are elevation in meters, relative to a local benchmark. Numbers 71, 72, 103, 106, 107, 118, and 123 refer to excavation/drilling locations.

Archeological Study of Fernandez Pueblo

The Office of Contract Archeology (OCA) of the University of New Mexico was on-site intermittently from August 1993 through June 1995. Their primary task was to define the dates of occupation of the Pero natives so that, if an anthropogenic solute was identified, the time to accumulate the observed solute mass and the overall travel time could be known. This was to be accomplished by comparing the glaze and pottery types present in the pot sherds at Fernandez Pueblo to known archeological sequences of pottery. A second task was to identify intact midden (waste) deposits so that the hydrologists would know where to drill in order to search for potential anthropogenic solutes.

For the purpose of this discussion, the OCA archeologists' most germane field work included: (1) establishing benchmarks with known coordinates for all other work on site, (2) excavating 111 auger holes on a grid system to search for areas of high-density midden material or cultural artifacts, and (3) excavating eleven 100 cm by 100 cm test pits within areas of suspected midden deposit (based on the auger hole results), to determine the densities of cultural artifacts and the relative amounts of midden fill present. Excavation of the test pits was normally halted when the pit bottom contained undisturbed geologic material, and thus no more cultural material would be produced by digging deeper; on average this occurred at a depth of 110 cm (Doleman, 1995). It was assumed that a large amount of midden fill (i.e., refuse and soil back-filled by the natives into their waste sites) present in any test pit would be a good indicator of where to dig for anthropogenic solute plumes. The test pits close to the pueblo, particularly on east side, had much greater cultural material density than those in other locations. For this reason,

the hydrologic and chemical soil sampling performed by hand auger and drill were concentrated on the east side of the pueblo. The OCA researchers found definite intact midden in three of the test pits. In total, seven of the eleven test pits had some cultural material present. A summary of their findings is given in Table 1.

Pottery sherds excavated from the test pits and auger holes were brought back to the UNM-OCA for taxonomic classification. Based on the absence of glaze B types (which begin in 1425 C.E. in the known record), and the small number of early 1300's types, the time of occupation was estimated to be C.E. 1300 to 1450 [Doleman 1995; Quemada 1995].

Hydrologic Field Investigation

Some exploratory boreholes were drilled in August 1993 with a hollow-stem auger rig; the only result of this work that concerns us here is that the hollow-stem auger proved ineffective at drilling through clays found at depths between 1000 and 1500 cm at the site. Because of this difficulty, all further mechanical drilling at Fernandez Pueblo was done using an air rotary rig.

In September 1994 a monitoring well was installed. Ground water was reached at 1740 cm bgs [Quemada, 1995] in a leaky confined sandstone aquifer below the clay. The equilibrium water level in the monitoring well was measured at 850 cm bgs in 1995, and at 800 cm bgs in 1999; thus the estimated confining pressure of the leaky confined aquifer is 920 ± 30 cm.

Seven hand auger holes and seven air rotary holes were drilled in or near the seven archaeological test pits that contained any traces of cultural material. These pits,

numbered 71, 72, 103, 106, 107, 118, and 123 (refer to Table 1 and Figure 2), and the boreholes in or near them were given the same number designations. The New Mexico Tech hydrology team drilled hand-auger holes in February 1995, just outside the boundaries of the test pits [Quemada 1995]. The hand auger holes were drilled until further downward progress was impossible. The final depths of the holes ranged from 130 cm to 305 cm. Soil samples were collected from each ~15-cm interval and transported to New Mexico Tech for gravimetric water content, Cl^- , Br^- , and NO_3^- analysis.

In March 1995 seven air-rotary boreholes were drilled, one through each of the seven test pits with any evidence, however slight, of midden material (Table 1 and Figure 2, above). These drilling operations were continued until water was reached, between 980 cm and 2100 cm below ground surface [Quemada, 1995], except at the locations designated 72 and 118, where forward progress was rejected by the hard rock just before water was expected. Samples were taken of the drill cuttings, every 150 cm and at each noticeable change in lithology; these were also transported to the laboratory at New Mexico Tech for gravimetric water content, Cl^- , Br^- , and NO_3^- analysis. Physical and chemical analyses of the hand auger and air rotary borehole samples were performed as described in Quemada [1995]. The gravimetric water contents were converted to volumetric water contents by the formula

$$\theta = w\rho_b \quad (1),$$

where θ = volumetric water content [-]; w = gravimetric water content [-]; ρ_b = dry bulk density of soil [M L^{-3}]. The dry bulk density was estimated using the equation

$$\rho_b = 1.51 + 0.25(f_s) \quad (2),$$

Table 1. Test pits which had midden content within them, along with the total excavated volumes of each. Adapted from Doleman [1995].

Test Pit	Excavated Volume (m ³)	Midden Content
71	1.3	100 cm of stratified (intact) midden deposits, including refuse-filled adobe borrow pit and an ash lens.
72	1.4	At least 70 cm of stratified (intact) midden deposits.
103	0.7	A pocket of charcoal-bearing deposits.
106	1.0	70-80cm of cultural deposits, including at least 20cm of apparently intact stratified midden.
107	0.7	40-50cm of stratified deposits, including 20-30cm of partially intact to somewhat eroded midden.
118	0.7	Middle levels...either intact or redeposited midden.
123	0.6	Possibly partially redeposited midden.

where f_s = sand fraction [-]. This estimation for bulk density was suggested by Maidment [1992].

In August 2000, I took water samples from the monitoring well for chemical analysis. Approximately three casing volumes of water were purged from the well prior to taking the final samples, to assure that pristine water from the leaky confined aquifer was obtained. Samples were analyzed for Cl^- , Br^- , and NO_3^- at the New Mexico Bureau of Mines and Mineral Resources by ion chromatography on a Dionex DX-600 with an AS-50 autosampler and standard conductivity detector that comes with the system, using Peaknet 6.0 software. Lower detection limits were 0.2 mg l^{-1} for Br^- and NO_3^- , and 1 mg l^{-1} for Cl^- . From analyses of the water in the monitoring well, the concentration of Cl^- in the sandstone aquifer water was $4.1 \times 10^2 \text{ mg/L}$, the Br^- concentration was 5.7 mg/L , and the NO_3^- concentration was $2.2 \times 10^1 \text{ mg/L}$.

Two 2-m deep trenches, one $\sim 76 \text{ m}$ long and the other $\sim 46 \text{ m}$ long, were dug in June 1995, situated as shown on Figure 2. The trenches provided detailed soil information on the near-surface soils. With my assistance, H. Edward Bulloch of the Bureau of Indian Affairs described soil horizons at seven locations along the trenches, and performed textural analyses on the drill cuttings from the borehole designated 72. The seven trench profiles plus the one borehole profile are included in Appendix C.

The chloride, bromide, Cl:Br ratio, nitrate, and water content profiles from the air rotary and hand auger holes are presented by Quemada [1995]. They can be separated into two groups: one with a clear midden signature (boreholes 71 and 72), and one without it (123, 106, 107, 118, 123) Figure 3 shows chloride, bromide, Cl:Br ratio, nitrate, and water content profiles from the air rotary and hand auger holes at boreholes

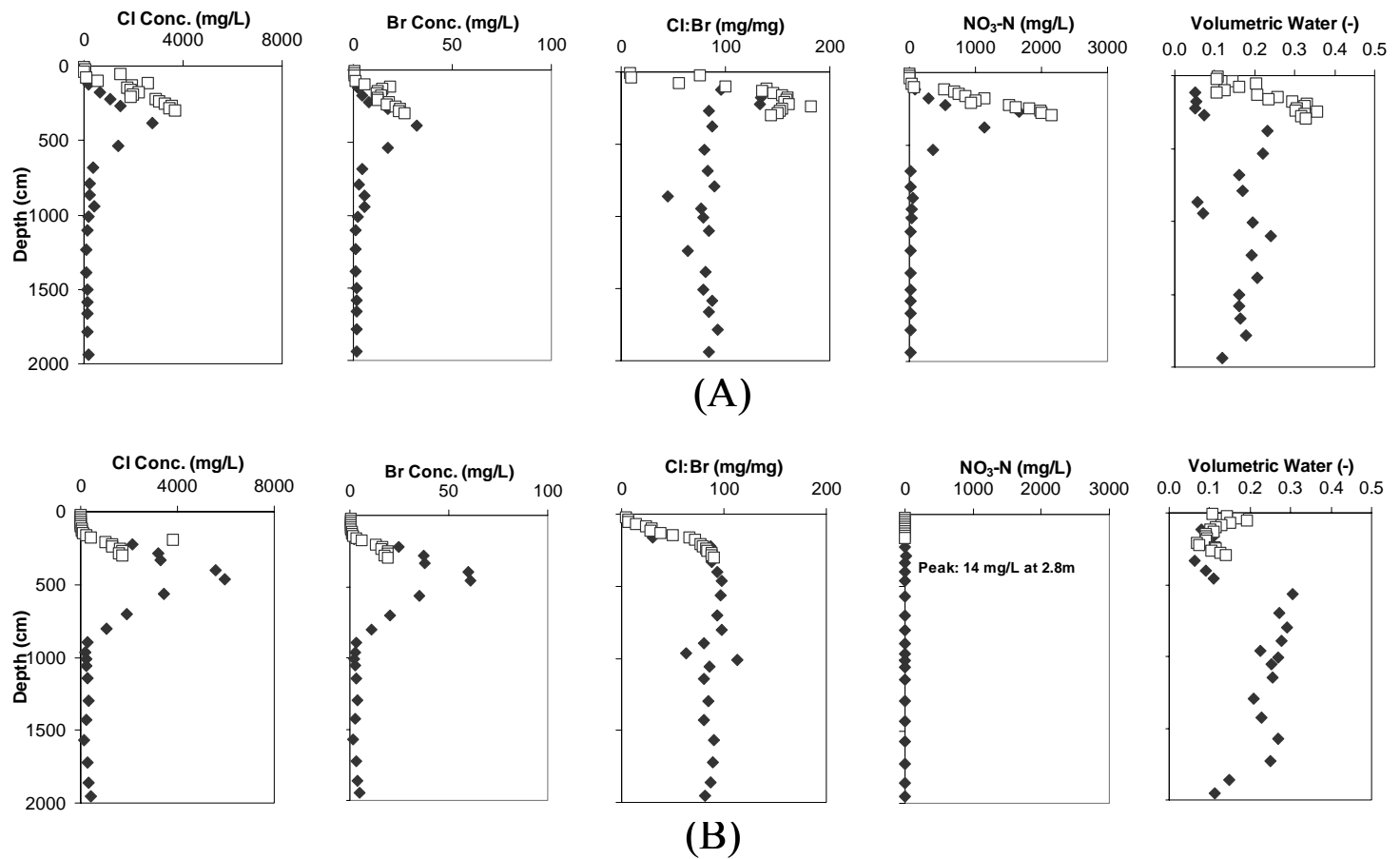


Figure 3. Chloride, bromide, Cl:Br ratio, nitrate-N, and volumetric water contents from two of the seven boreholes from which soil samples were taken for analysis. Depths shown are for the present-day.. (A) Profiles from borehole 71, through intact midden; (B) profiles from borehole 103, through pristine soil. Open squares represent hand auger samples, filled diamonds represent air rotary samples. Adapted from Quemada, [1995].

71 and 103. The depths shown are for the present-day, as opposed to the time of midden deposition. Sandy colluvium has accumulated over the surface since the time of midden deposition, so that total profile thicknesses for this time would be approximately 90 cm less than in the present. Confined water was found within 1 m of the bottom data points given in the figure, at 2100 cm bgs in borehole 71, and at 2070 cm bgs at borehole 103. The solute profiles from borehole 71 are representative of what was found beneath the thick intact midden (at boreholes 71 and 72), while the profiles from borehole 103 are representative of what was found beneath less impacted soils (at boreholes 103, 106, 107, 118, and 123). The large Cl^- and Br^- bulges at 200-900 cm depth in Figure 3 are common to all profiles, although the width, placement, and maximum concentrations vary somewhat from hole to hole. Bulges in Cl^- (and presumably Br^-) concentration like these are common in desert vadose zones, and so are not generally attributable to anthropogenic sources; they are thought to reflect environmental conditions that concentrate Cl^- from precipitation (e.g., Peck et al. [1981], Johnston [1987], Allison et al. [1985], Phillips [1994]). For all boreholes, the peak Cl^- concentrations are between 350 and 500 cm depth.

One interesting and previously unexplained feature, that is common to all seven profiles, is the much lower Cl:Br ratio in the top ~1 m of the subsurface, compared to that of rainwater. In the top meter of the borehole profiles, Cl:Br is 26 on average, while local measurements of Cl:Br in precipitation give values of 63 ± 14 [Quemada, 1995]. Preferential sorption of bromide over chloride by dead organic material and preferential uptake of bromide by plants are the most likely causes of the difference in Cl:Br ratio between the top meter of the soil and the rainwater. Research in humid climates has

suggested that bromide is preferentially sorbed by humus [Låg and Stiennes, 1976; Lundstrom and Olin, 1986], and is biologically transformed by some plants to bromo-organic complexes [Shotyk, 1996]. Gerritse and George [1988] made a column study of preferential sorption of bromide on surface soils from arid Western Australia, and inferred that bromide is preferentially sorbed by the organic materials. They found that, upon leaching these soils, the leachate initially had a high Cl:Br ratio of 300, reflecting precipitation in that area, but this value rapidly decreased to 10, reflecting the ratio of Cl⁻ to Br⁻ bound to soil organic matter. I hypothesize that the same phenomena—preferential sorption of Br⁻ over Cl⁻ to organic matter and preferential root uptake—occur at the Midden Project site where Br⁻ accumulates in the top meter of soil. During the laboratory analysis, in which soil samples are mixed with purified water [Quemada, 1995], some of the sorbed Br⁻ joins the Br⁻ already in solution from the pore water. This lead to an increase in the total amount of Br⁻ in the water and, thus, a decrease in the Cl:Br ratio. At our site, the accumulated Br⁻ mass in the first meter of the subsurface is small, relative to the mass in the Br⁻ solute peaks (Figure 3, Br⁻ profiles); presumably this reflects the fact that the amount of biomass and humic materials is small, as well.

Profiles drilled through thick midden deposits--71 and 72--show a peak in the Cl:Br ratio are at depth 230±30 cm bgs (profiles from borehole 72 are not shown, see Quemada [1995]). The uncertainty—±30 cm—represents the difference in depth between the Cl:Br peak at borehole 71 and the Cl:Br peak at borehole 72. This peak is absent from profile 103 and the other profiles without significant midden material. This is evidence that the peaks in these solute ratio profiles have their origin in the midden material, and that therefore the solutes are anthropogenic in origin. The time of the

pueblo occupation was 1300-1450 C.E., or 620 ± 75 years before 1995 when the boreholes were drilled.

The average apparent water recharge rate at the site should be calculated as:

$$q_r \approx \frac{\Delta z}{\Delta t} \theta_{avg} \quad (3)$$

where q_r = apparent recharge rate [$L T^{-1}$], Δz = travel distance since deposition, Δt = travel time since deposition, θ_{avg} = average water content in profile.

Quemada [1995] calculated an average apparent recharge rate from the Cl:Br ratio positions of $0.6 \pm 0.2 \text{ mm yr}^{-1}$, but in her calculation she used porosity in place of average water content in Eq. (3), and she did not take into account the sediment accretion on top of the midden since the time of its deposition.

Measuring from the present-day (1995) surface level to the mean plane of midden deposition at test pit 71, sediment has accreted about 90 cm since the time of midden deposition (accretion estimated from Figure 6 in Doleman [1995]). This sediment accretion thickness must be subtracted from the 230 ± 30 cm Cl:Br peak depth to get a true travel distance since deposition, because the solute does not travel through this accreted material on its way downward. Thus, the Cl:Br ratio peak is 140 ± 30 cm below the average plane of midden deposition, and this is the correct travel distance to use in Eq. (3). Therefore, over the 620 ± 75 years of transport since the time of the pueblo inhabitation, the average apparent recharge rate based on these Cl:Br peak positions and the present-day average near-surface volumetric water content of approximately 20%, is

$$= \frac{1400 \pm 300 \text{ mm}}{620 \pm 75 \text{ yr}} \times 0.2 = 0.4 \pm 0.2 \text{ mm yr}^{-1}.$$

In re-analyzing Quemada's data, I noticed a peak in nitrate concentration that is coincident with the Cl:Br ratio (Figure 3). This NO₃ peak is present in boreholes 71 and 72 (at depth 310±40 cm bgs), but is absent from the other boreholes. The NO₃ peaks are 220±40 cm below the zone of midden deposition, which gives an average apparent recharge rate of 0.7±0.2 mm yr⁻¹.

My revised recharge estimates based on Cl:Br and NO₃ positions given above are still uncertain for at least two reasons. (1) There is no phreatic water surface below, indicating that there is no net recharge occurring at the site unless the recharge flow includes a lateral outflow component, so that the recharge is accumulating somewhere off-site. The implications of not finding a phreatic aquifer during the drilling will be revisited below. (2) As Tyler and Walker [1994] pointed out, a solute that is nearer to the surface than about 2 times the rooting depth will tend to significantly overestimate the actual recharge, due to the water still being removed by transpiration. The dominant plant species surrounding Fernandez Pueblo is sand sage <*Artemisia filifolia*>. Weaver [1919] showed this plant to have a rooting depth in excess of 300 cm, although it is unclear how many samples were taken in his work. Roots have also been observed more than 400 cm below the surface in a Utah ecosystem dominated by sand sage [Pockman, 2000]. Canadell et al., [1996] summarized the known rooting depths of plant species worldwide by biome, and found that desert plant species had an average maximum rooting depth of 950±240 cm. By contrast, we measured rooting depths of 70 to 150 cm in our soil profiles along the trenches. Even though the nitrate peak (at 320 cm) is slightly deeper than two times our maximum measured rooting depth (2×150 cm = 300 cm), it seems likely that the Cl:Br and nitrate peaks are within 2 times the rooting depth

of the surface because these profiles were not performed with special attention paid to rooting depths and densities (e.g., no soil was sifted for rootlets, nor was any attention paid to whether a profile was taken directly underneath a sand sage bush).

Table 2 below highlights the difference in solute peak positions found in the solute profiles from within the midden (i.e., from boreholes 71 and 72). The data in Table 2 are all from the air rotary borehole profiles, as the hand auger drilling did not proceed deep enough to locate well-defined solute or solute ratio peaks in most cases. The reader can see from Table 2 that the anthropogenic signal peak depths are clearly higher in the profiles than are the environmental solutes. This difference in the solute positions has caused me to treat the environmental solutes and anthropogenic solute signals in fundamentally different ways, as will be discussed throughout the remainder of this thesis.

Chloride Mass Balance

The total amount of chloride represented in a profile can be used for determination of the duration of chloride accumulation. This is done with the chloride mass balance method (e.g., Phillips [1994]). The key assumptions of this method are: (1) that all chloride in a soil profile comes from surficial processes, i.e., precipitation and dry deposition; (2) chloride is conserved within the profile; and (3) the chloride deposition rate is known and constant. Thus the age of the chloride at any level in the soil profile is given by:

$$t(z) = \frac{1}{m_{cl}} \int_z^0 C(z')\theta(z') dz' \quad (4),$$

Table 2. Present-day solute signal peak depths, showing that the anthropogenic signal peaks (Cl:Br and NO₃⁻) are higher in the profiles than the environmental solute peaks (Cl⁻ and Br⁻). Depths shown are from air rotary samples.

Solute or ratio	Borehole 71 peak depths cm bgs*	Borehole 72 peak depths cm bgs*
Cl ⁻	380	500
Br ⁻	380	500
Cl:Br	225	230
NO ₃ ⁻	270	345

* Solute peaks are measured from present-day depths. Peak depths from the time of deposition would be 90 cm less.

where $t(z)$ = calculated age of chloride in the profile at particular depth z [T]; $C(z')$ = concentration as a function of depth [$M L^{-3}$]; $\theta(z')$ = volumetric water content as a function of depth [$L^3 L^{-3}$]; m_{Cl} = mass flux of chloride per unit time from the surface [$M L^{-2} T^{-1}$]. Of course, with soil samples from discrete intervals in a soil profile, as in our case, Eq. (4) must be approximated by an analogous summation. The surface chloride deposition rate was previously estimated by several different chloride collection methods by Moore [1997], for a location approximately 50 km northwest of Fernandez Pueblo. However, most of his methods were in use for only 5-6 months in the field. He reports that the method with the longest period of measurement (7 years) gives a chloride deposition rate of $46 \text{ mg } L^{-1} \text{ yr}^{-1}$ [Moore, 1997]. This value was the one used to estimate chloride ages.

The amount of chloride in soil profiles in the desert Southwestern United States tends to reflect surficial Cl^- deposition since the last large-scale climate change at the Pleistocene/Holocene boundary, presumably because downward fluxes were sufficient to wash excess Cl^- out for a brief time at the end of the Pleistocene, about 13-14 ka before present [Phillips, 1994; Plummer et al., 2001]. Hence, chloride profiles in the desert Southwest tend to reveal quite similar CMB ages throughout the Southwest, about 13-20ka, unless the profiles are deep enough and under dry enough hydrologic conditions to retain additional chloride from the dry period prior to this time frame. However, the chloride profiles at our site have a wide range of total chloride mass, representing from 8,000 to 69,000 years (mean 43,000 years) of chloride deposition if surficial processes were entirely responsible (see Table 3). The implications of this wide range of chloride

Table 3. Chloride mass balance ages through 10 meters depth, in the boreholes at Fernandez Pueblo.

Borehole	Chloride Mass† kg m ⁻²	Cl Mass Balance Age* ka
71	1.7	33
72	1.4	26
103	3.7	69
106	0.43	8
107	2.7	50
118	2.6	48
123	3.5**	65**
Average	2.3	43

† Chloride mass estimated from Quemada [1995].

* Age based on surface-only deposition and an annual total chloride deposition rate of 53.7 mg m⁻² a⁻¹, from Moore [1997].

** Confined water was encountered at 9.1 m depth in borehole 123, so chloride mass and chloride age are through 9.1m depth at this borehole.

ages, and the high mean age, are reviewed below (in the *Chloride Mass Balance, Revisited, and Upward Flow* section).

Soil and Water Data

Stratigraphic profiles were created for all air rotary and hand auger boreholes [Quemada, 1995]. These profiles were made at resolutions of approximately 15 cm for the hand auger holes, and approximately 1.5 m for the air rotary boreholes. These profiles are individually fairly simple—each shows a surface layer of sand dominated colluvium, which changes to a clay/mudstone at 1 m to 5 m depth. This clay/mudstone is presumed to be part of the Triassic Dockum formation. The profile from borehole 71 is shown as Figure 4, where the bottom of the profile at 2100 cm bgs represents where saturated conditions were reached.

Figure 5 shows relative elevations of the top surface, depth to water, and potentiometric level of water in the subsurface, derived from the air rotary drilling and subsequent measurement of the water levels in the boreholes. Based on these data, the aquifer is confined at all borehole locations where saturated conditions were identified, since the piezometric surface is higher than where saturated conditions were encountered (saturated conditions presumably indicated the top of the confined aquifer). The depth to confined water generally increases to the east. The one exception to this rule is at borehole 71. The eastward trend is discussed in detail in the Other Considerations section.

There is a relatively dry region of 1-2 m thickness just above the confined water in the borehole profiles that appears out of place (refer to the right-most plots of

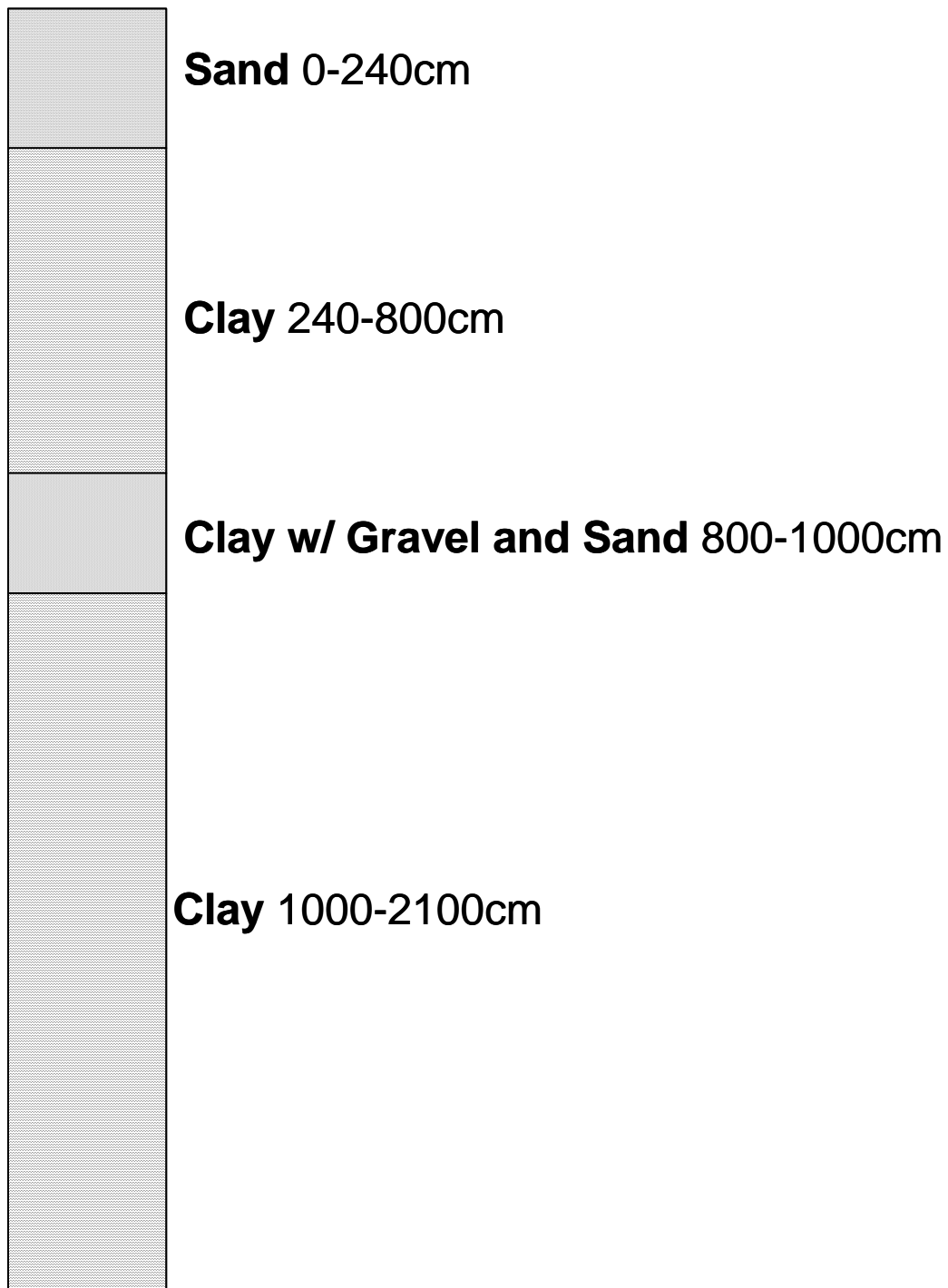


Figure 4. Present-day soil profile at Borehole 71 , adapted from Quemada, [1995].

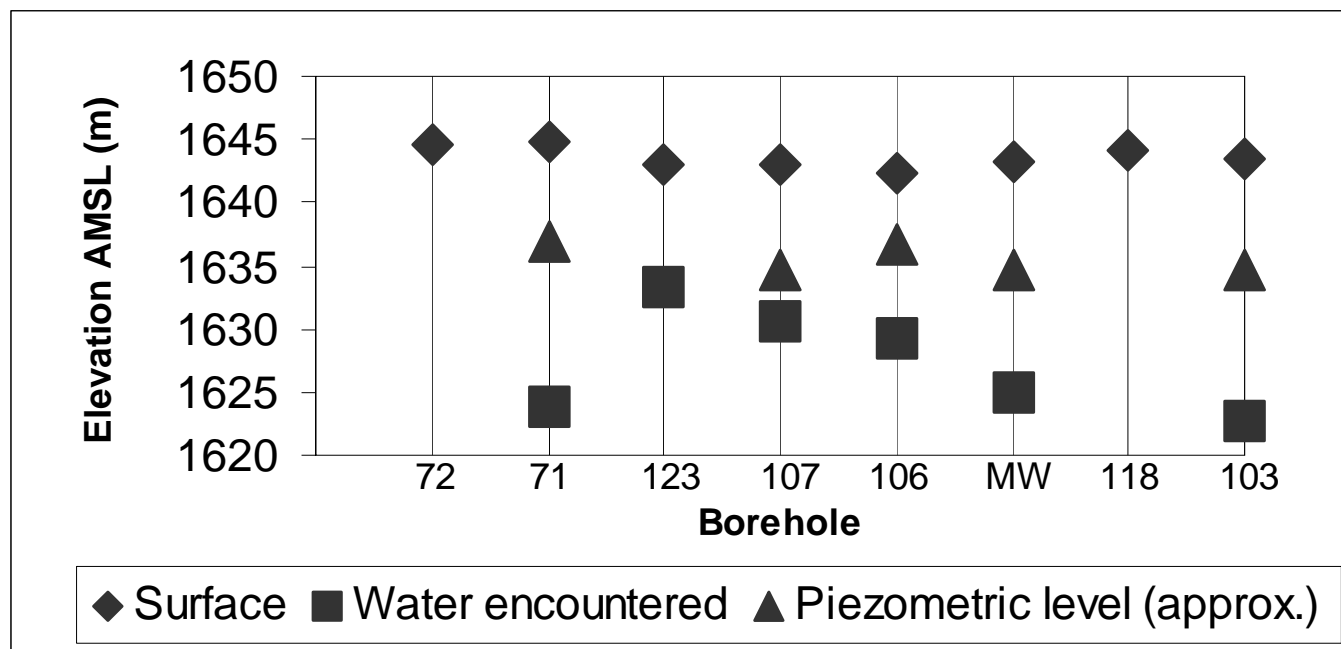


Figure 5. Plot showing relative elevations of the surface, the depth at which water was encountered, and the approximate piezometric level of the water in the boreholes drilled at the Fernandez Pueblo site. Boreholes are arranged on the plot by their East-West coordinates, from left (West) to right (East).

Figure 3 for example profiles from boreholes 71 and 103); we should naturally expect the confining layer to have a degree of saturation that is somewhere between that of the aquifer below and the relatively wet unsaturated zone above. This dry region is possibly due to the air rotary drill vaporizing the pore water present, as the drilling logs indicate that progress was often quite slow just before confined water was reached. However, the drilling log also reveals that progress was in some cases even slower through the unsaturated mudstone above, and that the confining layer is made of a slightly different material than the mudstone. A field texture analysis of this material showed that it contains a significant silt fraction, and is thus presumably more poorly-sorted than the mudstone. Therefore, one can infer that the confining layer may have a lower porosity than the clay/mudstone above it, which might also contribute to the lower gravimetric water content. Because the air rotary method of drilling may cause significant drying in soil samples, I conclude that the water contents in Figure 3 reflect the lowest possible water contents in the profile. The true water contents may be higher, but certainly will not be lower, than those measured.

Chloride Mass Balance, Revisited, and Upward Flow

The presence of the ~200 to ~1300 cm H₂O pressure potential at the top of the confined aquifer (Figure 5), with unsaturated conditions above, naturally leads to the assumption that some quantity of water, however minute, has been flowing upward through the unsaturated zone for however long the hydraulic system has been in this condition. The chloride masses in the borehole profile were re-examined, to see if

additional evidence of upward flux could be found. The following paragraphs explain this effort and its results.

In the absence of significant upward flow, the mass of chloride in the profile should represent the amount of chloride that has been deposited at the surface. Normally, there is 13,000-20,000 years' worth of Cl^- in profiles of the desert Southwest, according to Phillips [1994]. Since the average Cl^- mass from the profiles at the Midden Project site represents 43,000 years of accumulation, the Cl^- mass indicates the presence of an upward flow component.

The Cl^- masses in the profiles at Fernandez Pueblo are highly variable (Table 3). An obvious question then follows: Is the wide range of chloride masses at the site due to surface processes of lateral concentration and percolation, or is it caused by differences in upward fluxes from the confined aquifer below? I revisited the known field data in an attempt to see which of these processes it supports. A photogrammetric 20-cm interval topographic map of the site shows that none of the boreholes are in a modern local depression at this scale [Doleman, 1995]. Nor is there any obvious correlation between surface slope at the borehole locations and chloride mass below. But there is a strong correlation between the amount of chloride present in the environmental bulge (above 1000 cm bgs), and the average water content found in the unsaturated region between 500 cm bgs and the confined aquifer below. Table 4 ranks the boreholes in terms of: (1) the total chloride mass in the zone of accumulation (above 1000 cm, or above saturation at 920 cm in the case of borehole 123); (2) the average water content found in the unsaturated zone below 500 cm bgs; and, (3) the surface slope in the vicinity. A low surface slope should increase the infiltration rate locally.

There are no straight-forward equations that could be used to model the relationship of profile water content or surface slope to chloride mass. Instead, I determined the correlation coefficients of the ranks of these parameters. Such a non-parametric approach is quite robust and does not depend on the statistical distributions of the measured values. The correlation coefficients of the ranks of water content and slope to the ranks of chloride mass are reported on the bottom line of Table 4. By this analysis, the average water content between 500 cm depth and the saturated conditions below is well-correlated to the chloride mass present (R^2 of the rank comparison = 0.93); indeed, one can clearly see the correlation by inspection of the ranks listed in the 3rd and 5th columns of the table, only one ranking is transposed between the two sets. By contrast, the chloride mass found appears to have almost no correlation to the surface slope (R^2 of the rank comparisons = 0.01). This positive correlation between water content and Cl^- mass can be explained by well-known physical principles. For a given soil a higher water content leads to a higher unsaturated hydraulic conductivity. Since the water potentials in the aquifer and the root zone will each be similar from point to point at the field site, the higher water content will result in higher Cl^- fluxes, and thus higher Cl^- accumulation rates in the profile. Therefore, I consider the positive correlation between water content and Cl^- mass strong evidence for upward flow.

In summary, the following observations constitute the known evidence for upward flow at the site. (1) The water in the underlying sandstone lenses is under 200 to 1300 cm of pressure head, with unsaturated conditions above it indicating negative potentials; thus there is a driving force for upward flow. (2) There is a larger-than-normal Cl^- inventory in most of the profiles at the site, as compared to other sites

Table 4. A comparison of trends in chloride mass (represented by CMB age), water content between the root zone and the confined aquifer below, and the surface slope.

Borehole	Cl mass to 10m depth		Average water content between 5m depth and saturated zone		Surface Slope	
	kg/m ²	rank	vol/vol	rank	%	rank
106	0.43	1	0.162	1	1.0	7
72	1.4	2	0.164	2	13.	1
71	1.8	3	0.169	3	13.	2
118	2.6	4	0.204	5	2.8	6
107	2.7	5	0.175	4	3.3	5
123	3.5*	6	0.214	6	3.9	4
103	3.7	7	0.245	7	3.9	3
Correlation coefficient (R ²) between rank of Cl mass and rank of parameter:				0.93	0.01	

* Confined water was encountered at 9.1 m depth in TP-123.

in the desert Southwest. (3) The Cl⁻ mass in the environmental bulge is correlated to water content between 500 cm depth and the confined aquifer. (4) As previously discussed, other researchers have effectively demonstrated that upward flux from water table aquifers in arid and semi-arid areas does occur (Fontes et al., 1986; Scanlon et al., 1991; Gee et al., 1994; Plummer et al., 2001).

Modeling the Midden Project Data

This section describes some of the questions that remain after the basic analysis of the Midden Project data, and the main objectives in modeling the flow and transport processes at Fernandez Pueblo.

Outstanding Questions

Quemada [1995] successfully identified the Cl:Br ratio as an anthropogenic solute, and estimated recharge based on the present-day position of its peak. I modified this recharge estimate, and added the analysis of the nitrate data, which has strengthened the case for the anthropogenic origin of the Cl:Br ratio. But, this data set leaves us uncertain about processes at the Midden Project site. Despite the above arguments, the fundamental question of whether recharge (downward) flow is occurring remains unsolved. For example, these analyses provide no reason that a small amount of recharge and a small amount of discharge are not meeting in the unsaturated zone and discharging from the site as lateral outflow. And if recharge from precipitation and/or discharge from

the aquifer are occurring, what are the rate(s) of flow? As mentioned earlier, several researchers in the desert southwest have found that essentially no water leaves the root zone of plants over the long term [e.g., Fontes et al., 1986; Scanlon et al., 1991; Gee et al., 1994], while others [e.g., Stephens and Knowlton, 1986; Hakonson et al., 1992; Kearns and Hendrickx, 1998] indicated that there may be recharge occurring. So one basic question is, what could a modeling effort show about the possibility for groundwater recharge actually occurring? I address the question of recharge using mathematical modeling which permits the synthesis of much of the data and other site information; these efforts are discussed below.

Other questions, that relate to the modeling effort that is the body of this thesis, include the following. (1) Can the Midden Project data yield a simple conceptual model for water flow and solute transport at the site? (2) According to the model, what are the conditions that will lead to significant downward movement of the anthropogenic solutes? (3) Can these data be used to calibrate this conceptual model, just as data are used to calibrate models for nuclear waste repositories? The purpose of calibration is to establish that a computer model can reproduce field-measured potentials and solute concentrations [Anderson et al., 1992]. Successful calibration is a fair (certainly not absolute) indication that the model includes the necessary processes to make predictions about the future of a hydrologic system.

The questions posed above require numerical modeling, rather than a simpler back-of-the-envelope approach, because the shallow vadose zone (where the anthropogenic solutes reside) is a highly non-linear flow system with a high degree of temporal variability in saturation, flux, and even in flow direction. One expects, prior to

any modeling effort directed at the pueblo site, that the hydrologic system will change rapidly before, during, and after precipitation events, and that the system response will be highly dependent on antecedent moisture conditions, the season, and the details of the precipitation time series. Thus, the kinds of simplifying assumptions that typically make back-of-the-envelope calculations feasible—such as steady flow, or constant hydraulic conductivity—are not permitted by the hydrologic system being studied here.

Hypothesis of This Thesis

This thesis is a report on my work to create a conceptual model of water flow and solute transport at the midden project site using the known data, and a simulation effort that implements this conceptual model in the unsaturated flow and transport code HYDRUS-1D [Simunek et al., 1998]. This conceptual model is described in detail in the next section, Conceptual Model and Methods. I hypothesize that if the conceptual model created is able to adequately explain the present-day positions of the anthropogenic solutes, then we can use the conceptual model to explain processes and observations at the site, in particular recharge or discharge. This hypothesis was tested as follows: (1) determine whether the numerical model, i.e., the HYDRUS-1D implementation of the conceptual model, can reproduce the known NO_3^- and Cl:Br solute positions; (2) identify the physical parameters that control water and solute movement at the project site; and, (3) review the HYDRUS output in detail to determine the temporal scale of recharge events within the simulations. After these objectives were accomplished, the conceptual model of water and solute movement was refined by taking into account the HYDRUS model results.

II. CONCEPTUAL MODEL AND METHODS

This chapter describes the conceptual model of water flow and solute transport created for the Midden Project site, and how it was implemented in the HYDRUS-1D code. First, the soil profile and initial conceptual model inferred from the data gathered is introduced. The governing equations of water flow and solute transport in the HYDRUS-1D code are described and, along with the methods used to calculate root uptake and surface evaporation of water. The remainder of this chapter is devoted to the particulars of the simulation runs which are subdivided into three categories: (1) initial simulations (“dry” and “wet” scenarios), (2) sensitivity analysis, and (3) temporal scale of recharge events. The initial and boundary conditions for the simulations are described for each category of simulation, along with the data used, and the changes made from simulation to simulation.

Conceptual Model

Here the conceptual model of flow that was used throughout the HYDRUS simulations is discussed, along with some of the basic data that were needed to test this model. The soil profile that was used in the modeling is introduced first, followed by the root zone, the top boundary condition, the bottom boundary condition, and the initial

condition. As will be discussed in the next section (HYDRUS-1D Code), use of the HYDRUS code implicitly assumes that the Richards' Equation for the water balance, and the advection-dispersion equation for the solute balance, both apply to this problem.

Soil Profile

For simplicity, and to reduce the amount of computer time required to run the simulations, it was assumed that flow at the site could be modeled as a one-dimensional process. A 2-D profile simulation, that included the daily precipitation and evapotranspiration records that were to be used (see Top Boundary Condition subsection), would have required months' to years' running time per simulation on a desktop computer. In addition, the scant data available about the soil properties at the site could not justify a two-dimensional model. A typical (1-D) soil profile for the in-midden boreholes (71 and 72), that combines the detailed near-surface surface information from the trench profiles with the more depth-averaged information derived from the drill cuttings, is included as Figure 6. This soil profile, or some part thereof, was used in all of the modeling I have performed. The profile is presumed to be typical of the midden area at the time of anthropogenic deposition, whereas a modern profile would have an extra ~90 cm of sandy colluvium on top.

The somewhat arbitrary 200 cm thickness of the confining layer was based on the thickness of the region where an apparent drop in soil moisture was found at most holes just before confined water was reached. Figure 7 shows volumetric water contents for profiles 71 and 103, repeated from Figure 3. Initially, it was thought that the reduced

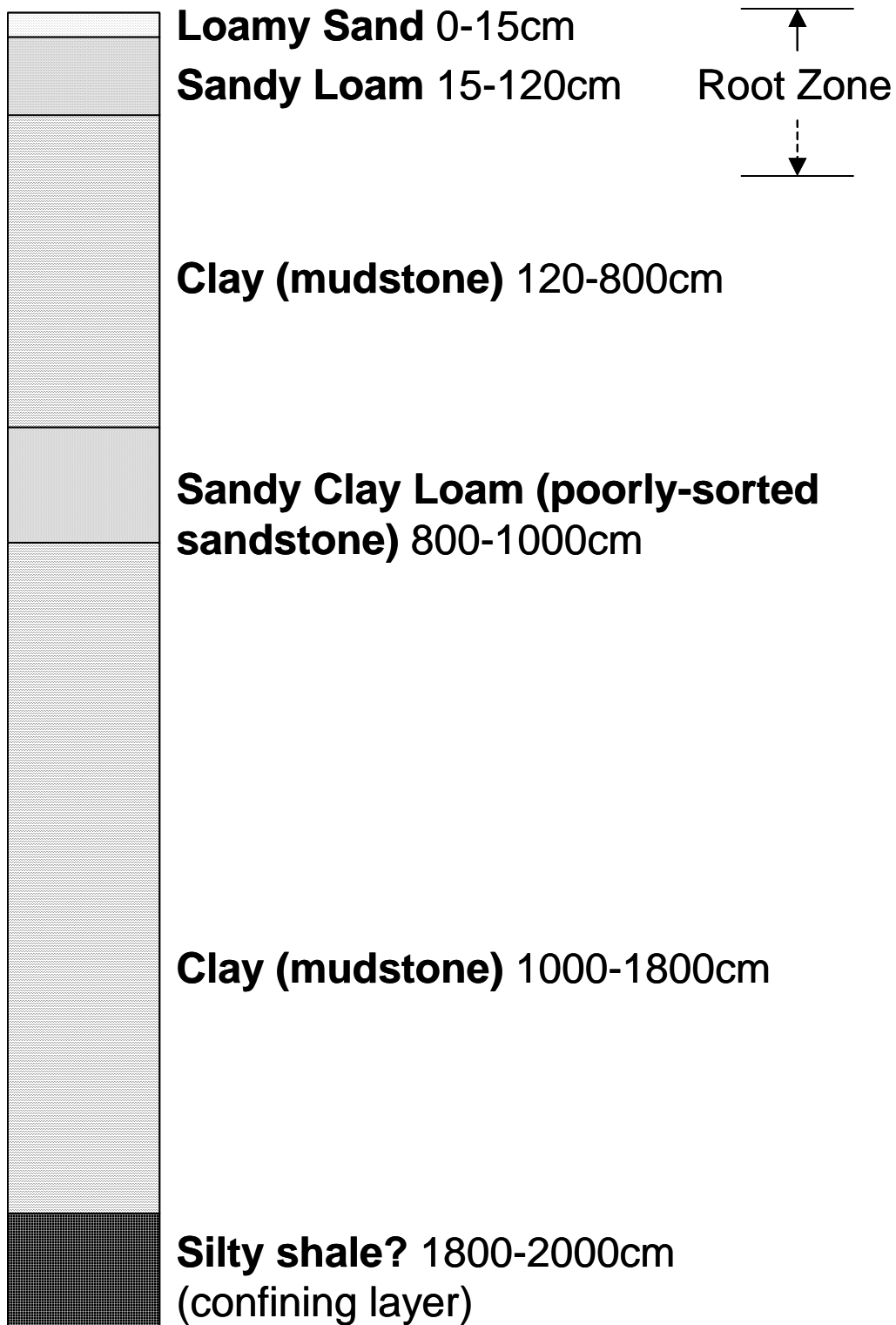


Figure 6. Typical soil profile at Fernandez Pueblo site, for the time of midden deposition.

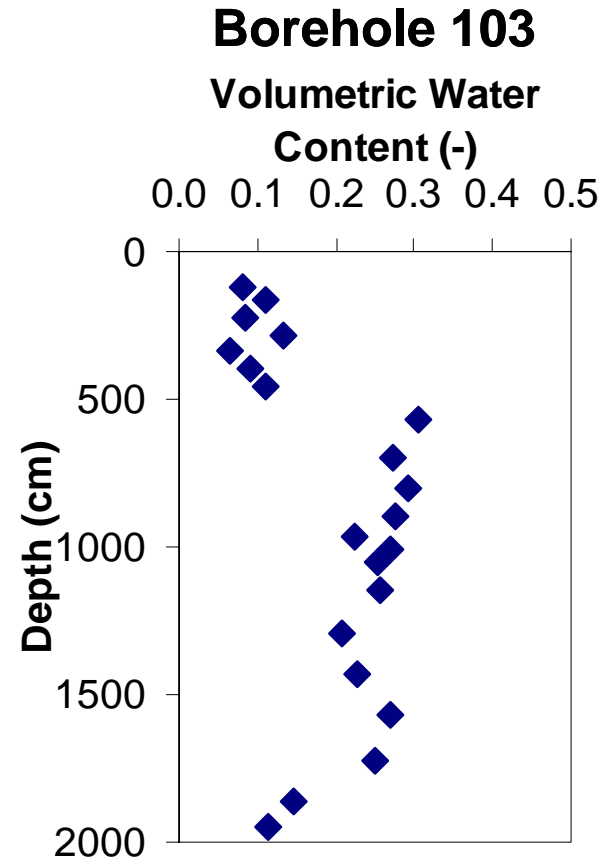
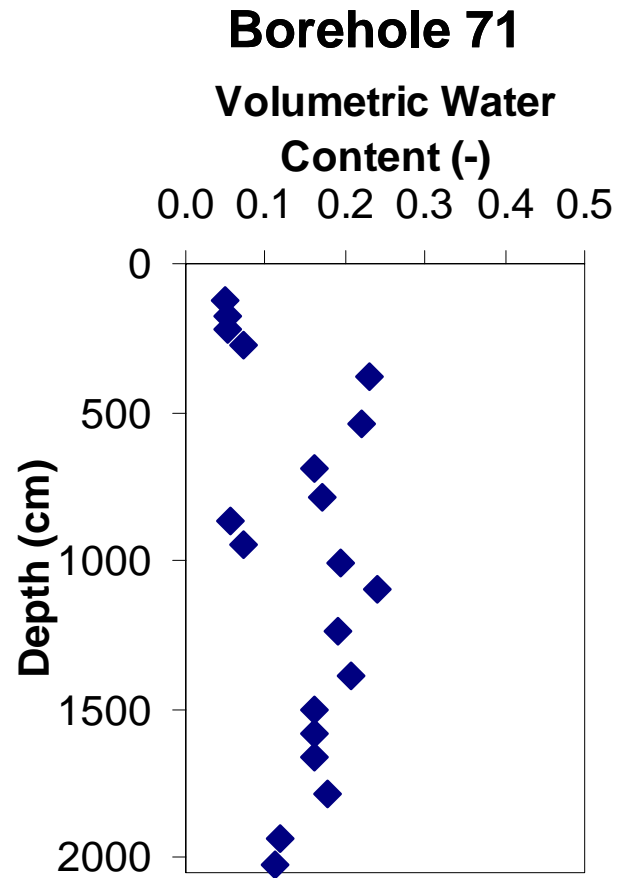


Figure 7. Estimated volumetric water content from boreholes 71 and 103, showing the reduced apparent water content in the bottom 200 cm. (These are larger copies of plots on Figure 3.)

water content in the confining layer was mainly due to the reduced porosity that is typically present in well-indurated, poorly sorted sediments, and the saturated water content in the simulated confining layer was restricted to reflect the actual (low) water contents. But as mentioned in the Previous Results section above, the drilling was often considerably more difficult just before saturated conditions were found. It is now thought that the apparent dryness of the rock reflects additional energy for water vaporization provided by the drilling process.

Based on the available texture data (Quemada, 1995; Appendix C) I assumed that, above the confining layer (at less than 1800 cm depth in the simulation profile, Figure 6), the apparent unsaturation is real, and not an artifact of the drilling. This means that the observed confining pressure (200-1300 cm H₂O) must be used up in the 200-cm-thick confining layer, so that negative matric potentials must exist above this confining layer.

Root Zone

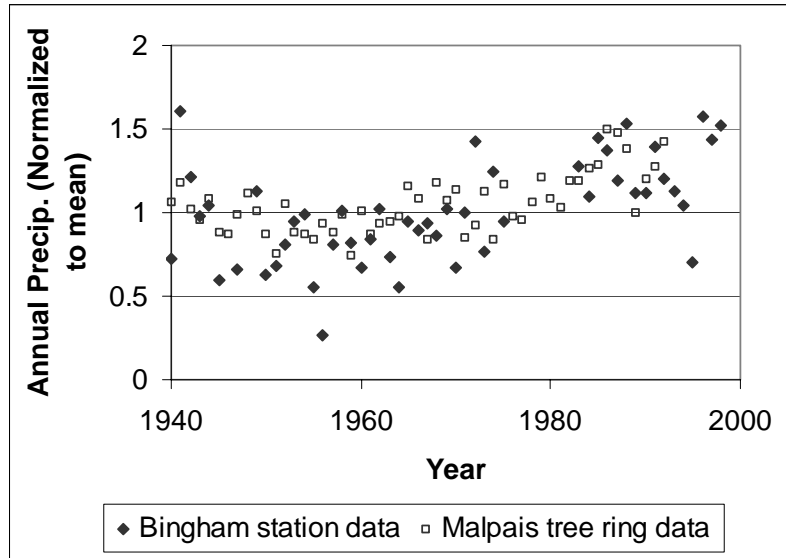
As stated in the Previous Results section of the Introduction, the shrub sand sage <*Artemesia filifolia*> is the dominant plant species at the site. Rooting depths for sand sage have been reported by others to be in excess of 300 cm [Weaver, 1919; Pockman, 2000]. We found rooting depths between 70 and 150 cm in the trench soil profiles (Appendix C). The conceptual model used in the modeling includes transpiration from roots with maximum depths between 100 cm and 300 cm.

Top Boundary Condition

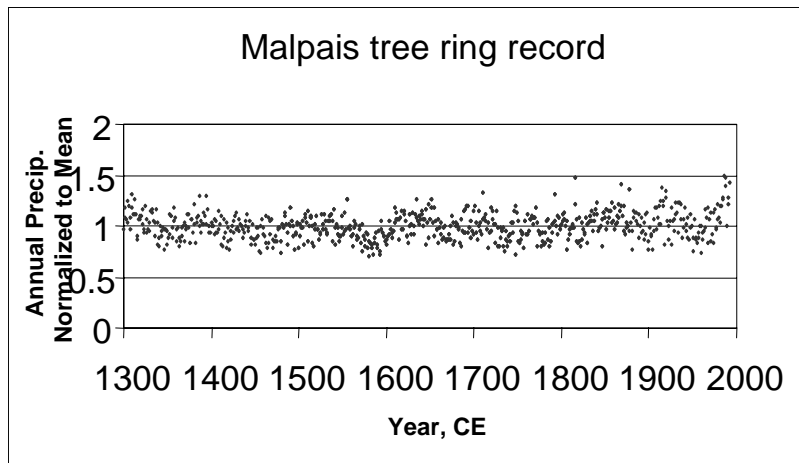
The top boundary condition—which was located at the surface of the profile at the time of midden deposition--needed to include the processes of precipitation and evapotranspiration. It was important that the data used to represent these processes have high temporal detail because brief, intense precipitation events have been proposed as a likely initiator of recharge in semi-arid regions [Stephens, 1994; Kearns and Hendrickx, 1997]. Typically, precipitation values are recorded daily at most weather stations.

Daily precipitation was taken from the Bingham 2 NE weather station at Bingham, NM, which is about 20 km south-southeast of Fernandez Pueblo. This precipitation record was used because it came from the closest known weather station, and because the weather station and the pueblo are at roughly the same elevation and both are within the same environment, the inter-mountain plains of the northern Jornada del Muerto. The mean annual precipitation from the Bingham station is 27.3 cm.

To assess whether climate change may be an important factor in modeling this centuries-long transport, the Bingham station precipitation data were compared to a 2,129-year precipitation record that was inferred from tree ring data compiled at Malpais National Monument, New Mexico, by Grissino-Mayer [1996]. These two data sets show the same general trends over the overlap period from the 1940s to the early 1990s—most notably, a drought in the late 1950s to early 1960s, and a wetter period from the early 1980s to the end of the record (Figure 8a). Thus we can infer that the Bingham time series of precipitation is fairly well correlated to the Malpais tree ring data, at least for the current record (the correlation coefficient between the two normalized data sets is $R =$



(A)



(B)

Figure 8. (A) A comparison of the Bingham station annual precipitation record used in modeling the Fernandez Pueblo solutes, with the far longer Malpais precipitation record inferred from tree ring data, from Grissino-Mayer [1996]. (B) the tree-ring series from the beginning of pueblo occupation, ca. 1300 CE. All time series are normalized to their means.

0.91 for 5-year smoothed averages). In addition, the Malpais record from the 1300's to the near-present shows that the precipitation time series has not changed much over this time frame (Figure 8b), although the 20th century has had the highest average annual precipitation. The mean precipitation in the overall 1300-1992 Malpais record is 37 cm, versus 39 cm in the 1940-1992 interval. Thus, there has been a slight increase in the annual precipitation in the relatively recent past in the Malpais record, but no drastic changes in climate. Because the modern Bingham station record is reasonably well-correlated to the modern Malpais record, I infer that climate change is a relatively unimportant factor near the Bingham weather station, and hence also around the pueblo site. Therefore the available 20th century Bingham station daily precipitation data were used in HYDRUS, without modification, as the precipitation series at the pueblo from the time of pueblo occupation to the present.

The Malpais dendrochronological precipitation record itself could not be used for the precipitation record, despite the fact that it has annual precipitation information back to the beginning of the pueblo inhabitation, ca. 1300 AD. The reason that this record is unsuitable is that the present modeling exercise required daily precipitation information, so that the near-surface unsaturated zone response to individual storm events could be captured. This was thought to be particularly important in modeling the anthropogenic solutes. The Malpais record, being inferred from year-by-year tree ring thickness, contains only the approximate total annual precipitation [Grissino-Mayer, 1996], and gives no information about the relative wetness of seasons or the intensities of particular storms. However, individual storm events are recorded within the daily Bingham station record, so the Bingham record was obviously the better choice for this modeling.

Potential evapotranspiration (ET_o) is the total amount of water vapor that the atmosphere could draw from the surface, if sufficient surface and near-subsurface water is available. There are no potential evapotranspiration data available from the Bingham weather station, nor from anywhere else within 100 km of the pueblo site that has similar hydrologic conditions. It was decided that the next-best data would come from a Chihuahuan desert site with quite similar hydrologic conditions. The potential evapotranspiration (ET_o) data used for the modeling were from Kearns and Hendrickx [1997], who applied the Penman method for inferring ET_o from environmental data gathered at the Leyendecker weather station near Las Cruces, NM. This station is about 192 km south-southwest of the pueblo site, but is in high Chihuahuan desert with a very similar climate. The daily average of the Leyendecker ET_o series data were deemed sufficient for the present modeling, because measurement of such values for a given site includes ~25% uncertainty [Bastiaansen, 2000]. This ET_o record is a one-year series of Julian day averages that was recycled over and over to form the ET_o record used in the HYDRUS simulations. For example, the ET_o 's from all January 1st's in the actual record (in this case the actual record was from 1983-1994 (Kearns and Hendrickx, 1998)) are averaged together to form the 1st day in the 365 day cycle. This ET_o value was also used in days 366, 731, 1096, etc, until the end of the simulation. It was understood that this ET_o time series would be slightly high for the midden project site, because (1) the Leyendecker station is at a lower elevation (1220 m, versus 1650 m at Fernandez Pueblo), and at a slightly lower latitude, and, (2) the daily average values used will tend to be higher than the actual ET_o on days with precipitation, when atmospheric demand is typically reduced due to lack of sun and higher humidity. Thus, I used these ET_o data as

maximum likely ET_0 value in some simulations, and modified these values downward for other simulations, as described below in the Preliminary Simulations and Sensitivity Analysis sections of this chapter.

There is no way of knowing when the pueblo natives interred the midden material, except that it occurred “sometime in their occupation of the pueblo” (1300-1450 A.D.). Thus, we cannot know the actual time series of anthropogenic solute addition within this time frame.

To simplify the surface boundary condition for solute transport, a generic solute was introduced with the precipitation for a time at the beginning of the simulations to simulate the movement of Cl:Br and NO_3^- , the anthropogenic solutes. The time of solute input varied in different simulations, as will be discussed below. This has the same effect as assuming that all of the midden material was deposited at the surface. The period of solute addition differed among simulations; the particulars are discussed in the Preliminary Simulations and Sensitivity Analysis sections below.

Bottom Boundary, Upward Flow

I have assumed that the chloride inventories in the borehole profiles reflect steady flux from the aquifer below, combined with chloride deposited at the soil surface with precipitation. I assume that this site was essentially washed clean of stored environmental chloride during the wet period of ~13-14 kyr before present, because other sites in the desert Southwest apparently had their chloride inventories removed at this time (Phillips, 1994; Plummer et al., 2001). The total chloride masses vary greatly from borehole to borehole (Table 3), so the flux from the surface and/or from the confined

aquifer below is not evenly distributed. Assuming that, estimation of the amount of upward flux is then possible by a simple mass balance:

$$\text{Total } Cl^- \text{ mass} = (M_s + C_b q_b) t_D \quad (5),$$

where M_s = mass flux from surface [$M L^{-2} T^{-1}$], C_b = concentration of solution in lower vadose zone [$M L^{-3}$], q_b = upward water flux from below (assumed to be constant), and t_D = time of chloride deposition in environmental solute bulge. This method assumes that the surficial chloride is evenly distributed. It turns out that the upward fluxes calculated by this method are quite small relative to the precipitation at the site. For borehole 103, where the highest upward flux is presumed because it has the highest chloride inventory, one calculates an upward flux q_b of 0.8 mm yr^{-1} using $M_s = 54 \text{ mg m}^{-2} \text{ yr}^{-1}$ from Moore [1996]; $C_b = 260 \text{ mg L}^{-1}$, the average Cl^- concentration found below the environmental bulge in borehole 103; and $t_D = 13,000 \text{ yrs}$. This is approximately 0.3% of the average annual precipitation rate of 27 cm yr^{-1} . Because the upward flux is so small, it is assumed that it is taken up by the plants at the bottom of the root zone and has little effect on the root zone's ability to absorb surface-derived moisture.

The bottom boundary in all simulations was a prescribed potential boundary that would drive upward flow from below the root zone, although the particular placement of the boundary and the prescribed potential value varied between simulations. The precise values used are given in the Wet and Dry Scenario, and Sensitivity Analysis discussions below.

Applying the maximum upward flux from the aquifer at borehole 103 (Eq. 5), 0.8 mm yr^{-1} , I estimate that the maximum accumulation of Cl^- from upward flux over the past ~700 years from the beginning of the pueblo occupation is 146 g m^{-2} . This is only 4% of

the 3700 g m^{-2} total Cl^- in the bulge at borehole 103. So, although solutes (including Cl^- , Br^- , and NO_3^-) are assumed to be entering the bottom of the profile with the upward flux from the confined aquifer, these were ignored in the modeling, i.e., $C_b = 0$ in the HYDRUS simulations.

Initial Condition

The time represented by the beginning of the simulations was about 1300 A.D., the time of first occupation of the pueblo. Because we cannot know the state of the water and solute system at that time, initial conditions for the modeling had to be assumed. I assumed that the uppermost layers of the soil profile have frequent changes in water content, due to changes in influx due precipitation and outflux through evapotranspiration and possible downward flux (drainage) below this zone. The thickness of this active zone was thought to be on the order of the maximum rooting depth of the plants on site. Below this active zone, I assumed that the water system is approximately in steady-state, reflecting equilibrium or near-equilibrium conditions between upward water flux from the aquifer below, and removal of this water near the surface by evapotranspiration. Modeling by Plummer et al., [2001], has indicated that water potential and content changes below the root zone are typically extremely slow in arid and semi-arid environments. The possibility of intermittent recharge pulses from large precipitation events breaking through the active zone was not discounted: one of the major reasons for the modeling effort was to see whether such events occurred.

The solute profiles at the site, as of 1300 C.E., were assumed to be the same as in the present-day, except that the anthropogenic solutes were not present. In other words,

the environmental solute bulges were in the same positions as they are today, and essentially negligible amounts of solute were in the rest of the profiles. Of course, there has actually been about 700 years of additional environmental solute accumulation in the meantime. One preliminary simulation was started with a solute peak at 400 cm depth, meant to represent the environmental solute bulge (see Preliminary Simulations section, below), while all other simulations had all concentrations set to zero in the initial condition.

HYDRUS-1D Code

Vegetation has been cited as the most important control on water movement in arid or semi-arid landscapes [Scanlon et al., 1997; Gee et al., 1994], so it seemed most important to apply a code that allowed for versatile input of root densities and plant water uptake characteristics. As mentioned earlier, I used the unsaturated liquid water flow and solute transport modeling software, HYDRUS-1D [Simunek et al., 1998]. As its name implies, this code only simulates one-dimensional problems. Reducing the potentially complex multi-dimensional flow beneath the pueblo to a one-dimensional process may be justified by the following considerations. (1) Subsurface hydraulic data for the site are quite limited; a more complex model would require additional data and/or a more complex sensitivity analysis. (2) Given the detailed, long upper boundary condition series that we desired to use, a multi-dimensional model would have been impractically expensive in computer time. (3) At least one model validation study in southern New

Mexico, with quite detailed hydraulic information, showed that two-dimensional computer models performed no better than one-dimensional models in predicting water and solute movement in heterogeneous porous media [Hills et al., 1994]. HYDRUS allows the use of realistic time-varying, user-prescribed boundary conditions that honor limits of prescribed daily potential evaporations and transpirations (E_o and T_o). E_o and T_o serve only as maximum limits in the code, not as any kind of scaling factors that are used to compute the actual fluxes. HYDRUS features the ability to easily set a root zone density profile, and potential transpiration can be set to zero for the winter when the plants are dormant. However, HYDRUS does not include vapor flux which, over a given season, can be a significant part of the water balance in the first ~200 cm of the subsurface [Scanlon et al., 1997], although over the time frame of many years and at deeper depth it becomes less significant. HYDRUS-1D was also not capable of accounting for surface sediment accretion. Figure 6 is presumed to reflect the depth of sandy soil and loamy sand for the time of midden deposition, and sediment accretion was assumed to take place after the solute transport had taken place. The validity of this assumption will be discussed in the Results and Discussion section.

HYDRUS-1D uses the Richards' equation for water flow and water mass balance [Šimůnek et al., 1998]:

$$\frac{\partial \theta(h)}{\partial t} = \frac{\partial}{\partial x} \left[K(h) \left(\frac{\partial h}{\partial x} \right) + \cos \alpha \right] - S(h, x) \quad (6)$$

where h = matric potential [L], $\theta(h)$ = volumetric water content [$L^3 L^{-3}$], $K(h)$ = unsaturated hydraulic conductivity [$L T^{-1}$], α = angle between the flow direction and the vertical positive-upward axis ($\alpha = 0$ in this study), and $S(h, x)$ is the sink term [T^{-1}]. Note that the sign of h in Eq. (6) is such that h becomes more positive (less negative) under

higher water contents (within a given horizon). The top boundary is a mixed boundary condition that limits the absolute value of the surface flux by the following two conditions:

$$\left| -K \frac{\partial h}{\partial x} - K \right| \leq E_0 \quad (x = 0) \quad (7),$$

and

$$h_A \leq h \leq h_s \quad (x = 0) \quad (8),$$

where $K = K(h)$; E_0 = maximum potential rate of evaporation under the current atmospheric conditions [$L T^{-1}$]; h_a , h_s = minimum and maximum pressure heads at the soil surface under the prevailing soil conditions. The bottom boundary condition of Eq. (6) in my simulations was always of the form:

$$h(x_b, t) = h_b, \quad (t > 0) \quad (9),$$

where x_b = position of bottom boundary, h_b = bottom boundary prescribed head value (constant for a given simulation).

The initial condition of Eq. (6) was determined by running the code in water-only mode, starting from an initial guess for the pressure heads. Once the pressure heads did not appear to be significantly changing over time below the root zone in these water-only simulations, the code was stopped, and the last recorded heads were used as the initial condition in the simulations that included solute transport. In this way, the anthropogenic solute that is to be modeled encounters pressure head conditions that are approximately in equilibrium with the boundary conditions. Of course, the heads right near the top boundary are highly variable in time due to precipitation events.

The functions $\theta(h)$ and $K(h)$ in (6) were determined by the van Genuchten relationships:

$$\theta(h) = \begin{cases} \theta_r + \frac{\theta_s - \theta_r}{\left(1 + |\alpha h|^n\right)^{(1-1/n)}} & h < 0 \\ \theta_s & h \geq 0 \end{cases} \quad (10),$$

and

$$K(h) = K_s S_e' \left[1 - \left(1 - S_e^{n/(n-1)} \right)^{1-1/n} \right]^2 \quad (11),$$

where θ_r = residual water content [$L^3 L^{-3}$]; θ_s = saturation water content [$L^3 L^{-3}$]; K_s = saturated hydraulic conductivity [$L T^{-1}$]; S_e = saturation index $\equiv (\theta - \theta_r)/(\theta_s - \theta_r)$ [-]; α , n , l = fitting parameters.

The sink term, S , in Eq. (6) represents transpiration by the vegetation. At any given point in the model, the sink term is given by

$$S(h, x) = \gamma(h) b(x) T_p \quad (12),$$

where $\gamma(h)$ and $b(x)$ are both factors that scale the potential transpiration T_p (both $\gamma(h)$ and $b(x)$ have ranges between 0 and 1). $\gamma(h)$ is known as the water stress response function, and reflects the plants' changing ability to take up water at different soil water matric potentials. For our simulations, the model of Feddes et al. [1978] is used to define $\gamma(h)$ (Figure 9). In this model, the plant's water-uptake ability is completely choked off near saturation due to lack of oxygen ($h \geq h_1$), increases linearly with decreasing h to a maximum of $\gamma = 1$ in the plant's optimal range of matric potential. Then, below a certain $h = h_3$, decreases linearly until the matric potential is less than or equal to the wilting

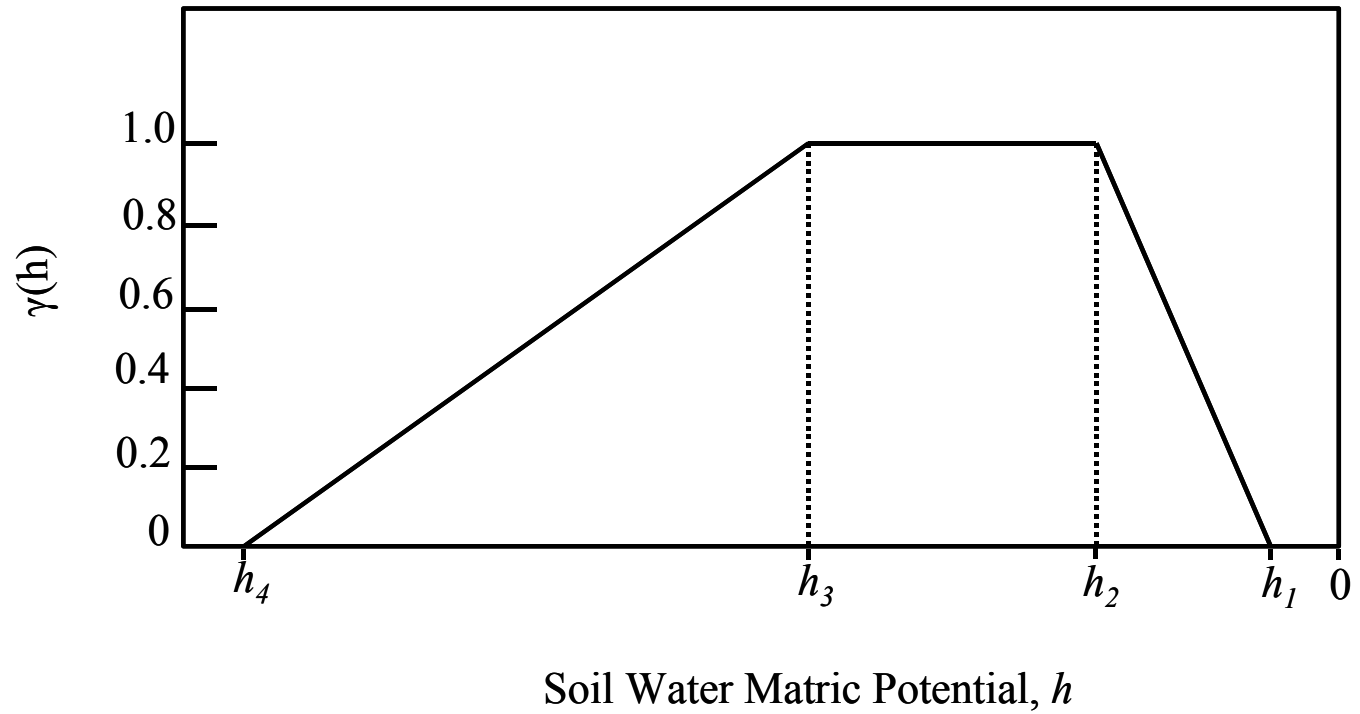


Figure 9. Model of water stress response function $\gamma(h)$. The horizontal scale is such that $h_4 < h_3 < h_2 < h_1 < 0$. Figure is after Šimůnek et al., [1998]. h_4 is the wilting point.

point of the plant (where $\gamma = 0$). The factor $b(x)$ in Eq. (12) accounts for the distribution of roots in the subsurface; $b(x)$ always integrates to 1 over the entire rooting depth. Hence $b(x)$ may be seen as a relative density function for plant roots within HYDRUS. Let the maximum rooting depth be r_{max} ; $b(x)$ in all simulations was then given by:

$$b(x) = \begin{cases} \frac{12}{7r_{max}}, & 0 > x > \frac{1}{3}r_{max} \\ \frac{6}{7r_{max}}, & \frac{1}{3}r_{max} > x > \frac{2}{3}r_{max} \\ \frac{3}{7r_{max}}, & \frac{2}{3}r_{max} > x > r_{max} \end{cases} \quad (13),$$

which always integrates to 1 over the entire root zone (x is upward-positive). This is an approximation to the root density profile for sand sage sketched in Weaver, [1919].

Evaporation is calculated by simply finding the Darcy flux between the top two nodes and removing this amount of water from the model if the flow is upwards, provided that this amount does not exceed the potential evaporation in the top boundary condition.

Conservative solute transport within HYDRUS is handled by the advection-dispersion equation, modified for unsaturated water flow conditions:

$$\frac{\partial[\theta(h)C]}{\partial t} = \frac{\partial}{\partial x} \left[\theta(h)D \frac{\partial C}{\partial x} \right] - \frac{\partial[q(h)C]}{\partial x} \quad (14),$$

where C = the solute concentration [$M L^{-3}$], D = hydrodynamic dispersion coefficient [$L^2 T^{-1}$], and $q(h)$ = specific discharge [$L T^{-1}$]. The top boundary condition for Eq. (14) was a third-type (Cauchy) condition:

$$-\theta D \frac{\partial C}{\partial x} + qC = -q_o C_o \quad (x = 0) \quad (15),$$

where q_o = net (downward) precipitation flux [$L T^{-1}$]; C_o = concentration of solute in q_o [$M L^{-3}$]. The bottom boundary condition for Eq. (14) was in all cases

$$C(x_o, t) = 0 \quad (16),$$

where again, x_o = position of the bottom boundary. As mentioned before in the Conceptual Model section of this chapter, the initial condition for Eq. (14) was in all but one simulation

$$C(x, 0) = 0 \quad (\text{all } x) \quad (17).$$

As mentioned earlier, one simulation was started with a solute peak at 400 cm depth, meant to represent the environmental solute peak (see Preliminary Simulations section, below).

The Richards' Equation for water balance, Eq. (6), is approximately solved using a mesh-centered finite difference scheme in HYDRUS-1D, whereas the ADE for the solute balance, Eq. (14), is approximately solved by a combination of Galerkin finite elements for the space derivatives, and finite differences for the time derivative.

HYDRUS automatically calculates mass balances for water and solute at every time step for which output is requested. For the details of this calculation, the reader is urged to consult the user's manual [Simunek et al., 1998]. An outline of their method is as follows. For a given output time, t^i , the mass balance error is roughly calculated by:

$$\varepsilon_a = m^i - m^0 - \Delta m_r + \Delta m_b \quad (18),$$

where ε_a = absolute error in mass balance; m^i, m^0 = masses in profile at the current output time and at time 0, respectively; Δm_r = change in mass due to root uptake; Δm_b = change in mass due to additions at the boundary. The percent error, ε_r , is calculated as

$$\varepsilon_r = \frac{|\varepsilon_a|}{\max[|m^i - m^0|, |\Delta m_r + \Delta m_b|]} \times 100 \quad (19).$$

Thus the absolute mass balance error is normalized to either the total change in storage in the system, or the total addition/removal of mass from the system by boundary processes and root uptake, whichever is greater. Note that ε_a and the quantities it is calculated from in (18) have units of mass for solutes, but units of length for water. This is because the length of a water column and its mass are functionally equivalent within a 1-D code with no changes in water density allowed, as is the case in HYDRUS-1D. Typically, the water mass balance calculated within HYDRUS indicated no more than 0.3% error, and the solute mass balance calculated within HYDRUS indicated no more than 0.2% error.

In addition to these mass balance calculations, I also checked the HYDRUS output for conservation of anthropogenic solute mass for four representative simulations, by separately checking the total solute mass in the system, C_{TOT} , at every output time, which I calculated as:

$$C_{TOT} = \sum_{all\ j} C_j \theta_j \Delta x_j \quad (20),$$

where C_j = anthropogenic solute concentration at node j ; θ_j = volumetric water content at node j ; Δx_j = length of profile interval controlled by node j . This was then normalized to the average solute mass over all output times to yield a percent error. Note that these calculations of solute mass and mass balance are only relevant after all of the solute mass has entered the system. The mass balance error by this method, for times after all of the solute mass has been added, was no more than 2% within the simulations. The increase in mass balance error shown by this method over the method used within HYDRUS might be explained by the fact that HYDRUS uses an integrated finite element approach

to calculate solute mass that takes solute gradient between nodes into account [Simunek et al., 1998], while my method, Eq. (20), does not use that gradient information.

Preliminary Simulations

Two preliminary simulations were created and the results were compared to the solute distributions in the real profile. The purpose of these simulations was to impose “typical” values on the unknown transport parameters on the conceptual model described above, and determine whether the present-day real anthropogenic solute positions could be recreated. These simulations used the full 20 m profile shown in Figure 6. Because unsaturated flow characteristics have not been assessed for the soils at the site, typical values of soil properties for the known soil textures were generated with the Rosetta neural network algorithm [Schaap, 1999]. The soil properties used in these simulations are provided in Table 5. The boundary and initial conditions for these simulations are described in broad outline within the Conceptual Model and HYDRUS-1D Code sections of this chapter; more detailed information on these conditions follows.

One major difference between these two simulations was in the parameters that affect top boundary “wetness”, including the amount of precipitation that occurs, and the soil-plant-atmosphere system’s ability to remove water from the system. The simulation with less precipitation and more potential evapotranspiration was dubbed the “dry scenario”, while the simulation with more precipitation and less potential

Table 5. Stratigraphic parameters used in preliminary simulations. θ_r , θ_s , α , n , K_{sat} , are van Genuchten model parameters.

Stratum	Depth	θ_r	θ_s	α	n	K_{sat}	Dispersivity
	cm				(cm H ₂ O) ⁻¹	(cm day ⁻¹)	(cm)
Loamy Sand	0-15	0.0485	0.3904	0.0347	1.7466	105.12	10
Sandy Loam	15-120	0.0387	0.387	0.0267	1.4484	38.25	10
Clay	120-800; 1000-1800	0.0982	0.4588	0.015	1.2529	14.75	10
Sandy Clay Loam	800-1000	0.0633	0.3837	0.0211	1.3298	13.19	10
Confining Layer *	1800-2000	0.09	0.11**	0.015	1.2529	1.48×10 ⁻⁴	10

* Confining layer is thought to be either indurated unweathered marine clay or silty shale

** In the preliminary simulations, θ_s was set low so that simulated water contents, which would be near saturation, would reflect observed water contents (Figure 3).

evapotranspiration was dubbed the “wet scenario”. The dry scenario had: (1) precipitation from the Bingham station in the relatively dry years 1954-1975, a twenty-two year repeating cycle with mean annual precipitation = 23.6 cm (3.6 cm below average); (2) a one year mean daily evapotranspiration cycle from the Leyendecker station, without modification; (3) a plant wilting point of -30000 cm H_2O ; and, (4) surface ponding was not allowed, i.e., surface potentials were never allowed to be greater than zero as if all excess water became surface run-off. The wet scenario had: (1) precipitation from the Bingham station in the relatively wet years 1983-1999, a sixteen year cycle with mean annual precipitation = 34.4 cm (7.2 cm above average); (2) a one year mean daily evapotranspiration cycle from the Leyendecker station, reduced by 25% on all days, and further reduced an additional 50% on days with precipitation, to account for the reduced atmospheric demand on rainy days; (3) a plant wilting point of -15000 cm H_2O ; and, (4) surface ponding was allowed if sufficient rain were to fall within a simulation, i.e., surface potentials were allowed to be greater than zero as if no run-off at the surface occurred.

The wilting points used ($-15,000$ cm H_2O for the wet scenario, $-30,000$ cm H_2O for the dry scenario) were somewhat arbitrarily chosen. Literature values have not been found for the wilting point of the dominant plant species at the pueblo site, *Artemisia filifolia* (sand sage). The HYDRUS model automatically assigns $-15,000$ cm H_2O as a default; this appears to be near the middle of the range of wilting points that HYDRUS has stored in a database of food crop data. Very low matric potentials ($<-100,000$ cm H_2O) have been noted in the near-subsurface in previous arid-zone research with other plant species [Scanlon et al., 1991]. However, assigning a wilting point of $-100,000$ cm

H₂O caused HYDRUS to crash in some circumstances. Sand sage is almost always found in areas with more available water than the more ubiquitous creosote (*Larrea tridentata*) or mesquite (*Prosopis glandulosa*) of south-central New Mexico [Atwood, 1983], so one may expect that appropriate wilting point values should not be extremely low. It was decided that doubling the default wilting point in HYDRUS would have to suffice for the dry scenario, hence the value $-30,000$ cm H₂O. Fortunately, it turns out that the wilting point chosen has little impact on the model outcome, as will be shown in the results of the sensitivity analysis (see Sensitivity Analysis in Results and Discussion, below).

The lower boundary condition needed to be constant positive pressure in the range found downhole (200-1300 cm H₂O) in the confined aquifer at the site, and located at 2000 cm bgs as per Figure 6. It was decided that the simulation confining potential should reflect the confining potential at the monitoring well (920 cm H₂O) because this was measured more accurately than other water level measurements. In hindsight, it would have been more meaningful to use the pressure head in borehole 71 within the midden (1090 cm H₂O), since this is the location from which the modeled soil profile (Figure 6) is derived.

This discrepancy should not be a serious factor in the model outcomes, because the unknown conductivity of the confining layer is a much larger source of uncertainty than the confining pressure used. For example, Freeze and Cherry [1979] give a range of saturated hydraulic conductivities of $\sim 9 \times 10^{-7}$ to $\sim 9 \times 10^{-3}$ cm day⁻¹ for shale, and $\sim 9 \times 10^{-6}$ to $\sim 3 \times 10^{-3}$ cm day⁻¹ for unweathered marine clay (the confining layer was thought to be best represented by one of those two lithosomes). I will show that use of different values

in this range for hydraulic conductivity of the confining layer makes the difference between a saturated condition above the confining layer, and no saturation, using the bottom confining head of 920 cm (see Results and Discussion). Presumably, I could set the bottom boundary head of the confining layer to 1090 cm while decreasing the conductivity of the confining layer, and simulate approximately the same heads and concentrations with the larger bottom boundary head as were simulated with the smaller head. The upward flux resulting from the positive pressure head had little impact on the principal goal of the simulation exercise, which was to see whether the present-day anthropogenic solute positions could be simulated.

One other difference between the wet and dry scenarios was that the initial condition of the solute profile was not zero everywhere in the wet scenario. Instead, a solute peak—meant to represent the environmental solute bulges at 350-500 cm bgs in the real solute profiles (Figure 3, and Quemada, 1995)—was started at 400 cm depth. This addition was not anticipated to affect the transport of the solute coming in at the top boundary, as will be discussed in the Results and Discussion section.

The results of the dry and wet scenario simulations were compared to the actual positions of the solute pulses.

A third preliminary simulation was created to help investigate the assumption that no saturation occurs above the confining layer at 1800 cm depth. This simulation was identical to the dry scenario described above, except that the saturated hydraulic conductivity of the confining layer was set to 9×10^{-7} cm day⁻¹, about 150× smaller than in the wet and dry scenarios. According to Freeze and Cherry [1979], p.29, this lower K_{sat} is in the range for an unweathered marine clay or shale, but is at the lower end of the

spectrum for either material. This simulation was named the “low K_{sat} scenario”, to distinguish it from the dry and wet scenarios in the Results and Discussion, below.

Sensitivity Analysis

After these initial simulations were run, additional simulations were created to see how sensitive the model was to uncertainties in those model inputs that affect the solute transport from the top boundary. This sensitivity analysis took the form of a 2^k *factorial design*, wherein each of the uncertain parameters is assigned a “high” and a “low” variant [e.g., Law and Kelton, 1999]. Ideally, the difference between these variants is to be of the order of the uncertainty of the individual parameter. It should be noted that the high and low variants chosen for parameters such as wilting point and unsaturated soil conductivity were necessarily somewhat arbitrary; such parameters exist in ranges without readily definable limits. A full 2^k factorial design requires 2^k simulations (k = number of uncertain parameters), one for each combination of uncertain parameters. In this case, because many parameters are unknown, some of them were lumped into groups. Our four parameters and groups of parameters chosen for sensitivity analysis were: (1) the precipitation, and potential evapotranspiration (together as a parameter group that was called the “top boundary condition”), (2) the hydraulic properties (K_{sat} , θ_s , θ_r , n , α) of the sandy loam and loamy sand at the top of the column (taken together), (3) the rooting depth of the plants on site, and (4) the wilting point of the plants on site. Thus, the full factorial design requires $2^4 = 16$ simulations. The simulations are termed

design points in the mathematical literature, and I have used this term to refer to particular simulations within the sensitivity analysis. Table 6 shows the simulation schedule for this sensitivity analysis.

An appropriate model response must be chosen to apply this sensitivity analysis. In our case, since transport of the anthropogenic solute is our primary concern, the distance that the simulated solute traveled from the source in a given time seemed most appropriate. Sensitivities were calculated on the basis of concentration peak depths after 88 years of transport. This time was used for two reasons: (1) previous experience in the preliminary simulations showed that solute movement after this time was slow enough that several hundred years' more simulation would typically cause no more than ~5 cm additional movement; (2) using 88 years, instead of some other number, made simpler the set-up of the top boundary condition input file for HYDRUS.

Once the 16 simulations were run, the sensitivity of the model to each of these parameters was then calculated as the average change in the model response (final solute plume depth after 88 years of simulation, in our case) as the parameter was changed from its high variant to its low variant, for all pairs of simulations in which the other three parameters were constant. For example (refer to Table 6), the wilting point sensitivity,

s_w , is:

$$s_w = \frac{(R_{10} - R_1) + (R_2 - R_9) + (R_{12} - R_3) + (R_4 - R_{11}) + (R_{14} - R_5) + (R_6 - R_{13}) + (R_{16} - R_7) + (R_8 - R_{15})}{8} \quad (21a),$$

where R_i = model response (final solute plume depth) in simulation i . This can be

Table 6. Sensitivity analysis schedule, showing the design points (simulations) and the high/low status of the four parameter groups for each simulation. High variant is indicated by a +.

Design Point	Wilting Point*	Rooting Depth#	Top Boundary Condition†	Soil Hydraulic Properties‡
1	-	-	-	-
2	+	-	-	+
3	-	+	-	+
4	+	+	-	-
5	-	-	+	+
6	+	-	+	-
7	-	+	+	-
8	+	+	+	+
9	-	-	-	+
10	+	-	-	-
11	-	+	-	-
12	+	+	-	+
13	-	-	+	-
14	+	-	+	+
15	-	+	+	+
16	+	+	+	-

* Wilting point: + = -15000 cm H₂O; - = -30000 cm H₂O.

Rooting Depth: + = 300 cm; - = 100 cm.

† Top Boundary Condition: + = more precip, less evapotranspiration; - = less precipitation, more evapotranspiration (see text for details).

‡ Soil Hydraulic Properties: + = van Genuchten parameters with higher saturated conductivity (loamy sand and sandy loam); - = van Genuchten parameters with lower saturated hydraulic conductivity (see text and Table 7 for details).

rearranged to yield a simpler form:

$$s_w = \frac{1}{8} \sum_{i=1}^{16} (-1)^i R_i \quad (21b).$$

In general, a simple equation using summation notation like Eq. (21b) will not always be possible, but long forms analogous to Eq. (21a) can always be written.

In this particular sensitivity analysis, because each model response, R_i , from each simulation i has dimensions of length [L], so do the sensitivities s_j (j = sensitive parameter group, e.g., soil hydraulic properties). Thus, the sensitivity s_j has a physical meaning: it is the average difference between the solute position at the end of simulations that used the high input variant of j , and the solute position at the end of simulations that used the low input variant of j . So this sensitivity, having the same units as the model response, may be compared directly to the overall responses of the model, and to the model sensitivity to other parameters.

For this factorial design type of sensitivity analysis, it is not important to know how a model responds to a particular parameter beforehand. If the modeler chooses the variants such that the model response is high when the low parameter variant is used (and vice versa), then the resulting s_j will be negative, but the magnitude of the sensitivity will not change. The following paragraphs describe the variants chosen for the four parameter groups.

The high and low variants for the top boundary condition were the same as used for the two preliminary simulations described above (“wet scenario” and “dry scenario”), except that plant wilting point was treated as a separate parameter. Thus, the high (wetter) variant included: (1) precipitation from the Bingham station in the relatively wet years 1983-1999, a sixteen year cycle with mean annual precipitation = 34.4 cm (7.2 cm

above average); (2) mean daily evapotranspiration from the Leyendecker station, reduced by 25% on all days, and further reduced an additional 50% on days with precipitation, to account for the reduced atmospheric demand on rainy days; and, (3) surface ponding was allowed if sufficient rain fell within a simulation, i.e., surface potentials were allowed to be greater than zero as if no run-off at the surface occurred. The low (drier) variant of the top boundary condition included: (1) precipitation from the Bingham station in the relatively dry years 1954-1975, a twenty-two year cycle with mean annual precipitation = 23.6 cm (3.6 cm below average); (2) mean daily evapotranspiration from the Leyendecker station, without modification; (3) surface ponding was not allowed, i.e., surface potentials were never allowed to be greater than zero as if all excess water became surface run-off.

The high and low variants for the soil hydraulic properties were chosen from available electronic databases, because the actual hydraulic properties of the soils were unknown. It was suspected that the saturated hydraulic conductivities of the loamy sand and sandy loam top layers were the most crucial members of the “soil hydraulic properties” group of parameters in the sensitivity analysis, because more water flow and solute transport should occur within the model when the soil was relatively wet, i.e., near saturated conditions. So, the high and low variants of the hydraulic properties were chosen based on the saturated hydraulic conductivities, K_{sat} , of the loamy sand and sandy loam. However, other van Genuchten parameters (α , n , θ_s , θ_r) were also different in the high and low variants of the hydraulic properties group, so all of these parameters contribute to the sensitivity study. Thus, these two variants that I am referring to as “high” and “low” are really but two realizations out of the infinite combinations of

parameters that could be put together. Table 7 below shows the hydraulic parameters that make up the high and low variants. The parameters that make up the high variant of soil hydraulic properties were chosen from the UNSODA unsaturated soil database managed by the National Risk Management Research Laboratory [Leij et al., 1999]. This database compiles raw data of θ vs. h that have been reported by various investigators, along with the saturated hydraulic conductivities. Three specimens each of loamy sand and sandy loam were found within UNSODA that had the same textures and structures as the loamy sand and sandy loam in the trench profiles (Appendix C). A single data set for each soil type was chosen based on which specimen had the highest K_{sat} . The water retention curve data ($\theta(h)$) for these high K_{sat} soils were each run through a non-linear inverse-squared routine (created in Microsoft[®] Excel[®]) to come up with the van Genuchten parameters that would be necessary to put into HYDRUS. The resulting van Genuchten parameters (along with K_{sat}) became the high variant of the unsaturated soil properties parameter group. It turned out that the K_{sat} 's used in the preliminary simulations were lower than the any of the K_{sat} 's found in UNSODA for the appropriate soil types. Thus, the van Genuchten parameters from the preliminary simulations were ultimately chosen to be the low variant for the unsaturated soil properties group.

As stated in the Previous Results section of the Introduction, the shrub sand sage <*Artemesia filifolia*> is the dominant plant species at the site. Rooting depths for sand sage have been reported by others [Weaver, 1919; Pockman, 2000] to be 300 cm or deeper. So the high (deeper) variant of rooting depth was chosen to be 300 cm. We found rooting depths between 70 and 150 cm in the trench soil profiles (Appendix C). Unfortunately, the HYDRUS model became numerically unstable when a rooting depth

Table 7. Stratigraphic parameters used in sensitivity analysis. θ_r , θ_s , α , n , K_{sat} are van Genuchten model parameters.

Variant (Realization)	Stratum	Depth	θ_r	θ_s	α	n	K_{sat}	Dispersivity
		cm				(cm H ₂ O) ⁻¹	(cm day ⁻¹)	(cm)
High*	Loamy Sand	0-15	0.0594	0.3982	0.0987	1.4663	558	10
	Sandy Loam	15-120	0.0469	0.4057	0.0278	1.6368	518	10
	Clay	120-600	0.0982	0.4588	0.015	1.2529	14.75	60
Low*	Loamy Sand	0-15	0.0485	0.3904	0.0347	1.7466	105.12	10
	Sandy Loam	15-120	0.0387	0.387	0.0267	1.4484	38.25	10
	Clay	120-600	0.0982	0.4588	0.015	1.2529	14.75	60

* The designations “high” and “low” have no meaning for most of the parameters, save for the K_{sat} ’s of loamy sand and sandy loam.

of 70 cm was used, so a rooting depth of 100 cm was used for the low sensitivity variant. Based on these records and observations, the high (deeper) variant of rooting depth was chosen to be 300 cm while the low (shallower) variant was chosen to be 100 cm deep. As stated before, I used a numerical approximation (Eq. 13) of the root density profile for sand sage shown in Weaver [1919].

The low variant of wilting point was set at $-30,000$ cm H_2O , while the high variant was set at $-15,000$ cm H_2O . These values were used for the same reasons cited above in the Preliminary Simulations section.

The $+920$ cm prescribed potential lower boundary at 20 m depth used in the preliminary simulations was replaced by a -2300 cm prescribed potential boundary at 6 m depth in the sensitivity analysis and subsequent simulations. This was done to reduce simulation time, and because the primary focus of this research has been on the anthropogenic solute transport. The potential -2300 cm was chosen for 600 cm depth because it was approximately the head found at this level with the first two simulations, which were near-steady at this level at the end of the simulations. Also, the flux that this new bottom boundary condition produced— 1.6 mm yr^{-1} —is twice the maximum upward flux calculated by the chloride mass balance (see Bottom Boundary, Upward Flow in Conceptual Model section, above), and thus is thought to serve as an upper bound on the impact of upward flow on the flow and transport process in the root zone. This upward flux is assumed to have had little impact on the modeling of the anthropogenic solute, in part because it represents only about 1-3% of the total water transpired over the long term in the various simulations, and did not penetrate more than ~ 10 cm into the root zone in the simulations (see Results and Discussion).

In all of the sensitivity design points, the initial condition for the solute was $C = 0$ for the entire profile, and the bottom boundary was a zero concentration boundary (type I). The initial condition for water was determined by (again) running the model without solute until an equilibrium condition was achieved below the zone of active precipitation flux and evapotranspirative uptake.

Temporal Scale of Solute Movement

The time scale of the solute movement within the HYDRUS model was investigated. The 8th design point of the sensitivity analysis was chosen for this study, because it was one of those that succeeded in moving the solute to the target zone that was inferred from the field data (see Results and Discussion, below). Output from a portion of the 8th design point of the sensitivity analysis, that indicated a downward solute movement event had taken place, was re-examined at different time scales. The data were analyzed first on an annual basis, next on a monthly basis, and finally on a daily basis, to see which of these scales the downward movement best corresponds to. This solute movement event was taken from late in the simulation. A second (earlier) downward movement event from the same simulation was examined for the same range in time scales, in the same way.

This work required “new” simulations only in the sense that the infiltration events needed to be identified in finer temporal scales than was used in the sensitivity analysis. In the sensitivity analysis, the time scale of output was one set of solute and water

profiles every 7.3 years; this frequency gave twelve output profiles for each 88-year simulation (design point). In this temporal scale study, design point 8 was re-run with annual output, so that infiltration events could be identified at that scale. Once the infiltration event was identified at the annual scale, a second simulation would begin at the beginning of the recharge event, and report monthly output, and so on until the temporal scale of the recharge event was identified.

Infiltration events were considered to occur when the solute center of mass position moved significantly. The solute center of mass is a finer measure of transport within the model than is solute peak position. This is because the solute peak position can only be determined to the nearest node position. For example, if the solute peak happened to occur where the profile was discretized to 3 cm per node, then the solute peak position can only be known within ± 3 cm. By contrast, the solute center of mass is by definition a weighted average of the solute position, and so has a continuous range.

III. RESULTS AND DISCUSSION

Unless otherwise noted, all of the plots in this section that feature HYDRUS output use the soil profile that has been assumed for the time of midden deposition. For comparison to present-day anthropogenic solute peak positions as in Figure 3, etc., one needs to increase the depths presented in these HYDRUS output plots by 90 cm.

Preliminary Simulations

The results of the initial two simulations (the “dry” and “wet” scenarios) are shown on Figure 10 for the top five meters of the profile. To avoid confusion, the wet scenario concentration profiles are shown without the environmental solute peak that was introduced at 400 cm bgs in the initial condition; this peak and its transport will be discussed below. Under the conditions simulated, the solute essentially came to a halt well before the 620 years of time since Native habitation has expired in both simulations. In the dry scenario, the solute peak stops at 70 cm bgs, while in the wet scenario, the solute peak stops at 100 cm bgs. Evidently the solute stops because downward water flux is reduced to nearly zero within the root zone; all of the available water is taken up by the plant roots and by the atmosphere, thus leaving none to transport the solute deeper into the profile. The movement of the center of mass of the anthropogenic solute in the dry

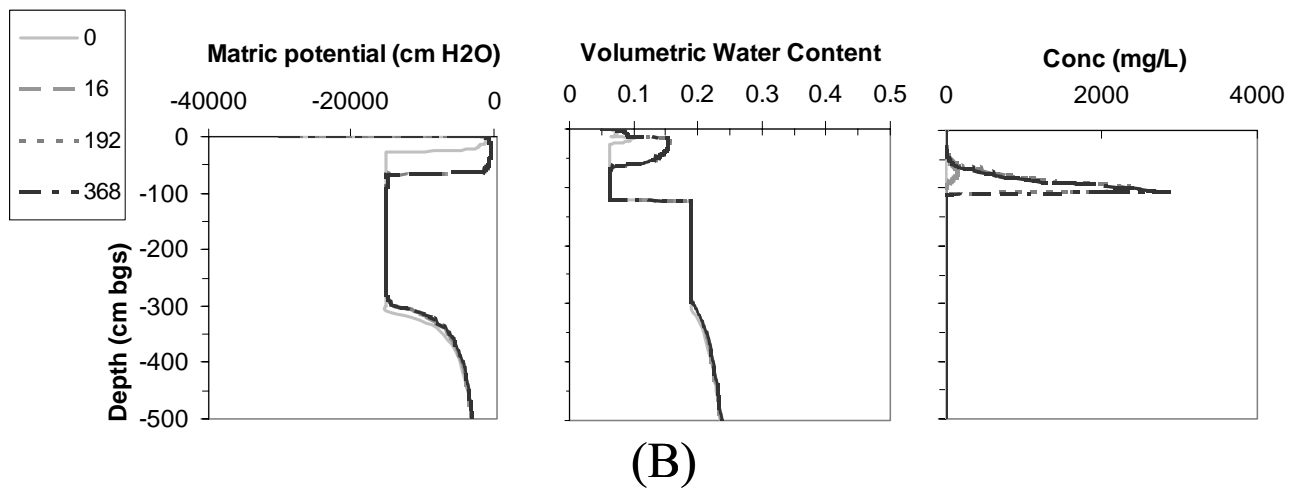
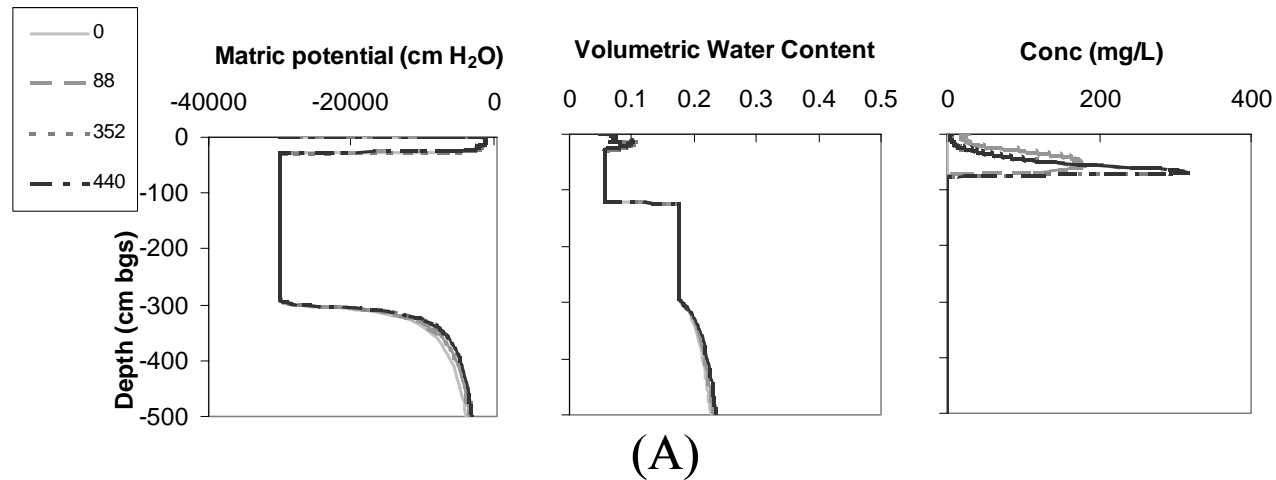


Figure 10. HYDRUS model results, with matric potential, water content, and concentration profiles from “wet” and “dry” scenarios (top 500 cm of overall 2000 cm profiles shown). (A) The dry scenario output. (B) The wet scenario output. On all plots, 0-15 cm is loamy sand, 15-120 cm is sandy loam, 120-500 cm is clay. Root zone is 0-300 cm.

scenario has slowed to less than 0.07 mm/yr at the end of 440 years of transport, and the movement of the solute center of mass in the wet scenario has slowed to less than 0.08 mm/yr at the end of 368 years of transport. These rates of travel would cause less than 1 cm of transport per century. With so little movement, the simulations were stopped, as they are somewhat expensive in terms of real computing time.

The field observed transport distance over the time since solute deposition was 180 ± 40 cm, reflecting the range of transport of the two anthropogenic signals from the zone of deposition to their present positions. As the reader can see from Figure 10, neither the simulated dry scenario with its more realistic precipitation record, nor the wet scenario with its highly optimistic precipitation record, caused the solute to travel this far. The depth of the solute peak in the dry scenario (Figure 10A) at 440 years is 68 cm, while the depth of the solute peak in the wet scenario (Figure 10B) at 368 years is 106 cm. At least three causes, alone or in combination, may be responsible for these simulated solutes falling short of the target range: (1) the model may not include all of the important solute transport processes (e.g., preferential flow or anion exclusion), (2) the assigned hydraulic properties of the simulated porous media may not be as conducive to movement as are the true hydraulic properties of the soils, (3) the actual wetness conditions that created the real current solute profiles were more extreme than those that were simulated. These possibilities are further explored in the sensitivity analysis.

Figure 11 repeats the results from the wet scenario, this time with the solute bulge that was started at 400 cm bgs. Recall that this plume was started here because that is the average solute peak position for the environmental Cl^- bulges shown in the real profiles (Figure 3 shows examples of Cl^- bulges from profiles 71 and 103). The reader can see

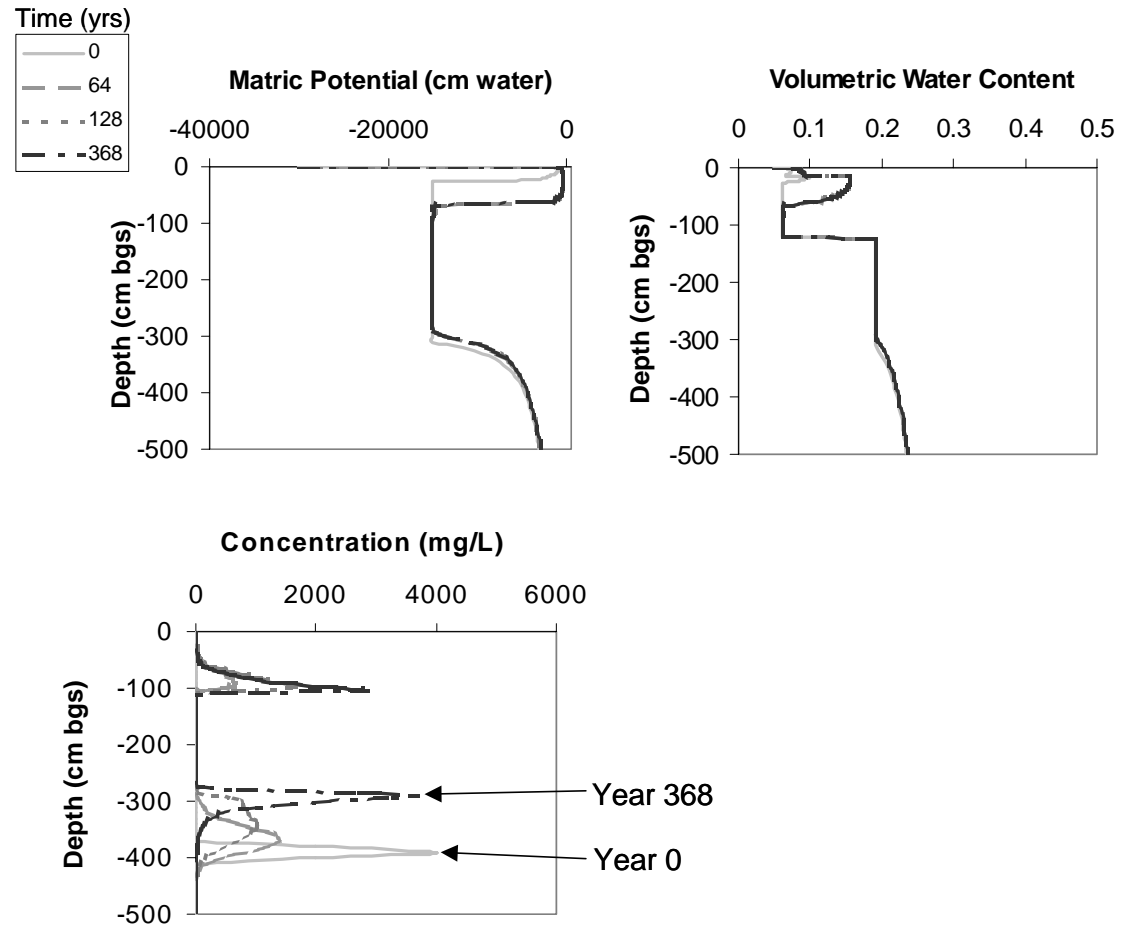
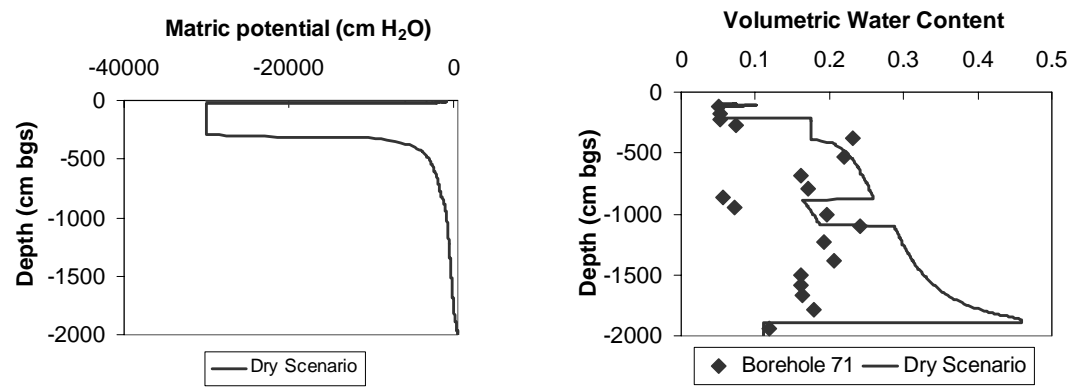


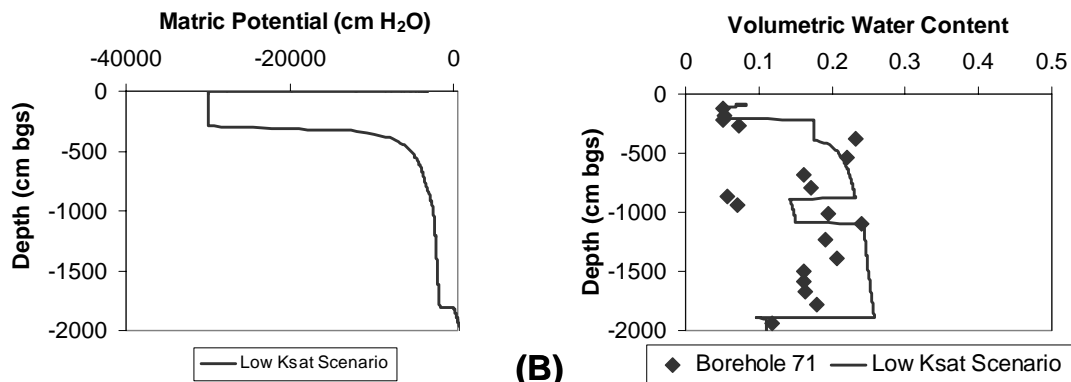
Figure 11. Repeat of wet scenario plots (Figure 10), with the simulated environmental solute peak included. Root zone 0-300 cm depth; loamy sand 0-15 cm depth; sandy loam 15-120 cm depth; clay 120-500 cm depth.

that the matric potential and volumetric water content plots on Figure 11 are the same as those shown for the wet scenario in Figure 10. The concentration plot on Figure 11 also has the same anthropogenic solute peak that is nearly stopped at 106 cm, but in this plot there is additional solute activity below. All of the solute peaks below 200 cm bgs on Figure 11 represent different stages in transport of the simulated environmental solute bulge begun at 400 cm bgs at time 0. The start position (Year 0) and final position (Year 368) of this bulge are indicated by the arrows. From its start position at 400 cm bgs, the solute travels upward with the discharge coming from the confined aquifer below. The solute is eventually pinned up against the bottom of the root zone, which is at 300 cm bgs, by the upward flow and the removal of water from the system by the plant roots. This suggests that the real environmental solute bulges may be likewise pinned against the bottom of the root zone of the sand sage at the pueblo site. In other words, the HYDRUS model predicts that the environmental solute bulge peak position, in reality approximately 400 cm bgs, could be an indicator of the rooting depth of the sand sage at the pueblo site.

Figure 12A shows the matric potential and water content plots for the entire profile, at time = 368 years, from the dry scenario. The 2000 cm plots for the wet scenario are the same as shown in Figure 12A below 300 cm depth (below the root zone), and are approximately in steady-state below the root zone as well. Steady-state for water may be defined as no changes in storage at any point within the flow domain. We know that the water simulated in the dry scenario at 368 years is nearly in steady state because the upward flux at every node in the HYDRUS model is nearly uniform, within 5% of 2.2×10^{-4} cm day⁻¹, or 0.8 mm yr⁻¹.



(A)



(B)

Figure 12. Complete matric potential and water content profiles from: (A) the dry scenario, and (B) the low K_{sat} scenario. Simulated water contents are 90 cm lower in profile than calculated, for direct comparison with known volumetric water contents from borehole 71. Rooting depth = 300 cm. Stratigraphy: loamy sand 0-15 cm; sandy loam 15-120 cm; clay 120-800 cm and 1000-1800 cm; sandy clay loam 800-1000 cm; confining layer 1800-2000 cm.

The points on the water content plot in Figure 12A are the observed volumetric water contents from boreholes 71. In general, water content is not a useful state variable for comparing simulation and reality because of its roughly exponential relationship with matric potential. Keeping this in mind, the dry scenario water content profile does a fair job of matching the actual water content in borehole 71, except in one important respect. In the simulated profile, there is ~25 cm of phreatic water ponding above the confining layer (above 1800 cm depth), which was not observed in any of the actual borehole profiles.

The third preliminary simulation, known as the “low K_{sat} scenario”, was created because the dry and wet scenarios failed to reproduce the unsaturated conditions throughout the clay above the confining layer. As was stated in the Methods section, this simulation used $K_{sat} = 9 \times 10^{-7}$ cm day⁻¹ for the confining layer, instead of the $K_{sat} = 1.5 \times 10^{-4}$ cm day⁻¹ used in the dry and wet scenarios. This simulation was otherwise identical to the dry scenario. Figure 12B shows the matric potential and water content results for the low K_{sat} scenario after 176 years of simulation. As the reader can see, the lower K_{sat} causes the entire positive pressure from below to be used up within the confining layer, so that no phreatic water stands above it. The upward flux in this case was 3×10^{-6} cm day⁻¹.

Therefore, the HYDRUS model can reproduce the unsaturated conditions found in the boreholes when a low but still reasonable K_{sat} is applied to the confining layer. However, this is not “proof” of any kind that there is no phreatic water at the site. It is important to note that saturated conditions could have existed in the real boreholes at the pueblo site, and simply escaped notice because insufficient time was allowed for water to

seep into the borehole from the surrounding clay. This possibility is largely irrelevant to the conceptual model or the solute transport, because the potential gradient from the confining layer to the root zone will drive the flow upward, whether or not the clay is entirely unsaturated above the confining layer. In other words, whether or not there actually is unconfined water to be found on the Midden Project site, has little bearing on the potential for upward flow. In either case, the simulations show that no recharge flow—downward flow below the root zone—is occurring.

A final note on Figure 12: Recall that the HYDRUS modeling was done using the profile presumed for the time of the midden deposition, and that a modern profile has accumulated an additional ~90 cm of colluvium on top compared to the time of midden deposition. The simulated water content plots in Figure 12 are set 90 cm lower in the profile than they were in the modeling, to enable direct comparison to the modern data from borehole 71. This adjustment does not make a dramatic difference in the fit of the data, except that water contents in the first 200-300 cm below ground surface match a little better.

Sensitivity Analysis

The raw results of the HYDRUS model sensitivity analysis are shown in Table 8. One discernible pattern in these raw data is that the solute peak has essentially halted within the root zone. Two exceptions to this pattern are design points 5 and 14, which will be discussed below. Profile plots of h , θ , and C from design points 1 and 8 are

Table 8. Results of the sensitivity simulations, showing the outcome of each of the design points in terms of the solute peak depth. Maximum rooting depth in the model is provided for comparison.

Design Point	Peak Depth at 88 yrs (cm)	Simulated Rooting Depth (cm)
1	50	100
2	90	100
3	106	300
4	66	300
5	118	100
6	88	100
7	95	300
8	151	300
9	86	100
10	56	100
11	64	300
12	109	300
13	80	100
14	98	100
15	142	300
16	100	300

shown on Figures 13 and 14; these are representative of the outcomes of the 14 sensitivity simulations in which the solute was halted. (Profile plots of h , θ , and C at various times, for all sensitivity simulations, are in Appendix B.) The halting of the solute peaks within the root zone indicates that the precipitation entering the model is in a quasi-steady state with the evapotranspirative processes that remove water from the system. This is the same qualitative result as was obtained in the preliminary simulations. Based on these results, the current model of the actual Cl:Br and NO_3^- signals is that they both still reside within the root zone of the sand sage. Thus, the modeling effort supports the notion that essentially no recharge is occurring at the Midden Project site, in that 14 of the 16 design points indicate that the anthropogenic solute is essentially stopped within the root zone.

The results from design point 5, which are essentially the same as from design point 14, are shown as Figure 15. In these simulations, unlike the others in the sensitivity analysis, a recharge process has evidently begun. This can be observed in the solute profile of Figure 15 (results of design point 5) by the bleeding of the solute below the bottom of the root zone. Thus, the solute would not be contained in the root zone if the sets of parameters used to create design points 5 and 14 are essentially correct. These design points have three of the four parameter groups in common: low variant of rooting depth, high variant of top boundary condition, and high variant of hydraulic conductivity.

I assert that the recharge scenario suggested by design points 5 and 14 suggest is unlikely to reflect reality. As was discussed in the Introduction of this thesis, there are several lines of evidence that point to upward flow from the confined aquifer; this evidence also discredits the notion of groundwater recharge. For example, I previously

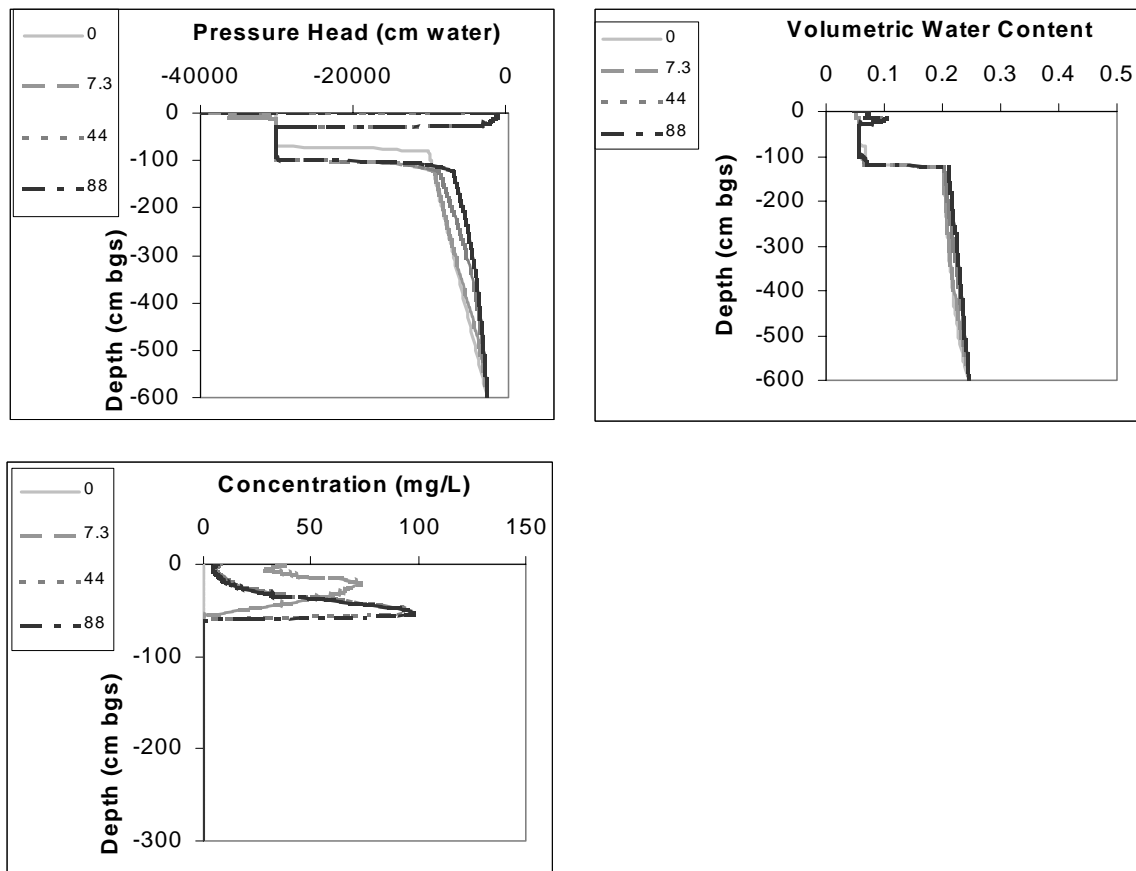


Figure 13. Pressure head, water content and concentration profile results from the sensitivity analysis, design point 1. Stratigraphy: sandy loam 0-15 cm; loamy sand 15-120 cm; clay 120-600 cm. Legend entries are time in years.

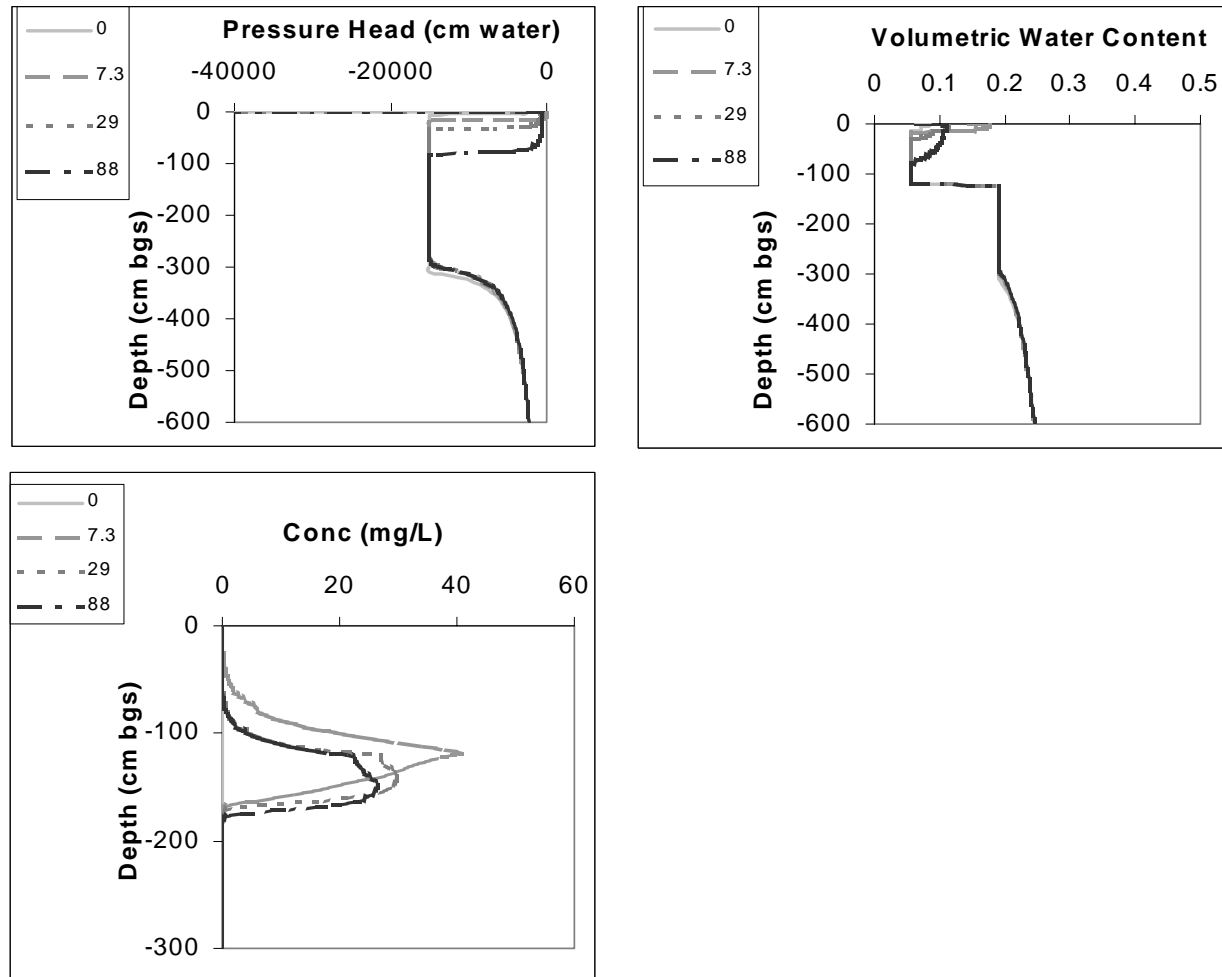


Figure 14. Pressure head, water content and concentration profile results from the sensitivity analysis, design point 8. Stratigraphy: sandy loam 0-15 cm; loamy sand 15-120 cm; clay 120-600 cm.

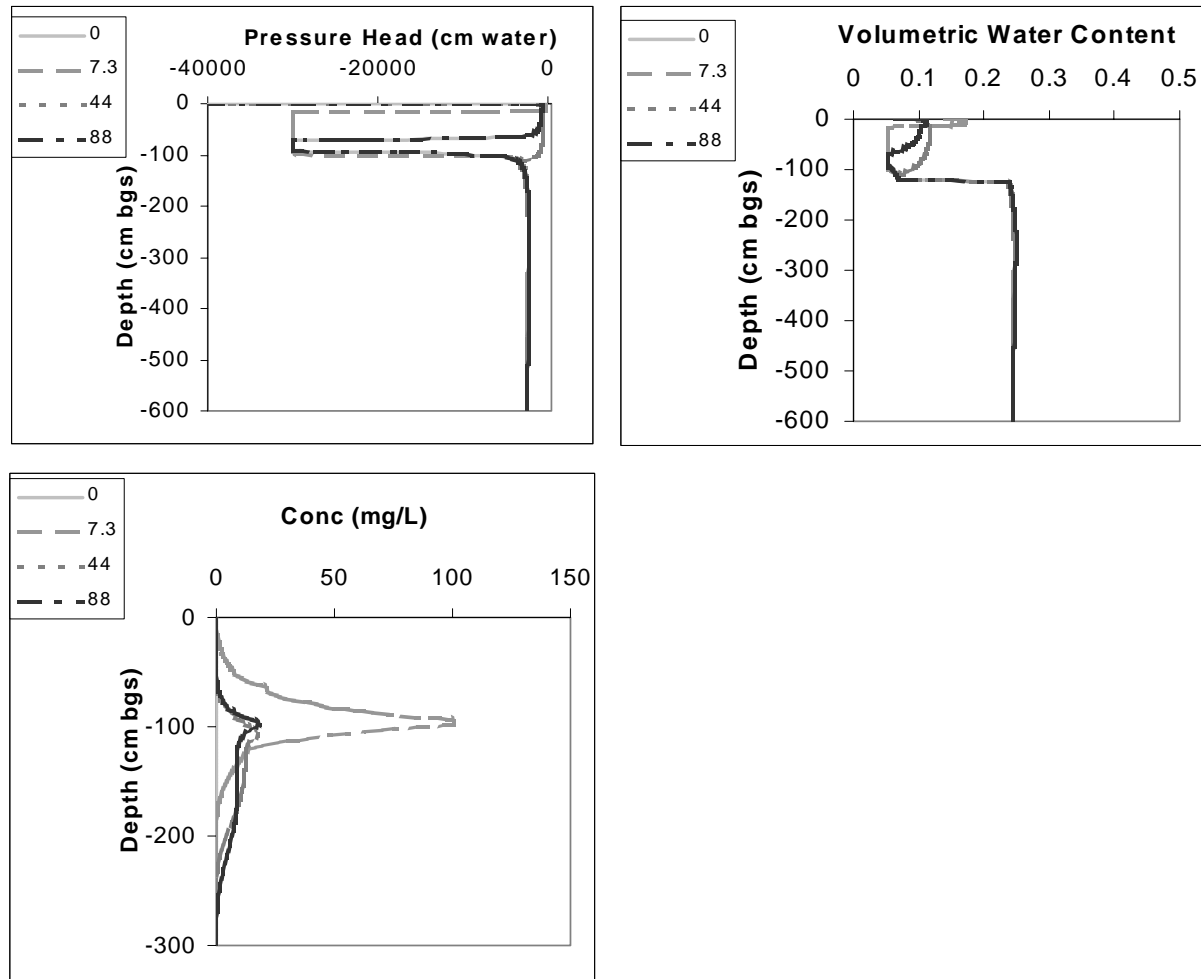


Figure 15. Pressure head, water content and concentration profile results from the sensitivity analysis, design point 5. Stratigraphy: sandy loam 0-15 cm; loamy sand 15-120 cm; clay 120-600 cm.

noted that the chloride inventories at the pueblo site are larger, on average, than those typically found in the desert southwest. If recharge were occurring, the pronounced Cl^- bulges in the real profiles (with peaks at approximately 400 cm bgs, see Figure 3) would tend to be non-existent or smaller than normal, rather than excessive. The environmental chloride would be washed through the profile to the top of the confining layer or laterally out of the region by the recharge flux. So, while the solute peak data from these two simulations were used to calculate the model sensitivities, the qualitative result that a recharge process occurs, as indicated by these two simulations, will not be further discussed.

The simulated solute reached the target range of 180 ± 40 cm in two of the sixteen simulations, design points 8 and 15, where the solute peak positions after 88 years were 151 cm and 142 cm, respectively. This places the modeled solute approximately concurrent with the real Cl:Br peak which is at 140 cm (average) below the mean plane of midden deposition. Note that these two design points also have three of the four parameter groups of the sensitivity analysis in common (Table 6). They both had the high variants of rooting depth, top boundary condition, and soil hydraulic parameters. Because it is possible to get the simulated solute within the target range in these simulations, I assert that the conceptual model outlined in the Conceptual Model and Methods chapter is adequate to explain the present-day positions of the anthropogenic solutes. It is therefore possible to calibrate the HYDRUS model with the known data from the Midden Project. The HYDRUS model predicts that the true soil hydraulic parameters are similar to the “high” variant of soil hydraulic parameters, particularly with respect to the higher saturated conductivities, and that the root zone . Thus, one of the

major objectives of this modeling work that was outlined in the Introduction has been accomplished (see Hypothesis of This Thesis section of the Introduction). This success must be qualified, however, because the position of the deeper NO_3^- peak (220 cm below the mean plane of midden deposition) has not been simulated. It is not known at this time whether reasonable soil hydraulic parameters could be found that would cause the simulated solute to reach this depth.

Using equations (21) for wilting point sensitivity and the analogous equations for the other three parameter groups, the raw data in Table 8 was converted into sensitivities. These are shown in Table 9. The parameters that affect the solute transport the most are the soil hydraulic parameters and the group of parameters known as the top boundary conditions (precipitation, potential ET, and whether surface ponding is allowed). Compared to these two, the maximum rooting depth has an intermediate effect, while the maximum wilting point assigned appears to have little effect on the model outcome. This last result is a positive one for the future of modeling similar problems in the unsaturated zone, because the wilting point of a plant turns out to be difficult to measure, and tends to have an ambiguous meaning once it is measured [Hillel, 1998, page 621]. The other three sensitivity parameters can be measured with some reasonable degree of accuracy in either field or laboratory. Thus, another of the objectives of this thesis has been completed, in that the parameters which control water movement and solute transport have been ranked in terms of their relative importance.

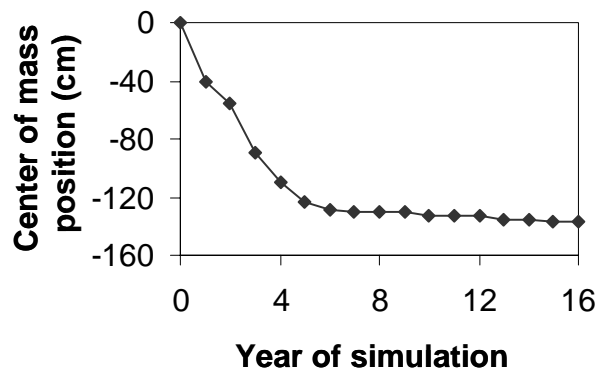
Table 9. The HYDRUS model sensitivities to the four parameter groups used in the analysis, by peak depth.

Parameter Group	Peak depth sensitivity
	cm
Wilting point	2
Maximum rooting depth	21
Top boundary conditions	31
Soil hydraulic properties	38

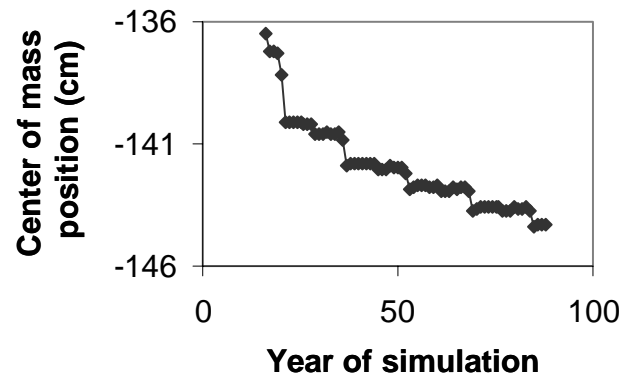
Temporal Scale of Solute Movement

Figure 16 shows the time series of the solute center of mass movement from design point 8 from the sensitivity analysis, broken into the first sixteen years (Fig. 16(A)), and the remaining 72 years (Fig 16(B)). The reader can see that the majority (over 80%) of the movement has already occurred by year six. Recall that 90 cm of sediment have accumulated at the midden since the time of midden deposition, and that one of the assumptions in the modeling is that this accretion essentially occurs after the solute transport has taken place (as discussed in the HYDRUS-1D Code section of the Methods). The fact that most of the solute transport occurs very early on in design point 8 supports this assumption. Moreover, inspection of the previously-discussed modeling results (Figures 10-11, 13-15) reveals that the majority of solute transport in all of these cases takes place early on in the simulations. So it would appear that this assumption that solute transport occurs prior to significant sediment accretion was reasonable, based on the model results.

In the later years of design point 8 the solute position is quite stable except that, once every sixteen years, a little downward movement takes place (Fig. 16(B)). It is important to note that this 16-year periodicity is a completely artificial pattern of solute movement, brought about by the use of repeating 16-year record of precipitation. This does not detract from the usefulness of looking at this downward movement event at temporal scales finer than 16 years, as is discussed here. Figure 17 shows 16 years of



(A)



(B)

Figure 16. Year-by-year simulated solute center of mass position for design point 8 of the sensitivity analysis. (A) The first sixteen years of simulation. (B) Years 17-88 of the simulation.

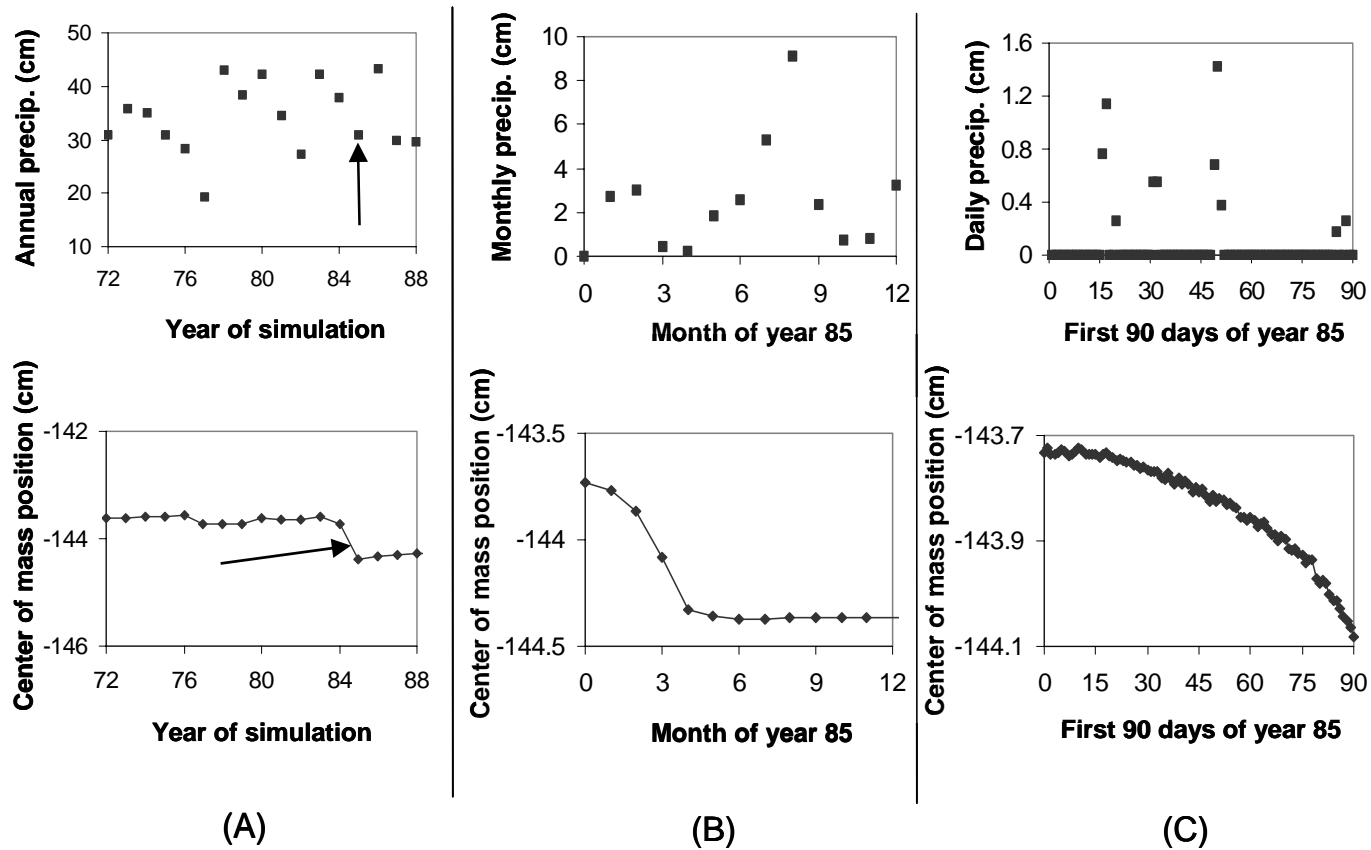


Figure 17. Precipitation and HYDRUS model solute center of mass at three levels of resolution in time, after 72 years of simulation in design point 8 of the sensitivity analysis. (A) 16 years covering the entire wet scenario cycle of precipitation. The arrow in the upper plot points to the total precipitation that occurs during the transport pointed at in the lower plot. (B) Monthly precipitation and center of mass position during year 85 of the simulation. (C) The first 90 days in the 85th year of the simulation.

output from the 8th design point, starting at the beginning of year 73. Panel A of the figure shows the total annual precipitation going into the model, along with the response of the anthropogenic solute center of mass, for the entire sixteen year cycle of the wet scenario (years 73 to 88 of transport). At year 85 there is a sudden drop in the solute center of mass, indicating that a transport event has occurred. Note that the total precipitation in year 85, 32.4 cm, was below the average of the wet scenario series, 34.4 cm. Thus downward flux is not well-correlated to annual precipitation for this flux event. Figure 17(B) focuses on the monthly center of mass output of year 85. These plots show that the downward flux is a response to wetting that takes place in the early months of the year (or perhaps the last months of the previous year), when transpiration is shut down for the winter, and the potential evaporation is low. There is no visible correlation between the high precipitation months of the monsoon season (July through September) and the time of relatively rapid downward flux. Figure 17(C) focuses on daily center of mass positions for January through March of year 85. These plots show that no apparent correlation exists between a given precipitation event, and the actual solute movement. Instead, the solute position appears to be more or less steady for the first ~20 days of the simulation, then begins an accelerating descent which slows down greatly by May. Of course, the total travel distance for the solute (measured by its center of mass) is only ~0.5 cm during this time. There is no simple correlation between solute movement and the amount of precipitation occurring during the winter months. The total precipitation during the winter months (Nov.-Mar.) of the year that transport occurs is 12.3 cm, which is the third highest winter precipitation of the sixteen years of the wet scenario. Significant solute movement does not occur in the two years with higher winter

precipitation. The maximum single-day precipitation event in the winter in which solute movement does occur is 1.3 cm, which is eclipsed at least 5 times in the winter months of the sixteen year record. Thus, according to the model, the total precipitation in winter would appear to be a moderate factor in moving the solute downwards, but a larger factor is the low evaporative demand and non-existent transpiration during these months. Despite the above analysis, individual storms could still be driving the downward flux. It may be that one of the January storms in year 85, for example, happens to occur on a day with an exceptionally low potential for evaporation, and this combination of modestly high precipitation and low evaporation leaves some water for downward percolation and thus transport of the solute.

Another solute movement event, in year 13 of the 8th design point simulation, was also investigated, and it showed all of the same trends noted above. This is not the same infiltration event that is seen repeating in a 16-year period later on in the simulation, because the precipitation year is different (in this case, the precipitation is from 1995, whereas the precipitation for year 85 of the simulation is from 1987). Figure 18 shows the result. As the reader can see on Figure 18(A), year 13 had very little total precipitation, 19 cm, and produced a very modest change solute center of mass position relative to the overall transport. But the change in solute position that did occur followed the same pattern found in year 85. The transport occurs in the winter and early spring (Fig. 18(B)), even though the majority of the precipitation occurs in summer. And the solute center of mass shows no obvious response to individual storms (Fig. 18(C)). Thus, the same pattern appears to occur for different recharge events within the model.

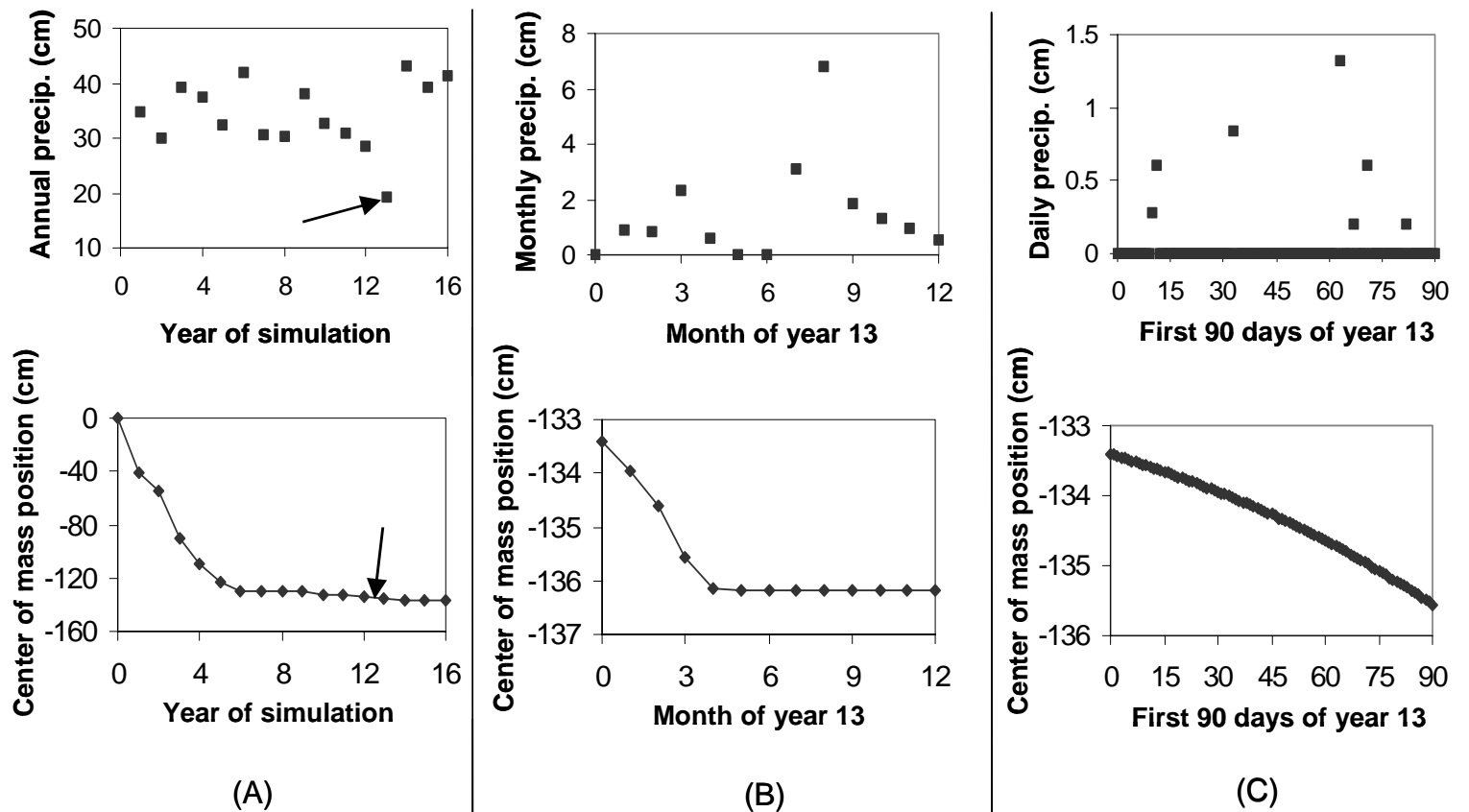


Figure 18. Precipitation and HYDRUS model solute center of mass at three levels of resolution in time, from the beginning 8th design point simulation of the sensitivity analysis. (A) 16 years covering the entire wet scenario of precipitation. The arrow in the upper plot points to the total precipitation that occurs during the transport that is pointed to in the lower plot. (B) Monthly precipitation and center of mass position during year 13 of the simulation. (C) The first 90 days of year 13 of the simulation.

An attempt was made to resolve whether downward solute movement events occur primarily due to antecedent moisture conditions (accumulation of infiltrating water from many storms) in the region near the solute peak, or due to individual storm events. If, after a precipitation event, the water content plots show that the resulting water pulse travels from the surface to 130 cm depth—where the anthropogenic solute bulge begins to arise within the profile—then it can be reasonably assumed that the anthropogenic solute moved primarily due to an individual storm. On the other hand, if the water pulse is completely attenuated and causes little or no increase in the water content at 130 cm depth, we can assume that accumulation of antecedent moisture is the primary cause of the downward transport. To pursue this issue, water contents within the model were plotted versus time at 0.1 cm, 1 cm, 10 cm, 50cm, 100 cm, and 130 cm depth, for the first 90 days of year 85 (i.e., January through March) of the design point 8 simulation. Recall that this is the time frame featured in Figure 17(C). Figure 19 below shows the resulting water content plots.

In the top plot of Figure 19 (1 mm bgs) the reader can see two major precipitation events occur over the 90 day period, one at ~20 days, and the other at ~50 days. At 10 cm depth (second-to-top plot in Figure 19), the two precipitation events have obviously attenuated somewhat in their impact, but are still clearly visible above the background. At 50 cm depth, the first precipitation event at ~20 days has become a step function, meaning that the increase in water content is beginning to be taken into storage, and less is being transmitted to deeper in the soil. The second water spike at 50 cm depth is still being transmitted, although the long tail after the spike indicated on the plot from day

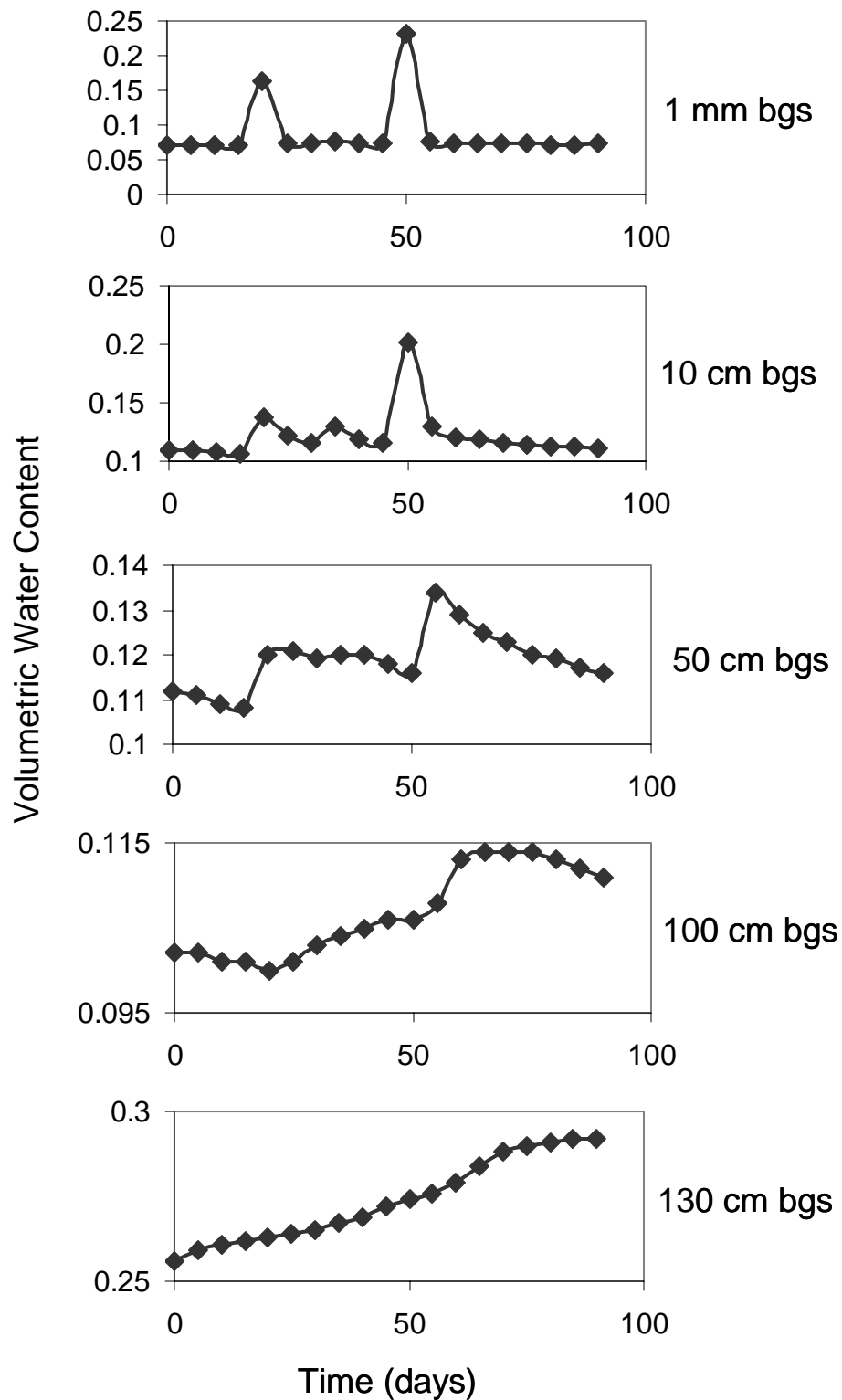


Figure 19. Volumetric water content through time, for the first 90 days in year 85 of the design point 8 simulation, for several depths below ground surface. Points are at 5-day intervals.

~55 to day 90 indicates that the water is moving more slowly at this level. At the 100 cm bgs level, both the first and second precipitation events markedly increase the water content, and both result in increases in storage which are mainly kept through day 90. Finally, at 130 cm bgs, the first precipitation event appears to be almost entirely subsumed into a general trend of increasing moisture that begins well before day 20 when this precipitation event occurred. However, the second, larger precipitation event at day 50 causes a more notable increase in the rate of water accumulation at this level. But no individual storm has caused the significant increases in water content at 130 cm bgs, from $\theta=0.26$ to $\theta=0.29$, by itself. Instead, water of several storms have added together create the wetter conditions necessary for downward solute movement. So, the third objective of this thesis that was identified in the Introduction—that of finding the time scale of downward solute movement events—has also been achieved. According to the model, solute movement events occur during wet seasons, due to accumulation of water storage from several intense precipitation events. Of course, this does not mean that a truly rare single event, like a 500-year storm, could not move the solute plume downward on its own.

Based on all of the above modeling efforts, an inference can be made about the final fate of the anthropogenic solutes. As was noted before, the HYDRUS model predicts that the Cl:Br ratio peak and the NO_3^- peak are essentially frozen in place, pending some large infiltration event to push them deeper into the profile. I infer that the anthropogenic peaks will remain in this situation while spreading slowly through diffusion, until a low frequency infiltration event takes place that is large enough to push them through the root zone. This large infiltration event may be either an accumulation

of smaller storms, or the melt from a large snow pack, a flood, or perhaps a more average precipitation event occurring after a fire has swept through and drastically decreased transpiration. Once this event occurs, though, the anthropogenic solutes will be merged with the environmental solute bulges. Unless the deeper infiltration is prolonged (Phillips [1994] has suggested this would occur during an ice age), the downward moving water pulse that is carrying the solute will diffuse and, under the influence of the prevailing upward gradient will eventually carry the anthropogenic solutes back up to the bottom of the root zone. The anthropogenic Cl^- and Br^- will then be indistinguishable from the environmental solutes, and all of the solutes will remain in this zone until another such intense low frequency infiltration event occurs.

IV. OTHER CONSIDERATIONS

In order to account for all the potentially important physical processes that may have taken place during the anthropogenic solute transport interval, the most complete software code for our purposes would have to include multi-dimensional non-isothermal liquid and vapor flow, water uptake by distributed roots in the near sub-surface, time-varying boundary conditions and root zone uptake, osmotic potential, anion exclusion, and accretion of sediment at the top surface. To date, there are few, if any, codes that take all of these processes into account and, in any case, the data set that was generated in the field and laboratory phases of this project is simply inadequate to constrain such a complex model. Below I discuss some of the potentially important processes that were ignored in the HYRDUS simulations discussed in the preceding sections of this thesis and the ways in which they may affect the modeling results.

Differing positions of Cl:Br and NO₃⁻

As stated in the Introduction, the Cl:Br ratio is 140±30 cm below the average plane of midden deposition, while the NO₃⁻ peak is 220±40 cm below the average plane of midden deposition. The reason for the difference in position of the Cl:Br and NO₃⁻

peaks is not known. One would expect that the nitrate would behave, if anything, less conservatively than the Cl^- or Br^- , as it is generally considered more reactive than the other species. It may be that the nitrate pulse was simply deposited prior to the Cl:Br. On the other hand, Wolff [1990] showed that the apparent advection of a ratio of solutes—an isotope ratio or our present Cl:Br ratio—is impacted by the dispersion of the denominator species. This effect is a mathematical artifact of applying the mass balance and flux models implicit in the advection dispersion equation on a *ratio* of species, and is completely independent of sorption, anion exclusion, or any processes which might cause the two species in the ratio to move differently. I have extended this work to unsaturated flow (see Appendix D), although the details do not concern us here. In the pueblo borehole profiles, the fact that the Cl:Br ratio signal lags behind the nitrate peak (Figure 6a) in the presence of a downward-increasing bromide concentration is consistent with this “dispersion-induced advection effect”, and preliminary calculations show that this effect cannot be ruled out as an explanation of the difference in apparent transport (see Appendix D). If this is true, then the nitrate signal is behaving more ideally than the Cl:Br ratio, and the modeling results should be compared to the nitrate signal alone. Recall that the “best” modeling results—the ones that indicated a successful calibration (design points 8 and 15 of the sensitivity analysis)—were able to match the Cl:Br solute positions, but that so far no simulations have put the solute deep enough to match the nitrate positions. Thus, if this dispersion-induced advection effect is truly the cause of the separation between the nitrate and Cl:Br peaks, then the model calibration effort could only be said to have come close in modeling the true solute positions. Additional simulations could be performed with higher K_{sat} 's for the loamy sand, sandy loam, and

clay layers for the site, to see if any reasonable soil hydraulic parameters can reproduce the nitrate plume.

Reverse Osmosis

From analyses of the water in the monitoring well, the concentration of Cl^- in the aquifer sandstone water was 410 mg L^{-1} , the Br^- concentration was 5.7 mg L^{-1} , and the NO_3^- concentration was 22 mg L^{-1} . If upward flow is present, then it would appear that ion filtering through reverse osmosis of the aquifer water is occurring, as the concentration found in the aquifer sandstone are larger than those found above the confining layer in almost all cases. Table 10 shows the average Cl^- concentration below the environmental solute bulge, and the Cl^- concentration in the soil samples taken just before confined water was reached. The reader can see that in most cases, the Cl^- concentrations in the unsaturated zone below the environmental bulge are less than the 410 mg L^{-1} found in the confined aquifer at the monitoring well. The main exceptions to this trend are just before confined water was reached at some locations, where some solute concentrations appear higher than those in the saturated zone. This may be due to ions being concentrated by reverse osmosis at the boundary, or may just be an artifact due to the air rotary drilling, which could have caused sufficient drying to cause a significant increase in the apparent pore water concentrations. The clay/mudstone at the site was composed mainly of a mixture of illite and smectite [Quemada, 1995]. Both of these clay minerals have high rates of isomorphous substitution for their structural cations and thus

Table 10. Average Cl⁻ concentrations below the environmental solute bulge, and the Cl⁻ concentrations just before confined water was reached. Chloride concentration in the confined aquifer water was 410 mg L⁻¹.

Borehole	Average Cl ⁻ concentration in unsaturated zone below environmental bulge mg L ⁻¹	Cl ⁻ concentration just before the confined aquifer was reached* mg L ⁻¹
71	190	190
72	290	**
103	260	420
106	120	150
107	320	590
118	300	**
123	530	1000

* The concentrations shown are for soil pore water found within 100 cm of reaching confined aquifer water.

** Confined water was not reached at boreholes 72 and 118.

significant electrical double layers, so it is not possible to rule out reverse osmosis on the basis of an electrically neutral porous medium. The Cl:Br ratios found from local bulk precipitation collectors ($63 \pm 14 \text{ g g}^{-1}$) [Quemada, 1995], within the unsaturated zone ($85 \pm 17 \text{ g g}^{-1}$), and within the aquifer (72 g g^{-1} , one set of measurements only) are all too close to be used to determine the origin of the unsaturated zone pore water. The nitrate concentrations, and associated Cl:NO₃ ratios, within the lower unsaturated zone cannot be compared to rain water and aquifer concentrations in any useful way, because nitrate concentrations vary greatly within the lower unsaturated zone [Quemada, 1995], so much so that comparison of these concentrations to potential sources is useless.

Laboratory experiments have shown that compacted clays act as osmotic membranes when they separate solutions of unequal ionic concentration [Marine and Fritz, 1981]. Graf [1982] showed that many brines of debated origin are probably created from entrapped sea water through reverse osmosis (forcing relatively clean water out) because an appropriate semi-permeable membrane material—such as shale—was surrounding the brine-laden formation, and sufficient hydraulic or overburden pressures to drive the dewatering process were present. One recent study showed that fluid pressures and solute concentrations in a shale formation are consistent with large (up to 200,000 cm H₂O) osmotic pressure anomalies [Neuzil, 2000]. Other researchers have shown that anion exclusion can be an important factor in unsaturated solute transport (e.g., Porro et al., [1993]). But direct evidence of reverse osmosis by sedimentary rocks in the unsaturated zone is scant, if it exists at all.

Instead of accepting the upward flux argument presented in the Introduction and Conceptual Model, one might suggest that preferential flow could be occurring, i.e., that

some precipitation is locally concentrated in the sandy soil in the top 1 to 6 meters, bypasses some part of the root zone via fractures other conduits, and hence supplies the mudstone beneath with water. This water would then either discharge off-site, or during dry conditions would be released upward to the root zone and hence to the atmosphere. Also, the osmotic potential difference across the confining layer could be assumed to balance the hydraulic pressure difference across the confining layer. This argument would neatly explain why the pore water below the environmental solute bulge has measured solute concentrations that are less than those found in the confined aquifer beneath. For this scenario to be consistent with the known facts, the osmotic potential gradient across the confining layer would have to be sufficient to balance the upward-driving forces of the pressure head in the sandstone and the upward-driving adhesive forces within the confining layer that would lead to matric suction. In any case, the downward flux model cannot explain why the chloride inventories at the site are on average so much larger than those in the rest of the American Southwest, or why there is a correlation between chloride mass and water content below the root zone (see Chloride Mass Balance, Revisited, and Upward Flow section of the Introduction).

Two-dimensional Stratigraphy

Unsaturated conditions prevailed at all drilling locations until confined water was encountered beneath the confining layer. In other words, there was no phreatic aquifer perched atop the confining layer. The elevation of the top surface of the confined aquifer

varied substantially considering the horizontal proximity of the boreholes (refer to Figures 2 and 5). Given the small ($\sim 1\text{m}^2$) sandstone outcrop to the West of the pueblo with strike that is almost due East, one would expect that material of the subsurface should have the same or similar characteristics. An inspection of the drill logs reveals that, at boreholes 71 and 72, an unsaturated sandy clay loam layer was encountered at about 8 to 10 meters depth that was absent from the other boreholes as an unsaturated body. Figure 20 shows the elevation that confined water was found versus the local east-west coordinate and local north-south coordinate that were used at the pueblo site. Ignoring (for the moment) the data point from borehole 71, the linear correlation of east-west coordinate and the elevation where water was encountered was quite good ($R^2=0.97$), while the correlation of north-south coordinate and the same elevation was poor ($R^2=0.23$). Presumably this means that the sandstone material that forms the aquifer is dipping, like the points on the graph (Figure 20), approximately due east at about eight degrees. This supports the eastward strike found at the outcrop, and gives us a basis for understanding the saturated hydrology of the subsurface. This sandstone body is most likely a lens within the Dockum mudstone, as is discussed in the geologic descriptions of the area [Quemada, 1995; Treadwell et al., 1995]. But what of the deeper water found at borehole 71 (and would almost certainly have been found at borehole 72 if drilling had continued for another meter or two)? There was a sandstone lens found at both boreholes 71 and 72 within a meter of the correct elevation to be correlated to the saturated sandstone at the other five holes, but this lens was clearly unsaturated [Quemada, 1995]. This sandstone lens formed that basis of the sandy clay loam layer which was included at 800-1000 cm depth in the Stratigraphic profile used in the simulations (see Figure 6). It

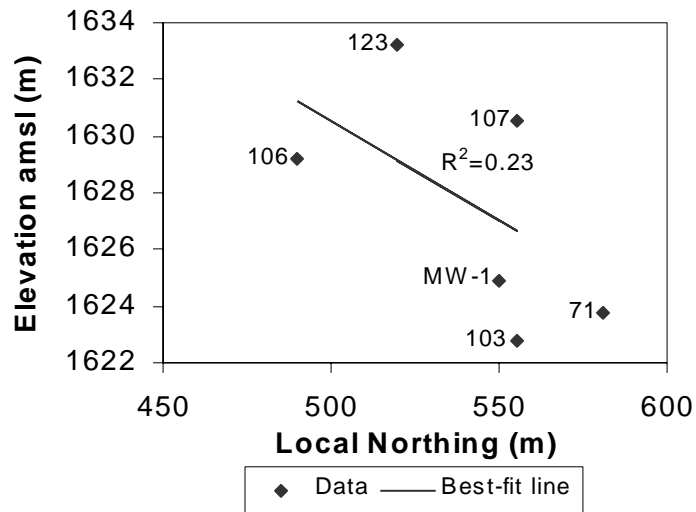
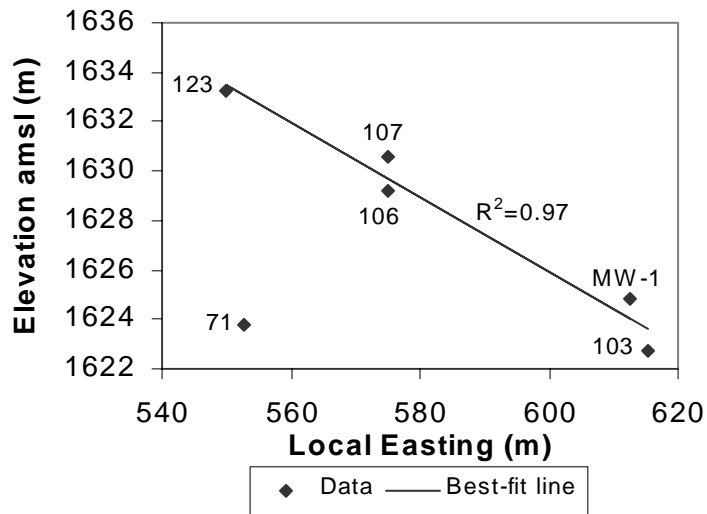


Figure 20. Elevation at which water was found during borehole drilling, plotted against local north-south coordinate, and against local east-west coordinate. Best-fit lines were created using all points except those for borehole 71. Point designated MW-1 is the monitoring well.

is not completely clear whether the unsaturated sandstone at boreholes 71 and 72 is continuous with the aquifer sandstone at the other holes and is unsaturated due its higher elevation, or whether it is separated from the aquifer sandstone by the mudstone, although the relative elevations involved appear to favor the latter idea. In any case, the aquifer that was eventually reached at borehole 71 was about 13 meters deeper than the eastward-dipping trend in the other boreholes would have predicted. This leads to the conclusion that the aquifer at 71 is a different water-carrying body than is present beneath the other holes, or is a different finger of the same larger sandstone body.

The aquifer at borehole 71 appears to be hydraulically connected to the aquifer found at the other boreholes, as the difference in the piezometric surface at each is within the level of uncertainty of the measurement (see Figure 5). Water level measurements at the time of drilling are considered partly suspect, as insufficient time may have been allowed for the water in some of the boreholes to come to equilibrium. Nevertheless, the measured water levels are fairly close, and I have implicitly assumed throughout this thesis that all of the confined water found in the various boreholes comes from a single hydrologic unit.

Since the beds of the Dockum formation are dipping at the site, one would expect some lateral flow component to be present, although the significance of lateral processes cannot be evaluated without extensive additional field work. Obviously, the one-dimensional profile that has been used in the present modeling efforts could not have taken lateral flow and transport into account. As was stated in the HYDRUS-1D Code section of the Methods, there is insufficient data to characterize a two-dimensional flow

process at the site, and a two-dimensional modeling effort would have been prohibitatively expensive in computing time.

Vapor Flux

Several neglected transport processes could influence the depth of anthropogenic solute travel. These include anion exclusion, preferential flow, and vapor flux; vapor flux is the one certain to be occurring. Milly [1996] showed that, for thermal vapor flux in the vadose zone, downward flux in the summer should theoretically be about 2 cm yr^{-1} at 1 m depth, while only 0.5 cm yr^{-1} passes 4 m depth. Note that these fluxes are not totals per year; rather, they are the maximum flux rates that occur in summer. These fluxes were derived using a perfect sine-curve top boundary temperature with an annual period, and temperature mean, amplitude and damping depth from a study by Scanlon [1994] in a Chihuahuan Desert site in Western Texas with similar environmental conditions to those at our pueblo site. If Milly's model and these parameters apply reasonably well to our site, no more than $\sim 0.75 \text{ cm yr}^{-1}$ of additional liquid water would be deposited by condensing surficial-driven vapor through 1 to 4 meters depth. This is an average volumetric water content increase of only 0.002.

In the summer, water that is converted to vapor could contribute to solute movement, because water vapor moves downwards from the surface through diffusion, and differentially condenses as the soil it encounters gets cooler with depth. Even so,

condensing water vapor that comes from above would be rapidly taken up by active roots (if the condensation occurs in the root zone) and transpired in summer.

In the winter, however, the surface-driven thermal vapor flux is upwards and gains mass as it goes, converting liquid water to vapor at all levels. Thus, winter vapor flux cannot contribute additional liquid water to the vicinity of the anthropogenic solutes. Other sources of water flux coming from below should be quite small. The upward liquid water flux from the confined source below is predicted to be $<1 \text{ mm yr}^{-1}$ (as discussed above in the Introduction), while geothermal vapor flux is generally no greater than 0.1 mm yr^{-1} [Milly, 1996]. Thus it appears that adding vapor flux to the modeling already completed may slightly retard downward solute movement in the winter by removing liquid water from the system, while the summer vapor-flux contribution of liquid water around the anthropogenic solute would normally be taken up by plant roots.

Anion Exclusion

I can only speculate on how much influence preferential flow and anion exclusion have had on the real solute transport at the midden site, as these processes are generally site-specific and there is scant data available from the pueblo site. Anion exclusion can cause a solute to move faster than the mean pore water, by forcing the solute to travel only through larger pores through which water travels at a faster velocity. In this case, because the water moving the anthropogenic solute stops at a certain depth, including anion exclusion in the model would not increase the depth at which the simulated

anthropogenic solute peak comes to a near-complete halt. Instead, it would simply cause the solute to get to this depth more swiftly than the average water molecule. Once the solute encounters static water, as has occurred in most of the simulations run to date, there is no way for it to move any further. Thus, including some anion exclusion process would have little effect on the modeling exercise. Anion exclusion can not be hypothesized to explain the difference in depth between the Cl:Br peak and the NO₃⁻ peak, because all three ions have the nearly the same hydrated radius (Cl⁻ and Br⁻ each have ionic radii = 0.33 nm, while NO₃⁻ has an ionic radius of 0.34 nm [Israelachvili, 1991]), and so would be affected by exclusionary pores in approximately same way.

Preferential Flow

Preferential flow could cause the anthropogenic solutes to travel deeper than would otherwise be possible. If macropores due to roots or animal borings are available, infiltration of intense precipitation events will be concentrated along these faster paths, thus carrying available solutes deeper than where such pathways are unavailable. Vertical unsaturated preferential flow through macropores comes to a halt where the macropores stop [Hendrickx and Flury, 2001]. Since macropores often are caused by soil flora and fauna or by drying and wetting processes, it is reasonable to assume that very few macropores will be found below the root zone at the midden site. Macropores could have pushed the solute signal down a little further but certainly not to a great depth in the unsaturated zone where no roots or soil fauna is found. It seems likely that one could

create a HYDRUS simulation including a preferential flow process that moves the solute to the depth of the actual NO_3^- peak (which has not been done as yet), using the same data as has been used before. But in the absence of supporting data, including preferential flow in the modeling would merely be a “curve-fitting” exercise, and would likely provide no additional insight into the overall transport process.

Solute Diffusion

Unless otherwise noted, all of the plots in this section that feature HYDRUS output use the soil profile that has been assumed for the time of midden deposition. For comparison to present solute peak positions as in Figure 3, etc., one needs to increase the depths presented in these HYDRUS output plots by 90 cm to account for sediment accretion in the intervening time.

The modeling problem presented in this thesis is mainly an advective one. The questions involved (How far does the model predict that the anthropogenic solute peak will travel?; Does the solute transport indicate that recharge has occurred?), are really questions about advective processes. Therefore, it was hypothesized from the beginning of the HYDRUS modeling effort that diffusive processes would have little bearing on the model outcome in terms of the solute peak positions, and would make more difficult the detection of small advective movements of the solute. Small advective movements were of particular interest in the temporal scale of solute movement study, and would have been more difficult to conduct with diffusion included. This difficulty would come about

because any particular movement of the solute plume could be due to either advection (which would indicate an infiltration event) or diffusion (which would not). Thus, determining when an infiltration event occurred based on slight movements of the solute plume, as was done in the temporal scale study, would become impossible. So, the modeling presented thus far was conducted with no diffusive transport, although dispersion was included as indicated in Tables 5 and 7.

Later, I decided to investigate the assumption that diffusion is unimportant in the measurement of the anthropogenic solute transport, because the real transport process would necessarily include diffusion, and because diffusion can play a dominant role in solute movement in flow systems with very slow velocities such as were shown in the simulations. The investigation took the form of another 2^k factorial design, in which the model sensitivity to *including* vs. *not including* diffusion was compared to the model sensitivities of the “top boundary condition” and “soil hydraulic parameters” groups described above in the Methods and Results and Discussion sections. Thus there were 3 parameter groups in this factorial design, which required 8 simulations. To simplify the task, four simulations from the previous sensitivity analysis were chosen that were to become half of the eight simulations necessary for this new study. These were formerly design points 4, 8, 12, and 16, which all had the “high” variants of wilting point (-15000 cm H₂O) and rooting depth (300 cm). These four simulations also have between them all four possible combinations of high and low variants in the parameter groups “top boundary condition” and “soil hydraulic parameters” (see Sensitivity Analysis section of the Methods, above), and a diffusion coefficient $D^* = 0$. Then, four new simulations were created that were identical to the four already made, except that they included a bulk

fluid solute diffusion coefficient of $D^* = 1.3 \text{ cm}^2 \text{ day}^{-1}$. This is roughly the mean diffusion coefficient reported for Cl^- , Br^- , and NO_3^- for a wide range of concentrations and for several different cations in Weast [1986]. Table 11 shows the sensitivity analysis design for these simulations, with letters “*a*” through “*h*” used to name the design points to distinguish them from the simulations in the previous sensitivity analysis. As before, the model outcome that was used to evaluate model sensitivity to the parameter groups was the simulated anthropogenic solute peak position after 88 years of simulation. The model sensitivities to the parameter groups were calculated by formulas analogous to Equation (21). For example, the diffusion coefficient sensitivity, s_{D^*} , was calculated by:

$$s_{D^*} = \frac{1}{4} \sum_{i=1}^8 (-1)^i R_i \quad (22).$$

where R_i = model response (peak depth) in simulation i .

Table 12 shows the solute peak depths for the eight design points of the diffusion sensitivity analysis, and the relative model sensitivities to the top boundary condition, soil hydraulic properties, and diffusion coefficient parameter groups. These results show that the top boundary condition and soil hydraulic properties groups are much more important factors in determining the solute peak position, than is the diffusion coefficient. The negative model sensitivity to the diffusion coefficient indicates that diffusion slightly retards the solute peak movement, but compared to the other parameters, this movement is slight. Thus it appears that diffusion is not significant in determining the anthropogenic solute peak position in the HYDRUS modeling.

Table 11. Sensitivity analysis schedule for the diffusion investigation, showing the design points (simulations) and the high/low status of the three parameter groups for each simulation. High variant is indicated by a +.

Design Point	Top Boundary Condition*	Soil Hydraulic Parameters*	Diffusion Coefficient#
a†	+	+	-
b	+	+	+
c††	+	-	-
d	+	-	+
e‡	-	+	-
f	-	+	+
g‡‡	-	-	-
h	-	-	+

* Top Boundary Condition and Soil Hydraulic Parameters: for details of the “+” and “-“ variants, see the Sensitivity Analysis section of the Methods.

Diffusion Coefficient: + = 1.3 cm² day⁻¹; - = 0 cm² day⁻¹.

† Was design point 8 in the previous sensitivity analysis.

†† Was design point 16 in the previous sensitivity analysis.

‡ Was design point 4 in the previous sensitivity analysis.

‡‡ Was design point 12 in the previous sensitivity analysis.

Table 12. Results of the diffusion sensitivity analysis.

Design Point	Solute Peak Depth at 88 Years (cm)
a	151
b	136
c	100
d	96
e	66
f	64
g	109
h	106

Parameter	Model (Peak Depth) Sensitivity (cm)
Soil Hydraulic Parameters	34.5
Top Boundary Condition	44
Diffusion	-6

Of course, diffusion will continue on past 88 years of simulation, so design point *b* (a simulation with diffusion) was continued to 161 years, and the solute peak depth was plotted with time to see if it would move significantly past the position it obtained after 88 years. Design point *b* was chosen for this because, of all of the simulations that included diffusion, it did the best job of moving the simulated solute down to the real solute peak positions (180 ± 40 cm). Figure 21 shows the result. The solute peak is at 136 cm bgs after 88 years of simulation, and is at 139 cm after 161 years of simulation. In between these times, the solute peak moves around between 133 cm and 148 cm. For reference, the solute peak position in design point *a*—which was the same as design point *b* except that diffusion was excluded in *a*--was 151 cm. Thus, it seems that including diffusion in the model makes the solute peak position less stable, but would not significantly change the outcome of this particular simulation.

Another way of seeing the same result is to look at a succession of concentration profiles from design point *b*, as is shown in Figure 22. This figure shows, as in other simulated solute profiles shown before, that the solute peak quickly reaches its near-steady position, and then essentially maintains the same position through time. The solute peak remains steady even while the solute mass is diffusing (mainly downward) through the rest of the profile. From all of these results I infer that, while diffusion may be an important process for solute transport in slowly moving flows, it does not appear to have a significant impact on the eventual solute peak positions.

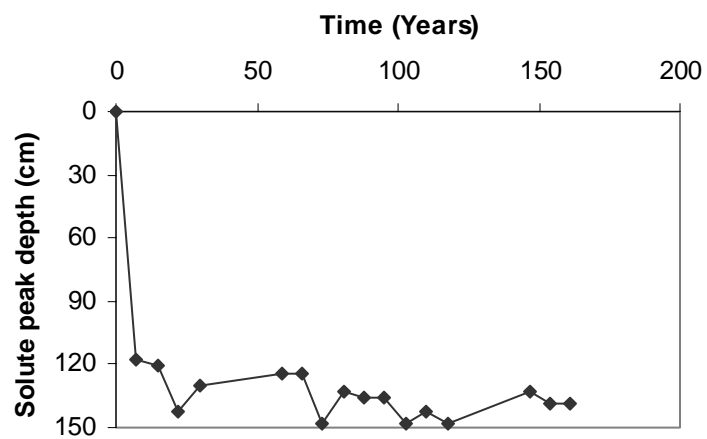


Figure 21. Peak concentration position of the simulated anthropogenic solute from design point *b* of the diffusion sensitivity analysis. The simulation has been extended to 161 years to examine the trend of movement beyond the 88 years used in the sensitivity analysis.

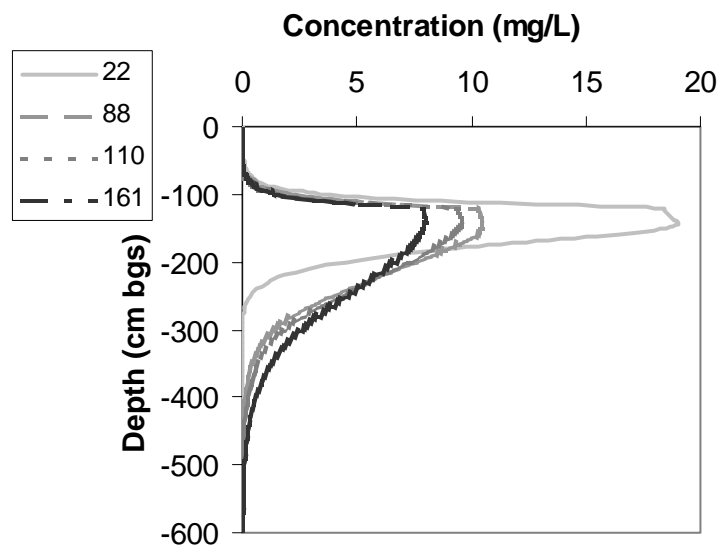


Figure 22. The solute profile from design point *b* of the diffusion sensitivity analysis, extended through 161 years. The different colored lines represent different snapshots in time.

V. CONCLUSIONS

Two solute signals of anthropogenic origin were identified at an ancient pueblo site in central New Mexico, the Cl:Br ratio and NO_3^- . Both of these signals were clearly present in the two boreholes drilled through thick intact midden material, while neither was present beneath the five boreholes that were drilled through relatively pristine soil. These solute signals had distinct peaks at depths shallower than the environmental peaks of chloride and bromide. These signals were somewhat separated in the subsurface; the Cl:Br signal has traveled 140 ± 30 cm while the NO_3^- peak has traveled 220 ± 40 cm in the 625 ± 70 years since the midden was deposited.

There is no phreatic water evident at the site, indicating that there is no downward recharge accumulating. There are three indicators of upward flow below the root zone at this site:

- (1) A near-subsurface (~800-2100 cm) confined aquifer with unsaturated material above indicates that the hydraulic potential gradient beneath the root zone should be upward (neglecting osmotic potential).
- (2) There is a correlation between the total amount of chloride mass in the environmental solute bulge and the average water content in the unsaturated zone below the roots.

(3) The average chloride mass balance age calculated for the profiles at this site (43 Kyr) is larger than those generally found in the American Desert Southwest, which usually have chloride inventories of 13-20 Kyr.

The conceptual model that was tested with the HYDRUS code assumed that upward flow is coming from the confined aquifer below, that the Cl:Br and NO₃⁻ signals below the thick midden are anthropogenic, and that precipitation, evaporation, and transpiration are enough to explain the anthropogenic solute positions.

The modeling effort has lacked some potentially significant physical processes, including vapor flux, anion exclusion, preferential flow, and solute diffusion. Of these, only preferential flow could move the simulated anthropogenic solute peak farther down into the profile. Inclusion of preferential flow in the model at this point is not warranted because nothing is known about the potential or distribution of this process at the site.

Despite the limitations of the modeling effort, several insights have emerged as a result of the HYDRUS simulations:

(1) According to the modeling results, the environmental solute peaks are held in place at the base of the root zone at ~400 cm bgs, between the upward flux from the aquifer below and the removal of water by the transpiring plants.

(2) A large majority of the anthropogenic solute transport appears to occur early in the simulations (within the first 5-10 years). The anthropogenic solute appears to be essentially trapped in place. New solute movement is predicted to occur in a winter with the right combination of precipitation and low evaporation (and transpiration), which will send it deeper. A corollary to this result predicts that, given enough time, an infiltration event will occur that is intense enough that

the solute will come to rest at the same level as the environmental solute bulge at ~4 m bgs.

(3) Because the anthropogenic solute is predicted to remain trapped in the vicinity of the root zone, the model clearly predicts that no recharge is taking place at the site. This modeling result is supported by much of the same evidence that indicates upward flow from below, including the correlation between chloride mass and water content in the lower vadose zone,

(3) The conditions that promote downward movement in the near subsurface, after the first few years of transport, are not simply correlated to individual storm events. Winter conditions appear more favorable than summer due to reduced evaporative demand and dormant plants.

(4) Of the four parameter groups included in the primary sensitivity analysis, solute transport in the model is most sensitive to the assigned soil hydraulic properties of the sandy soils above 120 cm depth, and to the combined precipitation and potential evapotranspiration (top boundary condition). Variations in rooting depth had an intermediate effect on solute transport, while the wilting point assigned had almost no effect. This last point is fortunate for desert vadose zone modeling in general (at least, to whatever extent the current study reflects the goals of vadose zone research), as wilting point is often considered an ambiguous concept or an immeasurable parameter.

(5) A secondary sensitivity analysis showed that inclusion of diffusion in the model is relatively unimportant in determining the position of the simulated anthropogenic solute.

The simulated anthropogenic solute peaks in the various preliminary and sensitivity analysis simulations essentially halted at 50 to 151 cm bgs, which is of the same order of magnitude as the travel distance of the actual anthropogenic solutes. In two of the simulations, the simulated solute made it to the target range, which was bracketed by the mean positions of the two anthropogenic solutes. Based on this agreement between simulation and reality, I assert that this archaeological site has provided calibration for the conceptual model that was developed. The model predicts that the true hydraulic conductivities are high in the range of those tested, and that the true rooting depth of the sand sage at the site is approximately 400 cm. This shows that archaeological analogs can yield useable calibration data for hydrologic modeling.

Suggestions for Future Work

If another season of study at Fernandez Pueblo is allowed by regulations and funding, there are two avenues that could be pursued. First, there are some items that could help constrain the model of the anthropogenic solute transport. The hydraulic parameters of the sandy loam, loamy sand, and clay should be ascertained, and the rooting depth of the sand sage at this particular site could be found. Knowledge of the rooting depth would also verify or refute the notion that the environmental solute peaks are at the bottom of the root zone, at ~400 cm bgs. In addition, as mentioned before, it would be helpful to perform some simulations with vapor flux included, so some method

of measuring or (more likely) estimating the top boundary condition of this process would need to be found.

Second, there are projects which might give assistance on the question of upward flow. A complete balance of potentials (including osmotic potential) at the bottom of the profiles should be worked up, perhaps near borehole 123 or an analogous location where upward flow appears significant based on the chloride mass analysis. This work could help resolve the issue of whether upward flow is possible, likely, or certain. Soil samples from near the bottom of the root zone should also be taken by some soil moisture-conserving method, so that hydraulic potentials, and perhaps gradients, in this region could be obtained by relative humidity (water activity) measurement.

Other solutes could be investigated for clues to the age of the environmental solute profiles. The amount of calcite (CaCO_3) deposited in a semi-arid or arid zone profile can indicate the age of the profile [Jan M.H. Hendrickx, personal communication]. The amount of carbonate present in soil profiles at the pueblo site might be useful in helping to confirm the assumed ~13,000 years of time since the near-subsurface was washed relatively clean of chloride accumulation during a wet period, although one should check the carbonate present in the confined aquifer water at the same time given that the upward flow process may be contributing carbonate in addition to chloride. Finally, intact samples of the unsaturated mudstone and siltstone could be taken for laboratory determination of their anion exclusion and reverse osmosis capabilities.

In the modeling, a more detailed sensitivity analysis could be performed that treats separately the top boundary condition group of parameters (evaporation, transpiration, and precipitation), and treats separately the soil hydraulic properties (K_{sat} ,

$\theta_s, \theta_r, \alpha, n$). However, it would seem to be much more preferable to measure the soil hydraulic properties (particularly for the loamy sand, sandy loam, and clay that the anthropogenic solutes have traveled through), and use them to constrain future modeling efforts.

VI. REFERENCES

- Allison, G.B., Stone, W.J., and Hughes, M.W., 1985. Recharge in karst and dune elements of a semi-arid landscape as indicated by natural isotopes and chloride. *J. Hydrol.* 76:1-26.
- Allison, G.B., Gee, G.W., Tyler, S.W., 1994. Vadose-zone techniques for estimating groundwater recharge in arid and semiarid regions. *Soil Sci. Soc. Am. J.*, 58:6-14
- Anderson, M.P., and Woessner, W.W., 1992. *Applied Groundwater Modeling*. p9. Academic Press. San Diego, CA.
- Atwood, T.L., 1983. Ecology of a sand sage community in southern New Mexico. Master's Thesis. New Mexico State University. Las Cruces, NM.
- Bastiaanssen, W.G.M. 1995. *Regionalization of surface flux densities and moisture indicators in composite terrain*. PhD Thesis, Wageningen Agricultural University, Wageningen, The Netherlands. p. 273.
- Davis, S.N., Whittemore, D.O., and Fabryka-Martin, J., 1998. Uses of chloride/bromide ratios in studies of potable water. *Ground Water*. 36:338-350.
- Doleman, W.H., 1995. Second progress report: Phase 1 archeological testing at Fernandez Pueblo (LA781). UNM/OCA Report No. 185-502a. University of New Mexico/Office of Contract Archeology. Albuquerque, NM.
- Feddes, R.A., Kowalik, P.J., and Zaradny, H., 1978. *Simulation of Field Water Use and Crop Yield*. John Wiley and Sons. New York, NY.
- Fetter, C.V. 1993. *Contaminant Hydrogeology*. p.272-4. Macmillan. New York, NY.
- Fontes, J.C., Yousfi, M., and Allison, G.B., 1986. Estimation of long-term diffuse groundwater discharge in the northern Sahara using stable isotope profiles in soil water. *Journal of Hydrology*, 86:315-327.
- Freeze, R.A., Cherry, J.A., 1979. *Groundwater*. p.29. Prentice Hall, Inc. New York, NY.

- Gee, G.W., Wierenga, P.J., Andraski, B.J., Young, M.H., Fayer, M.J., and Rockhold M.L., 1994. Variations in water balance and recharge potential at three western desert sites. *Soil Sci. Soc. Am. J.*, 58:63-71.
- Gerritse, R.G. and George, R.J., 1988. The role of soil organic matter in the geochemical cycling of chloride and bromide. *J. Hydrol.*, 101:83-95.
- Graf, D.L., 1982. Chemical Osmosis, reverse chemical osmosis, and the origin of subsurface brines. *Geochimica et Cosmochimica Acta*, 46:1431-1448.
- Grissino-Mayer, H., 1996. A 2129-year reconstruction of precipitation for northwestern New Mexico, U.S.A. Pages 191-204 in *Tree Rings, Environment and Humanity*. J. S. Dean, D. M. Meko, and T. W. Swetnam, editors. Radiocarbon. Tucson, AZ.
- Hakonson, T.E., Lane, L.J., Springer, E.P., 1992. Biotic and abiotic processes. In Reith, C.C., and Thompson, B.M., (ed's.), *Deserts as Dumps*. University of New Mexico Press, Albuquerque, NM.
- Hendrickx, J.M.H., and Walker, G.R., 1997. Recharge from Precipitation. In Simmers, I., (ed.), *Recharge of Phreatic Aquifers in (Semi-) Arid Areas*. A.A. Balkema, Rotterdam, The Netherlands.
- Hendrickx, J.M.H., and Flury, M., 2001. Uniform and preferential flow mechanisms in the vadose zone. In: D.A. Feary (Editor), *Conceptual Models of Flow and Transport in the Fractured Vadose Zone*, National Research Council, National Academy Press, Washington, D.C. pp. 149-187.
- Hillel, D., 1998. *Environmental Soil Physics*. p.620-2. Academic Press. San Diego, CA.
- Hills, R.G. and Wierenga, P.J., 1994. INTRAVAL Phase II model testing at the Las Cruces Trench site. *Report NUREG/CR-6063*, U.S. Nuclear Regulatory Commission, Rockville, MD.
- Isrealachvili, J., 1991. *Intermolecular and Surface Forces*. Academic Press. New York, NY. p. 55.
- Johnston, C.D., 1986. Distribution of environmental chloride in relation to subsurface hydrology. *J. Hydrol.*, 94:67-88.
- Kearns, A. K., Hendrickx, J.M.H., 1998. *Temporal Variability of Diffuse Groundwater Recharge in New Mexico*. New Mexico Water Resources Research Institute Technical Completion Report No. 309. New Mexico State University. Las Cruces, New Mexico.
- Law, A.M., and Kelton. D.M., 1999. *Simulation Modeling and Analysis*. 3rd Ed. McGraw-Hill. New York, New York.

- Leij, F.J., Alves, W.J., van Genuchten, M Th., and Williams J.R., 1997. *The UNSODA Unsaturated Hydraulic Database User's Manual Version 1.0*. National Risk Management Research Laboratory. Cincinnati, Ohio.
- Maidment, D.R., 1992. *Handbook of Hydrology*. McGraw-Hill Professional Book Group. New York, NY. p.535.
- Marine, I.W., and Fritz, S.J., 1981. Osmotic model to explain anomalous hydraulic heads. *Water Resources Res.*, 17:73-82.
- Mera, H.P., 1940. Population changes in the Rio Grande glaze-paint area. Laboratory of Anthropology Technical Series, Bulletin No. 9. Santa Fe, New Mexico.
- Miller, B., and Chapman, N., 1995. Postcards from the past: archaeological and industrial analogs for deep repository materials. *Radwaste Magazine*. January, pp. 32-42.
- Milly, P.C.D., 1996. Effects of thermal vapor diffusion on seasonal dynamics in the unsaturated zone. *Water Resources Res.*, 32:509-518.
- Moore, J.W., 1997. *Monitoring infiltration of atmospheric chloride across the land surface in central New Mexico*. Master's Thesis. Department of Earth and Environmental Sciences. New Mexico Institute of Mining and Technology. Socorro, New Mexico.
- National Resource Council, 1995. *Technical Bases for Yucca Mountain Standard*. Nat'l Acad. Press, Washington, D.C.
- Neuzil, C.E., 2000. Osmotic generation of 'anomalous' fluid pressures in geologic environments. *Nature*, 403:182-184.
- Osburn, G.R., 1984. Geology of Socorro County: New Mexico Bureau of Mines Open File Report 238, scale 1:200,000. New Mexico Bureau of Mines and Mineral Resources. Socorro, New Mexico.
- Peck, A.J., Johnston, C.D., and Williamson, D.R., 1981. Analyses of solute distributions in deeply weathered soils. *Agric. Water Manage.*, 4:83-103.
- Phillips, F.M., Mattick, J.L., Duval, T.A., Elmore, D., and Kubik, P.W., 1988. Chlorine 36 and tritium from nuclear weapons fallout as tracers for long-term liquid movement in desert soils. *Water Resour. Res.*, 24, 1877-1891.
- Phillips, F.M., 1994. Environmental tracers for water movement in desert soils of the American southwest. *Soil Sci. Soc. Am. J.*, 58:15-24.

- Plummer, M.A., Walvoord, M.A., and Phillips, F.M., 2000. Time-scale of the response of soil moisture in thick desert vadose zones to changes in surface boundary conditions and implications for preservation of paleoclimate signals. *EOS Transactions*, 81 (48) H72B-26, abstract, AGU Fall meeting supplement.
- Pockman, W., 2000. Personal communication based on work presented at New Mexico Tech Hydrology Seminar in April, 2000. Department of Biology, University of New Mexico. Albuquerque, NM.
- Porro, I., and Wierenga, P.J., 1993. Transient and steady-state solute transport through a large unsaturated soil column. *Ground Water*, 31:193-200.
- Quemada, L.F., 1995. Identification of a natural soil-water tracer at an ancient Indian midden. Master's Thesis. Department of Earth and Environmental Sciences, New Mexico Tech. Socorro, New Mexico.
- Sangster, B., Blom, J.L., Sekhuis, V.M., Loeber, J.G., Rauws, A.G., Koedam, J.C., Krajnc, E.I., van Logten, M.J., 1983. The influence of sodium bromide in man: a study in human volunteers with special emphasis on the endocrine and central nervous system. *Jour. Chem. Toxic.*, 21:409-419.
- Scanlon, B.R., Wang, F.P., Richter, B.C., 1991. *Field Studies and Numerical Modeling of Unsaturated Flow in the Chihuahuan Desert, Texas*. Report of Investigations No. 199. Bureau of Economic Geology, University of Texas at Austin. Austin, TX.
- Scanlon, B.R., 1992. Evaluation of liquid and vapor water flow in desert soils based on chlorine-36 and tritium tracers and nonisothermal flow simulations. *Water Resources Research*, 28:285-297.
- Scanlon, B.R., Tyler, S.W., Wierenga, P.J., 1997. Hydrologic issues in arid, unsaturated systems and implications for contaminant transport. *Reviews of Geophysics.*, 35:461-490.
- Schaap, M., 1999. Rosetta Lite Version 1.0 (software). U.S. Salinity Laboratory. Riverside, CA.
- Šimůnek, J., Šejna, M., and van Genuchten, M. Th., 1998. *The HYDRUS-1D Software Package for Simulating the One-Dimensional Movement of Water, Heat and Multiple Solutes in Variably Saturated Media (User's Manual), Version 2.0*. U.S. Salinity Laboratory. U.S.D.A. Riverside, CA.
- Stephens, D.B., 1994. A perspective on diffuse natural recharge mechanisms in areas of low precipitation. *Soil Sci. Soc. Am. J.*, 58:40-48.
- Stephens, D.B., and Knowlton, Jr., R., 1986. Soil water movement and recharge through sand at a semi-arid site in New Mexico. *Water Resour. Res.* 22:881-889.

Treadwell, C.J. and Garcia, A., 1995. Geology and Geomorphology of Fernandez Pueblo. Draft Report. University of New Mexico Office of Contract Archaeology.

Treiber, M., and Krusinger, A.E., 1979. Inferential techniques for soil depth determinations, Part II: *Artemisia filifolia torr.* (sand sagebrush). Research Note, Report Number ETL-0176. U.S. Army Engineer Topographic Laboratories. Ft. Belvoir, VA.

Tyler, S.W., and Walker, G. R., 1994. Root zone effects on tracer migration in arid zones. *Soil Sci. Soc. Am. J.*, 58:25-31.

van Genuchten, M. Th., 1987. A closed-form equation for predicting the hydraulic conductivity of unsaturated soils, *Soil Sci. Soc. Am. J.*, 44:892-898.

Weast, R.C., Astle, M.J., and Beyer, W.H., 1986. *CRC Handbook of Chemistry and Physics*. CRC Press, Inc. Boca Raton, FL.

Weaver, 1919. *The Ecological Relation of Roots*, Pub. No. 286., Carnegie Institution of Washington. Washington D.C.

Wierenga, P.J., Hendrickx, J.M.H., Nash, M.H., Ludwig, J., and Daugherty, L.A., 1987. Variation of soil and vegetation with distance along a transect in the Chihuahuan Desert. *Journal of Arid Environments*, 13:53-63

Wolff, M., 1990. Dispersion induced advection of an isotope ratio. Master's Thesis. Department of Earth and Environmental Sciences. Socorro, New Mexico.

Wu, Y.S., and Pruess, K., 2000. Numerical simulation of non-isothermal multiphase tracer transport in heterogeneous fractured porous media. *Advances in Water Resources*, 23:699-723.

Zyvoloski, G.A., Robinson, B.A., Dash, Z.V., and Trease, L.L., 1996. Users Manual for the FEHMN Application. Los Alamos National Laboratory. Publication LA-UR-94-3788. Los Alamos, New Mexico.

APPENDIX A. THE DRILL FOAM ISSUE.

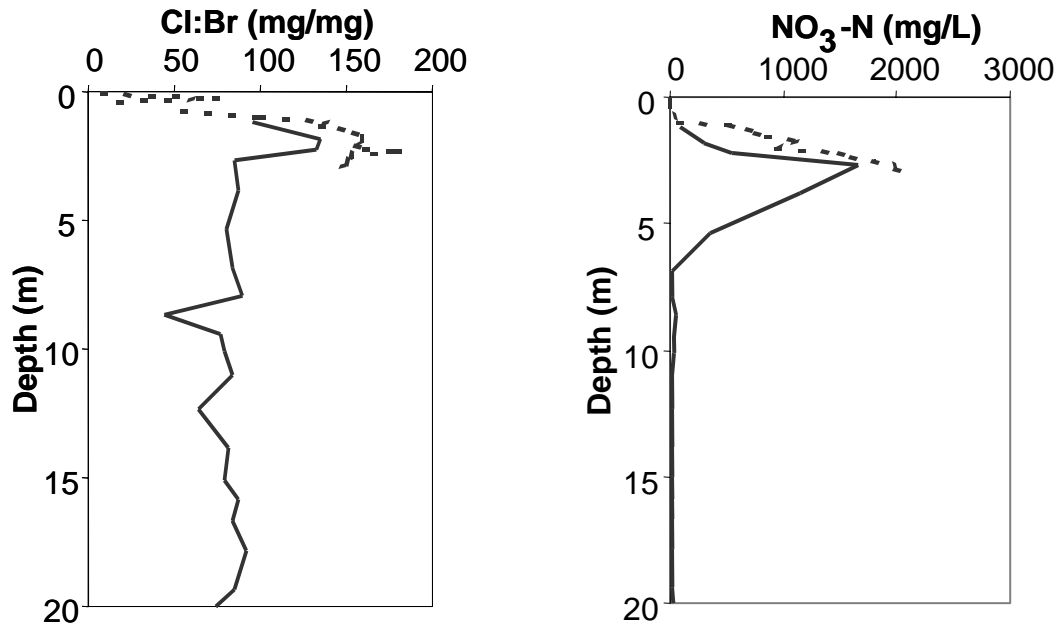
The following paragraph is a summary of information contained in Quemada [1995]. Caving of surface sands into the borehole was a serious problem at test pits 71 and 72 during drilling, due to the relatively large amount of eolian sand accumulated near the pueblo since the time of its occupation. Unfortunately, a drill foam was added to the borings at these locations, to prevent further mixing of the near surface sands with the samples to be taken from further down hole. This drill foam (DDF Foamer, Denver Co.) is an anionic surfactant that contains Cl^- , Br^- , and NO_3^- , and so could potentially throw off the analysis. Quemada noticed a peak on the HPLC chromatograms of those samples that were contaminated with surfactant that was never present on the chromatograms for samples that could not have been contaminated. The magnitude of this peak, along with a chemical analysis of the surfactant, were used to adjust the chloride, bromide, and nitrate concentrations of soils from the air rotary holes at 71 and 72.

One way to assure that the anthropogenic solute peaks are genuine, and not artificially created by the addition of the drill foam, is to compare the Cl:Br and nitrate profiles from the air rotary holes drilled at test pits 71 and 72, to the profiles derived from the hand auger holes which were drilled less than one meter away from the air rotary holes. The increases in NO_3^- and Cl:Br that we find in the air rotary boreholes are plainly evident in the hand auger boreholes, where drill foam contamination could not have

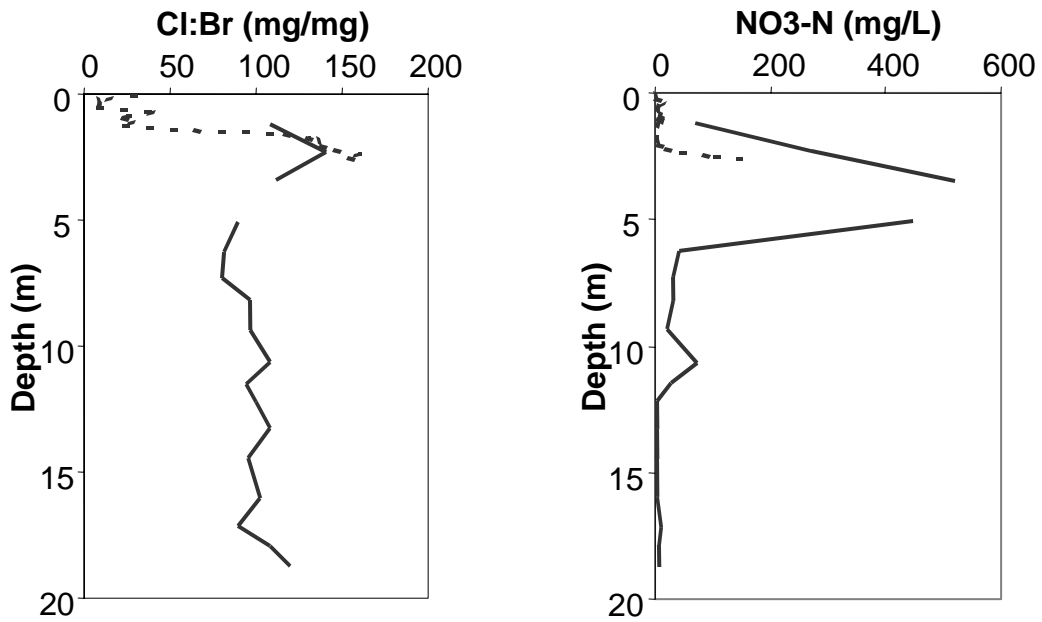
occurred (Figure A1), although it was not possible in all cases to dig deep enough with the hand auger to get to the solute peaks. Therefore, it seems only reasonable to suggest that the drill foam contamination does not qualitatively affect the air rotary profiles because the anthropogenic solutes are certainly not artifacts of the drill foam addition.

Reference

Quemada, L.F., 1995. Identification of a natural soil-water tracer at an ancient Indian midden. Master's Thesis. Department of Earth and Environmental Sciences. Socorro, New Mexico.



(A) Borehole 71



(B) Borehole 72

— Air rotary - - - Hand Auger

Figure A1. Cl:Br and NO₃-N solute profiles from the two boreholes within the midden. (A) Borehole 71 profiles. (B) Borehole 72 profiles. Data from Quemada [1995].

APPENDIX B. PLOTS FROM THE SENSITIVITY ANALYSIS.

The following sixteen pages show the output states of matric potential, water content, and solute concentration from the design points of the sensitivity analysis. For details on the sensitivity analysis, refer to Chapter 2.

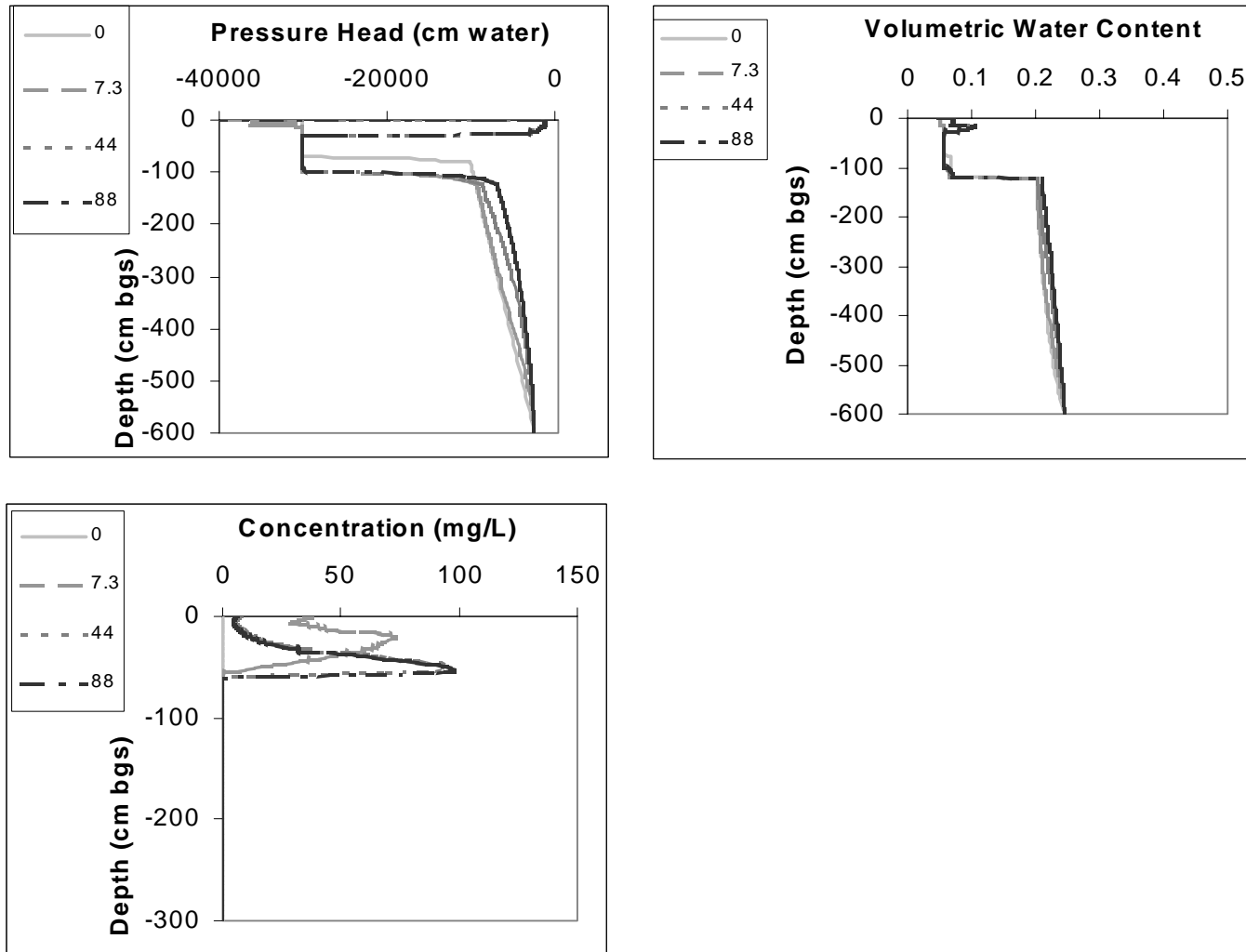


Figure B1. Plots of HYDRUS output from sensitivity analysis, design point #1.

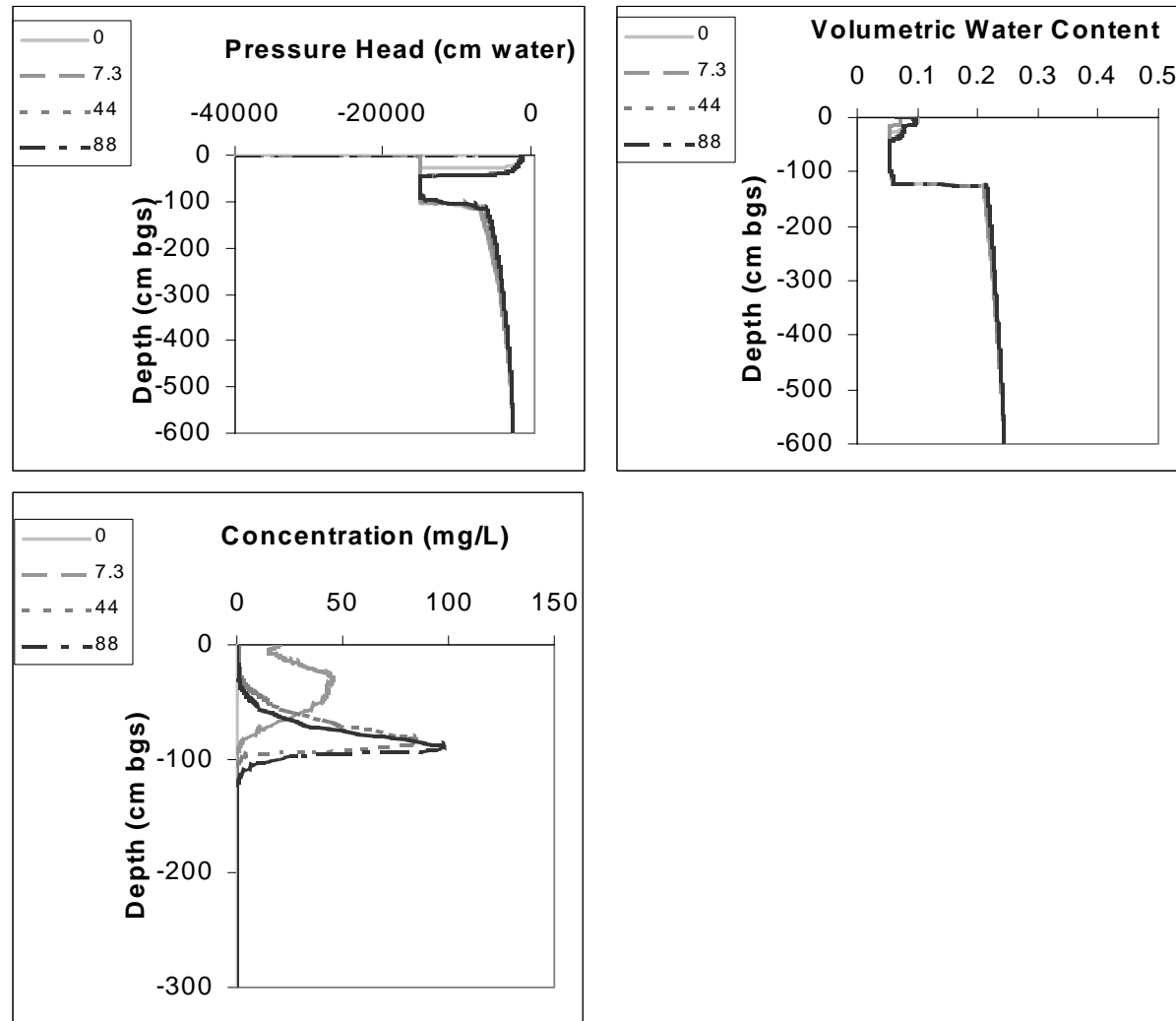


Figure B2. Plots of HYDRUS output from sensitivity analysis, design point #2.

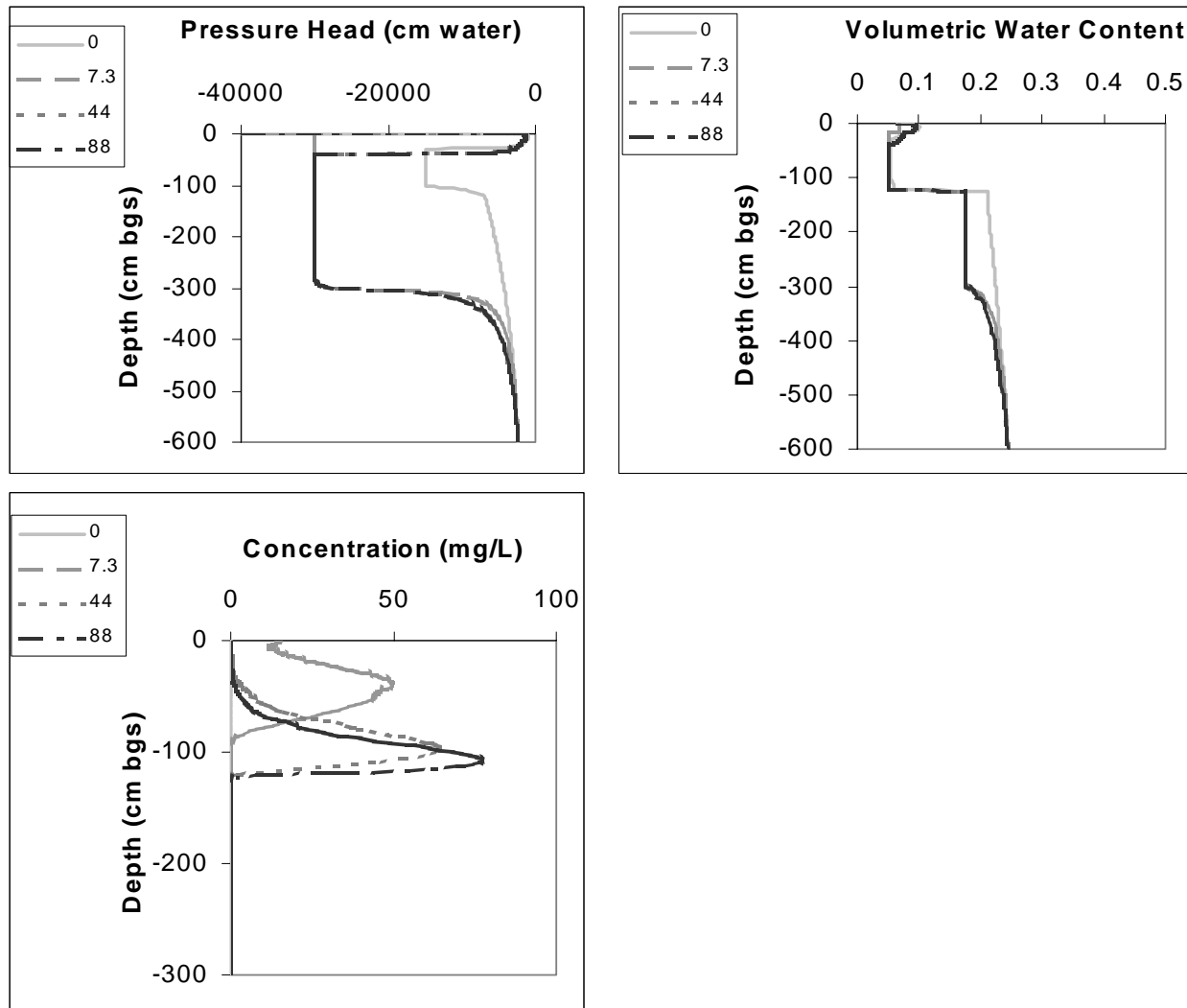


Figure B3. Plots of HYDRUS output from sensitivity analysis, design point #3.

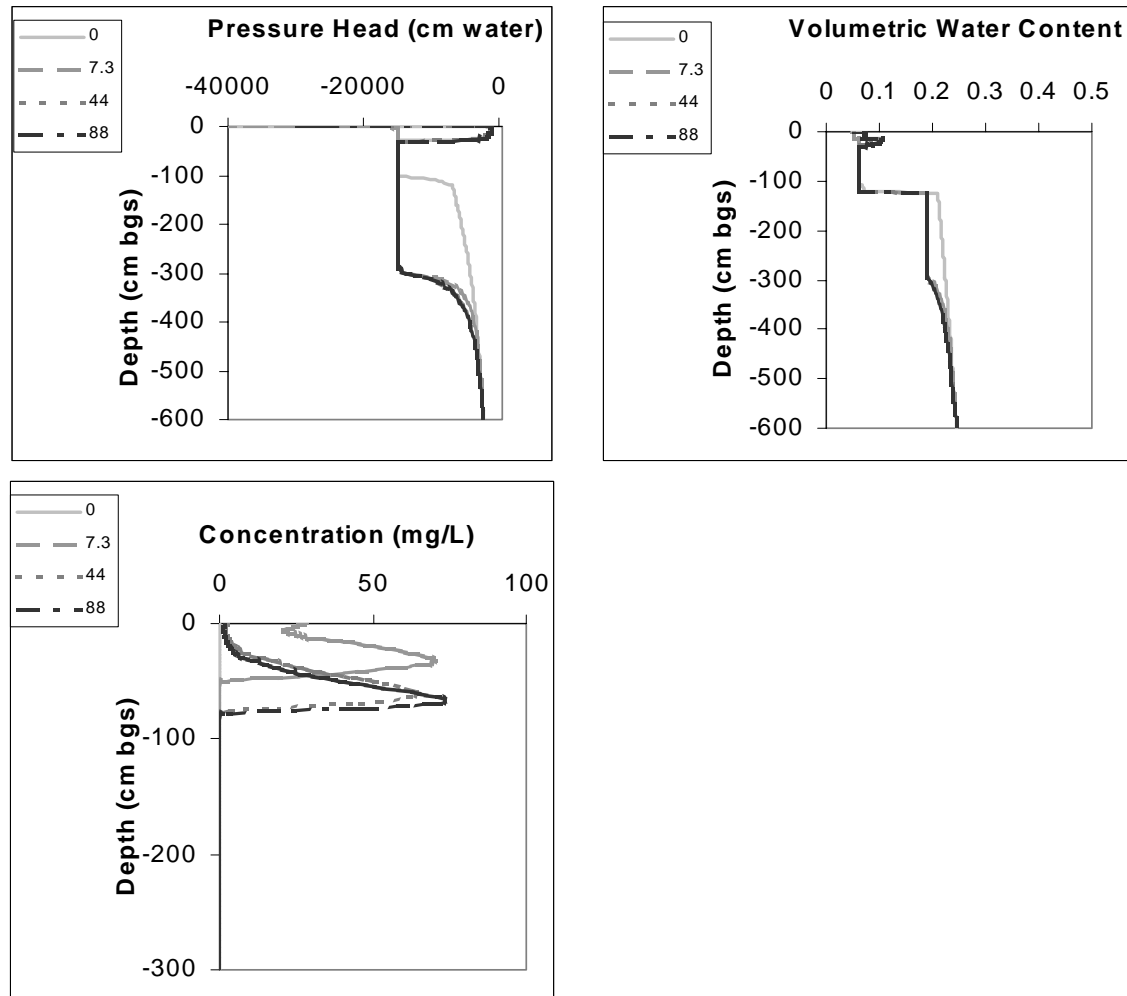


Figure B4. Plots of HYDRUS output from sensitivity analysis, design point #4.

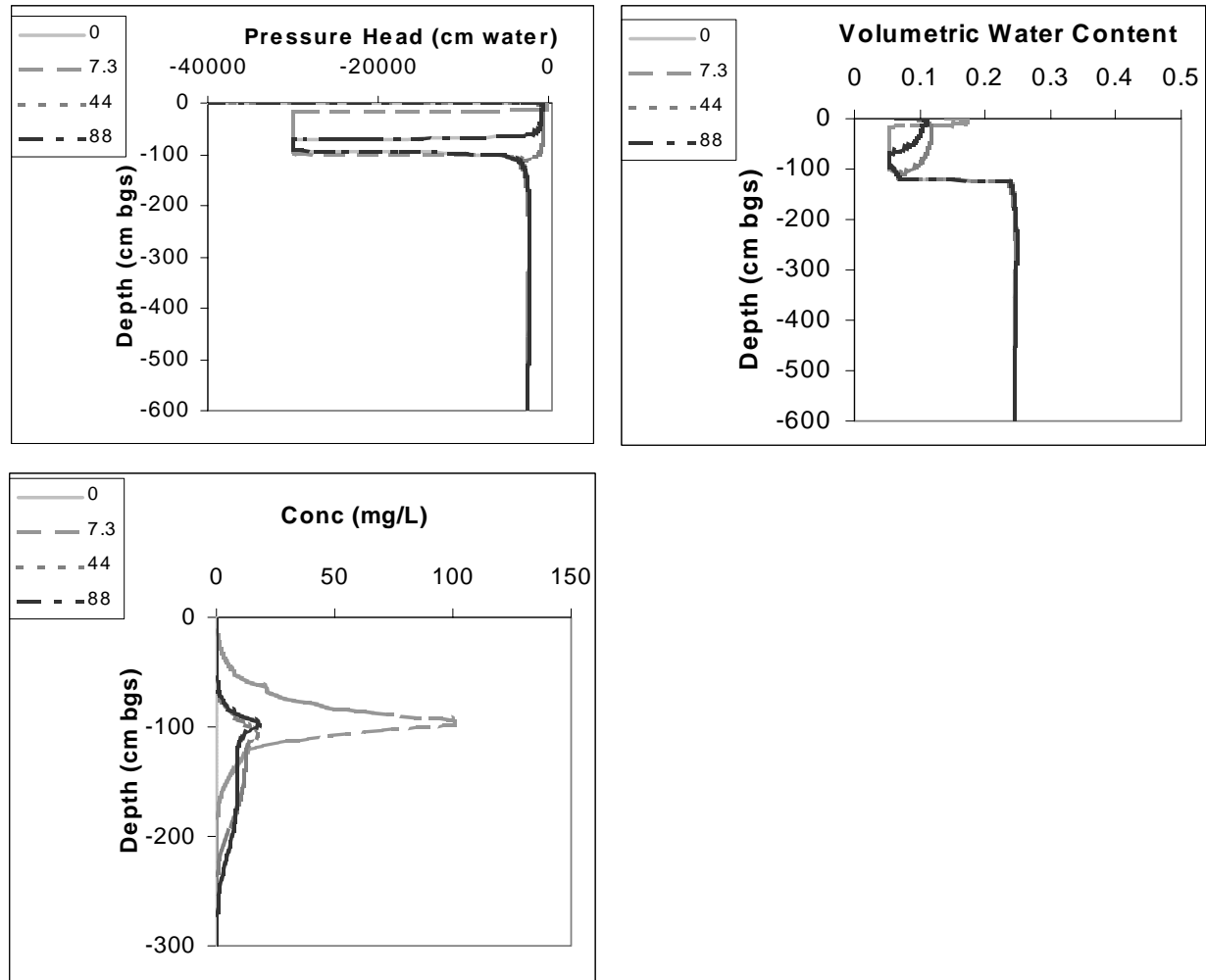


Figure B5. Plots of HYDRUS output from sensitivity analysis, design point #5.

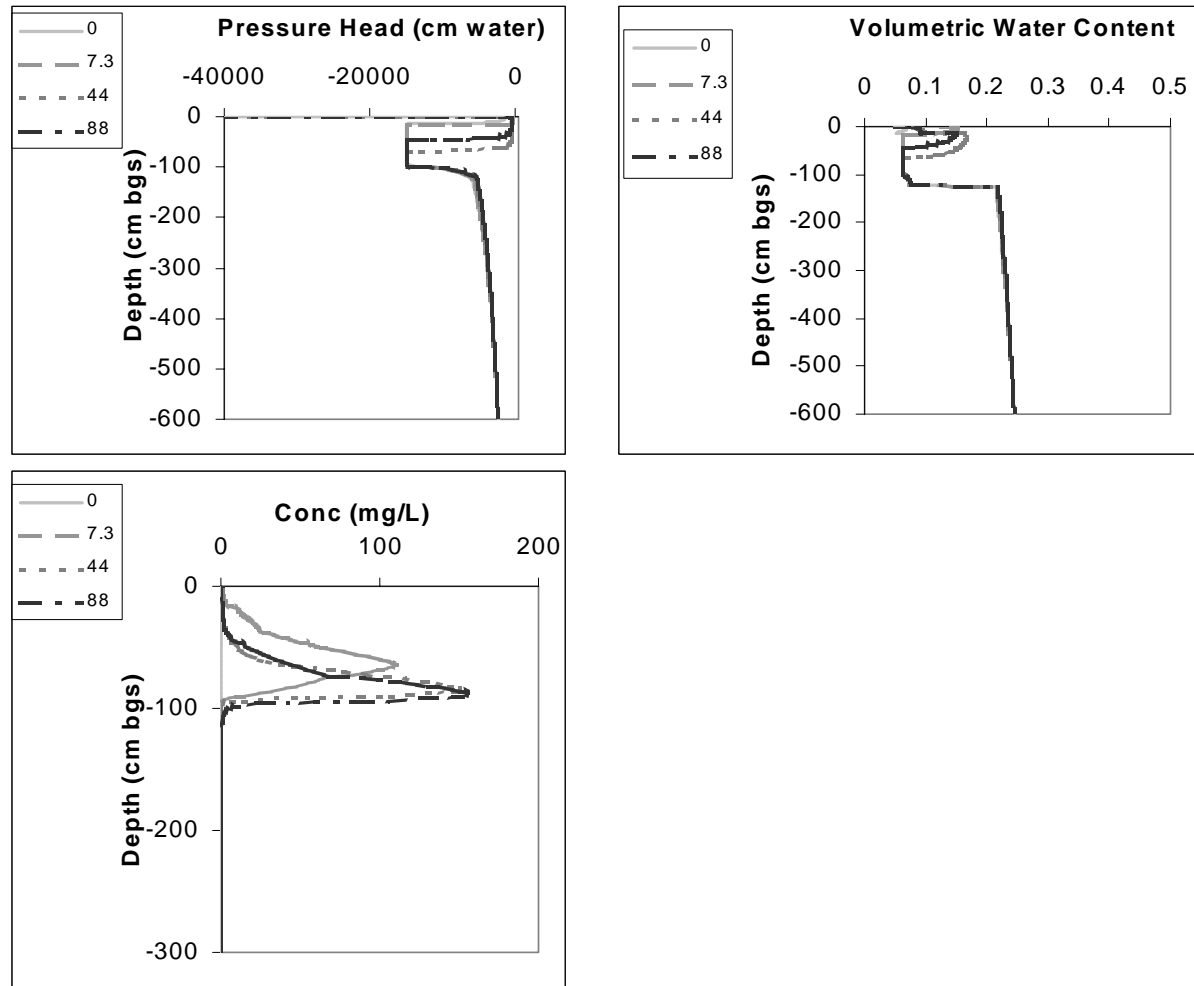


Figure B6. Plots of HYDRUS output from sensitivity analysis, design point #6.

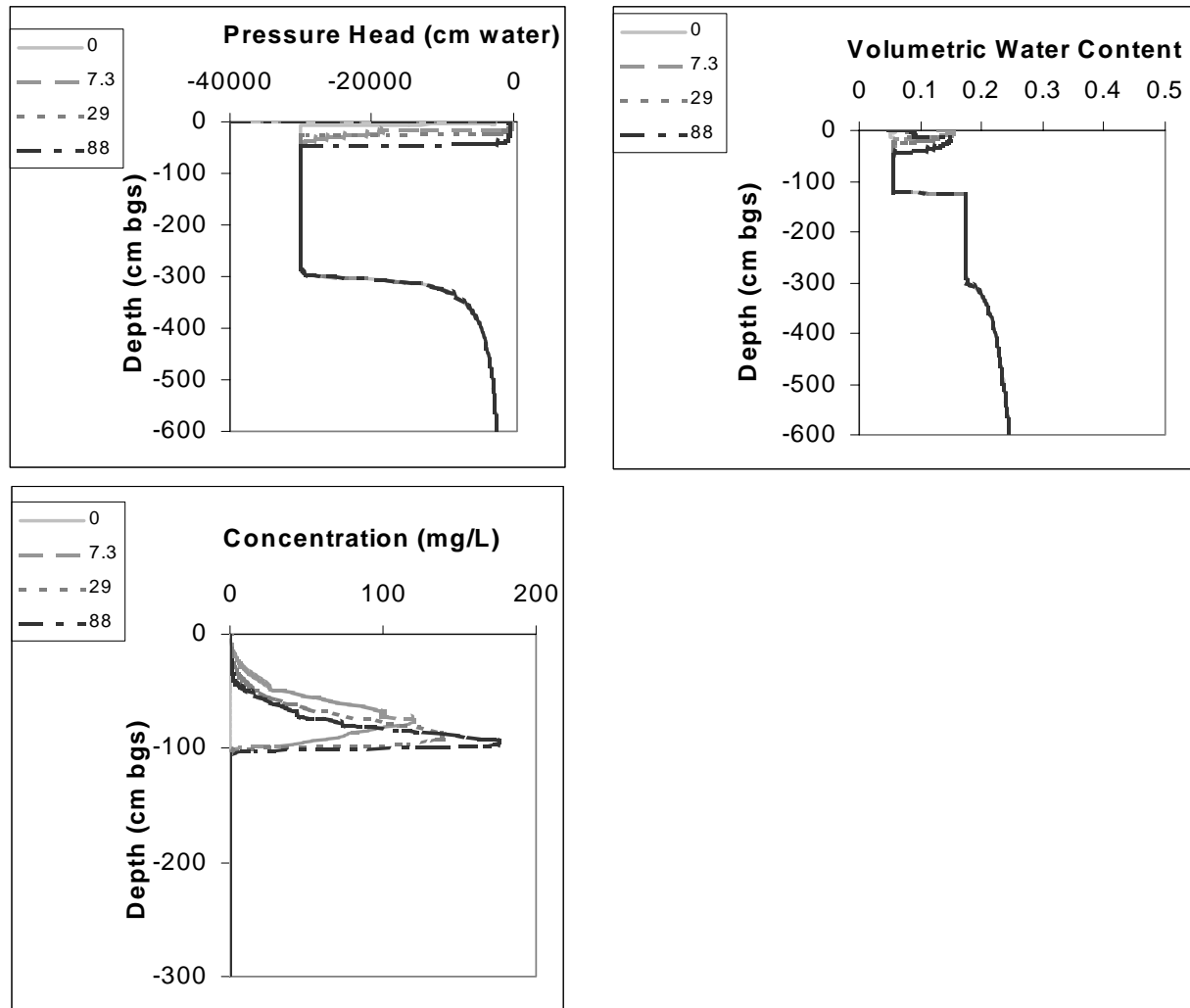


Figure B7. Plots of HYDRUS output from sensitivity analysis, design point #7.

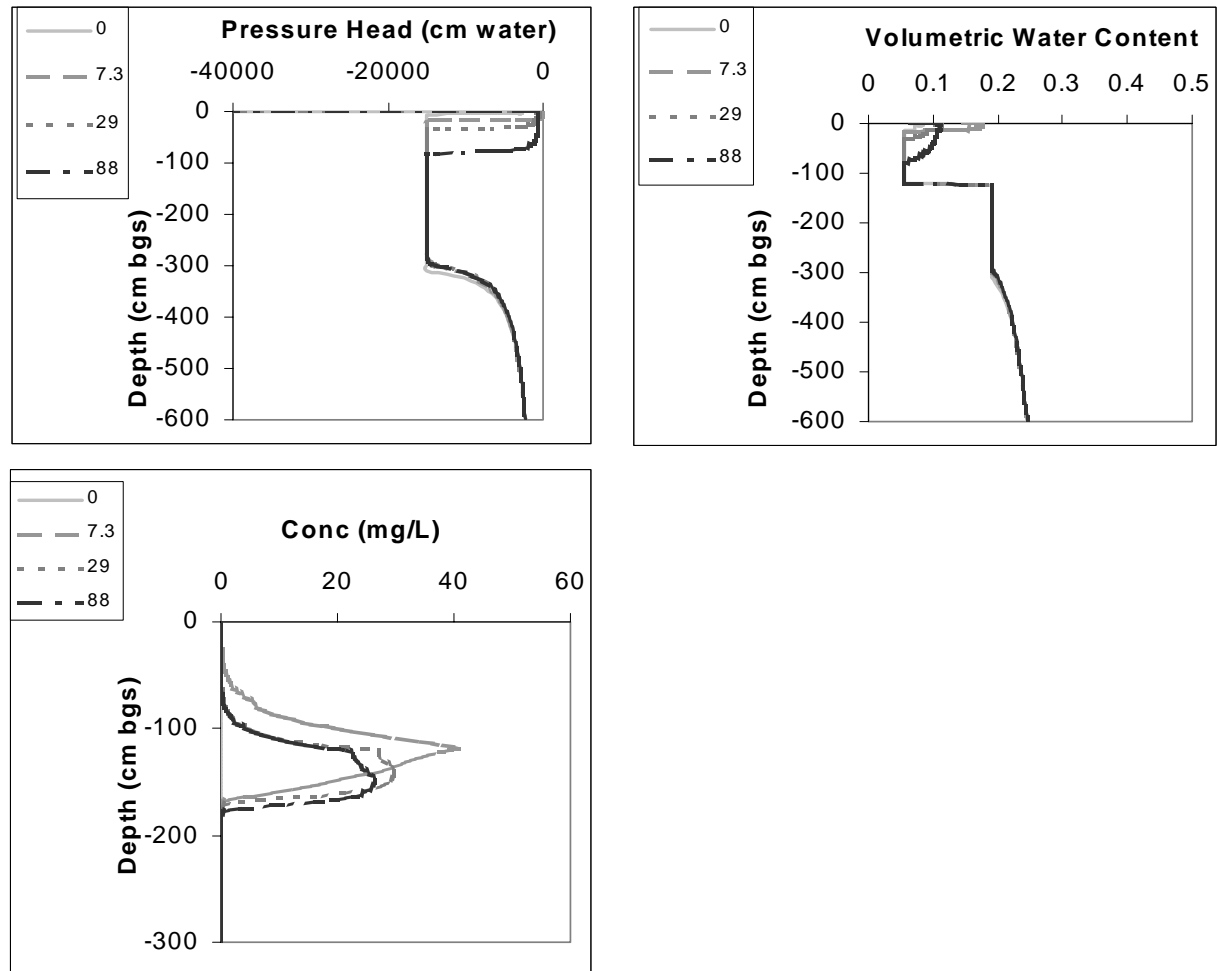


Figure B8. Plots of HYDRUS output from sensitivity analysis, design point #8.

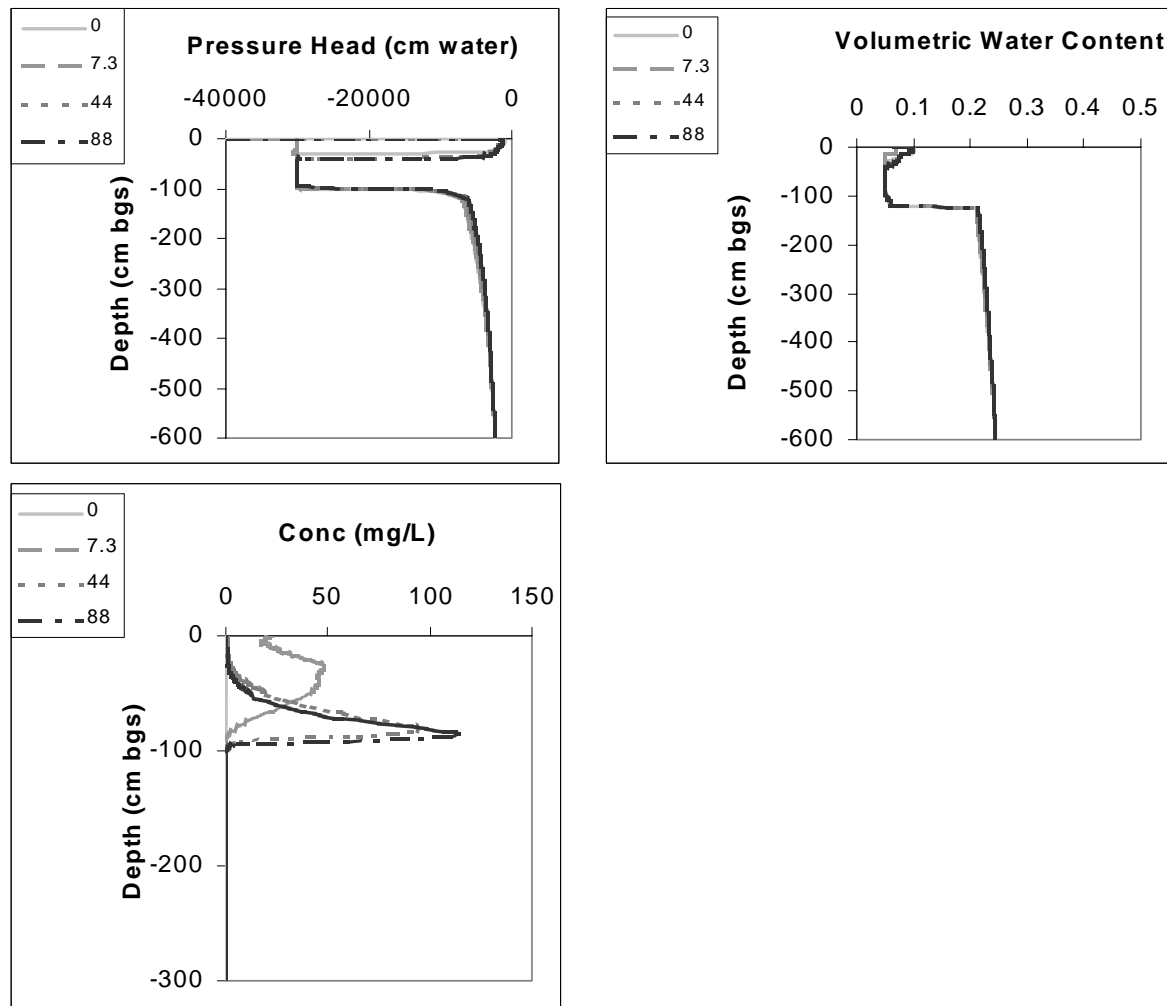


Figure B9. Plots of HYDRUS output from sensitivity analysis, design point #9.

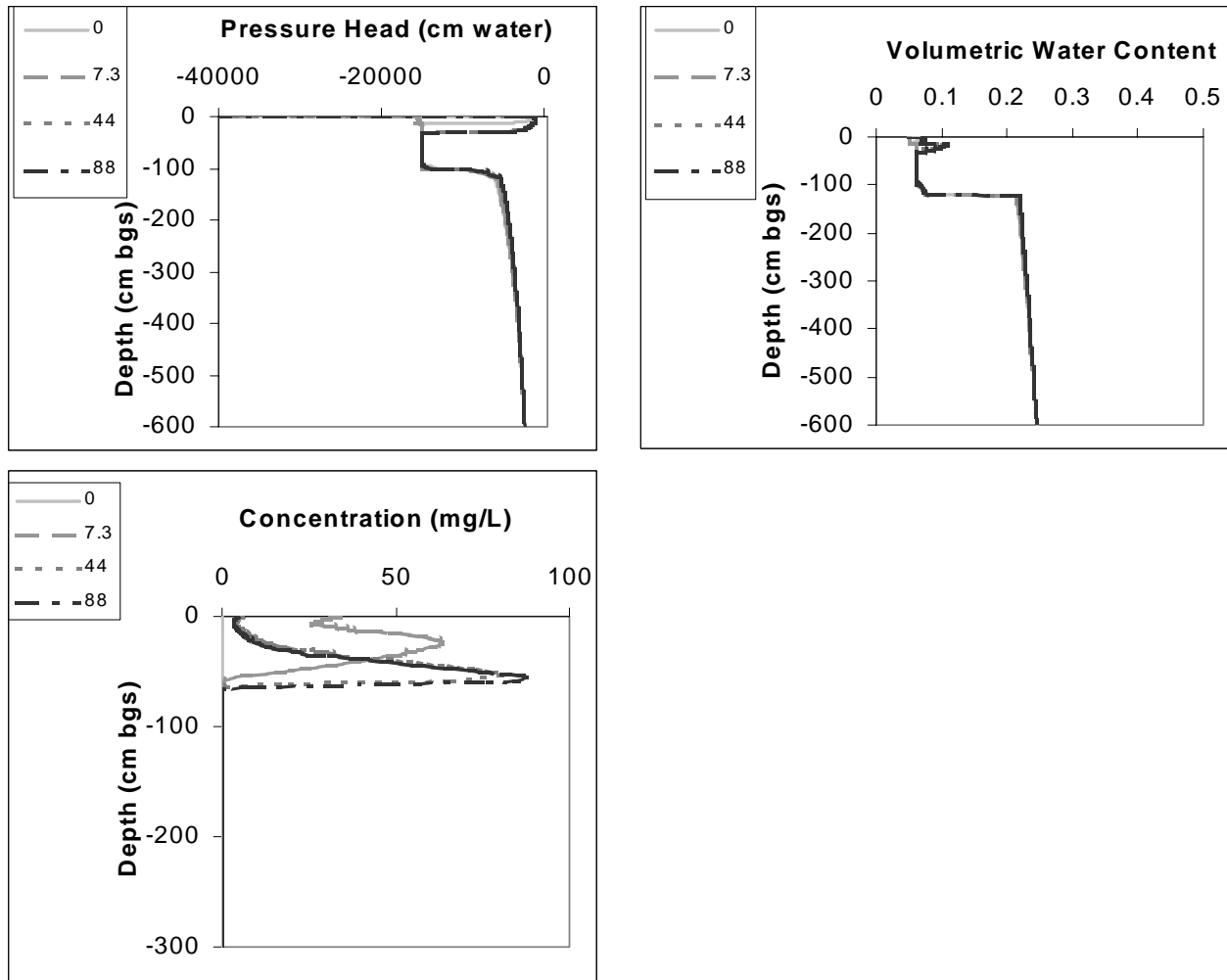


Figure B10. Plots of HYDRUS output from sensitivity analysis, design point #10.

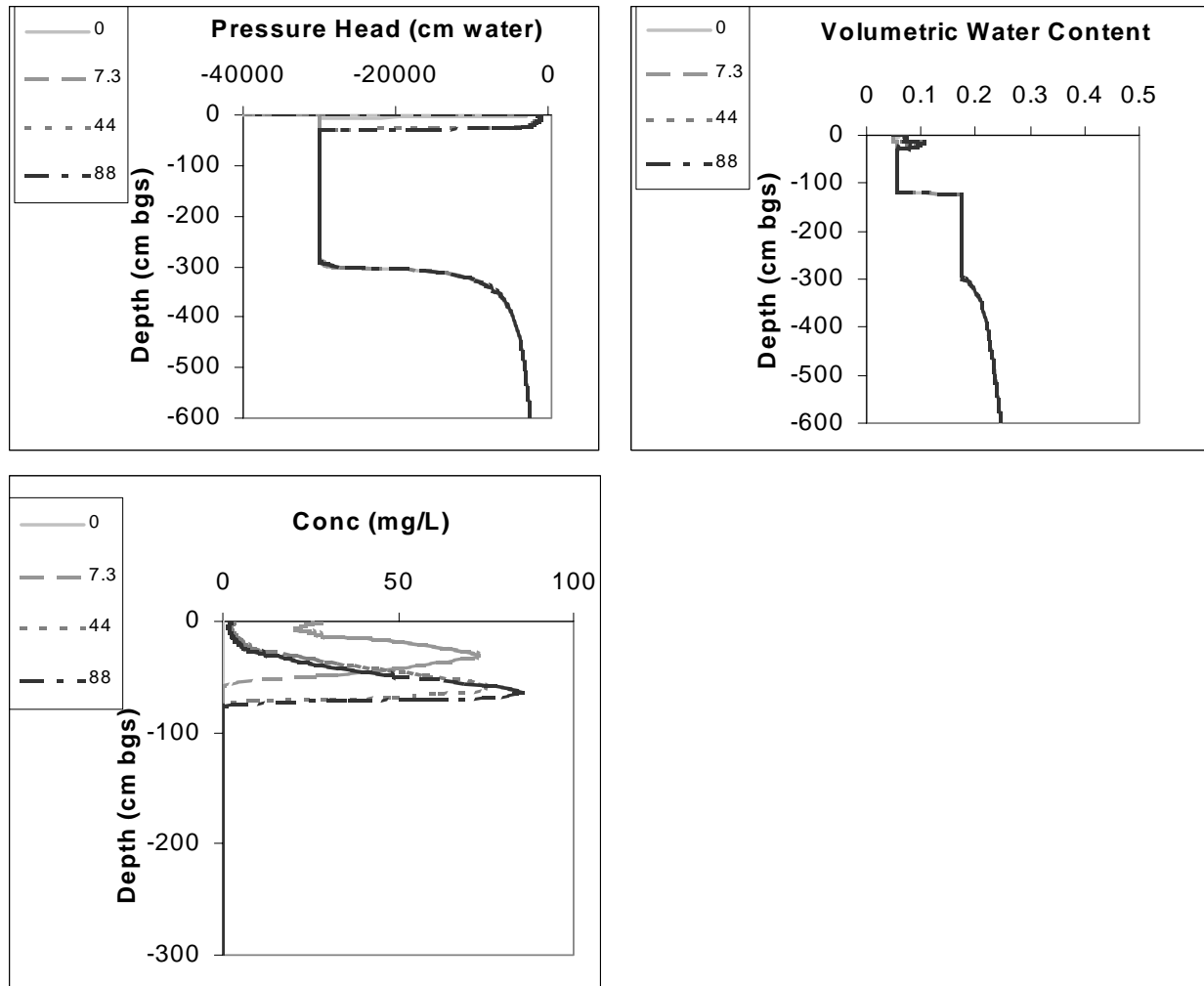


Figure B11. Plots of HYDRUS output from sensitivity analysis, design point #11.

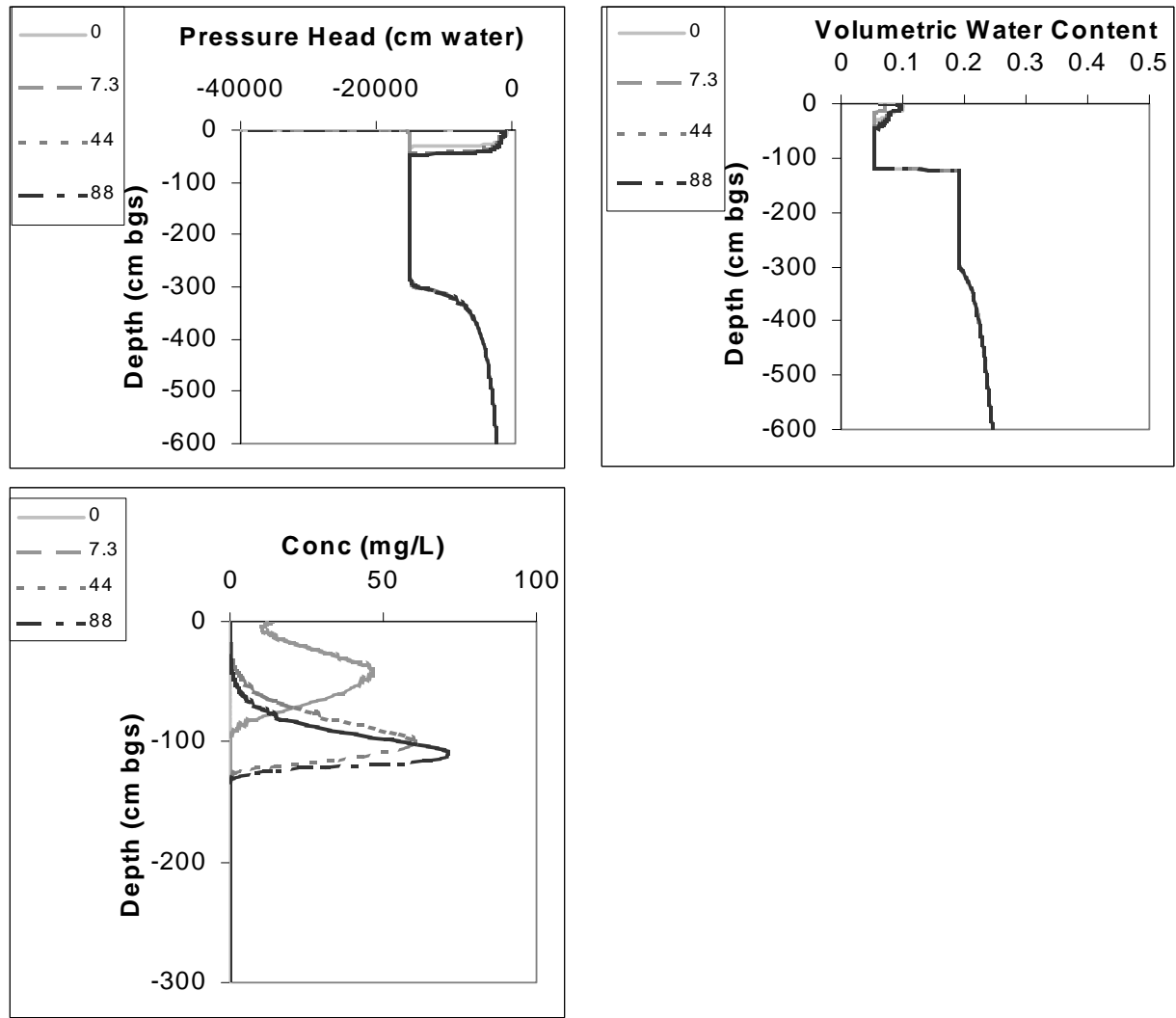


Figure B12. Plots of HYDRUS output from sensitivity analysis, design point #12.

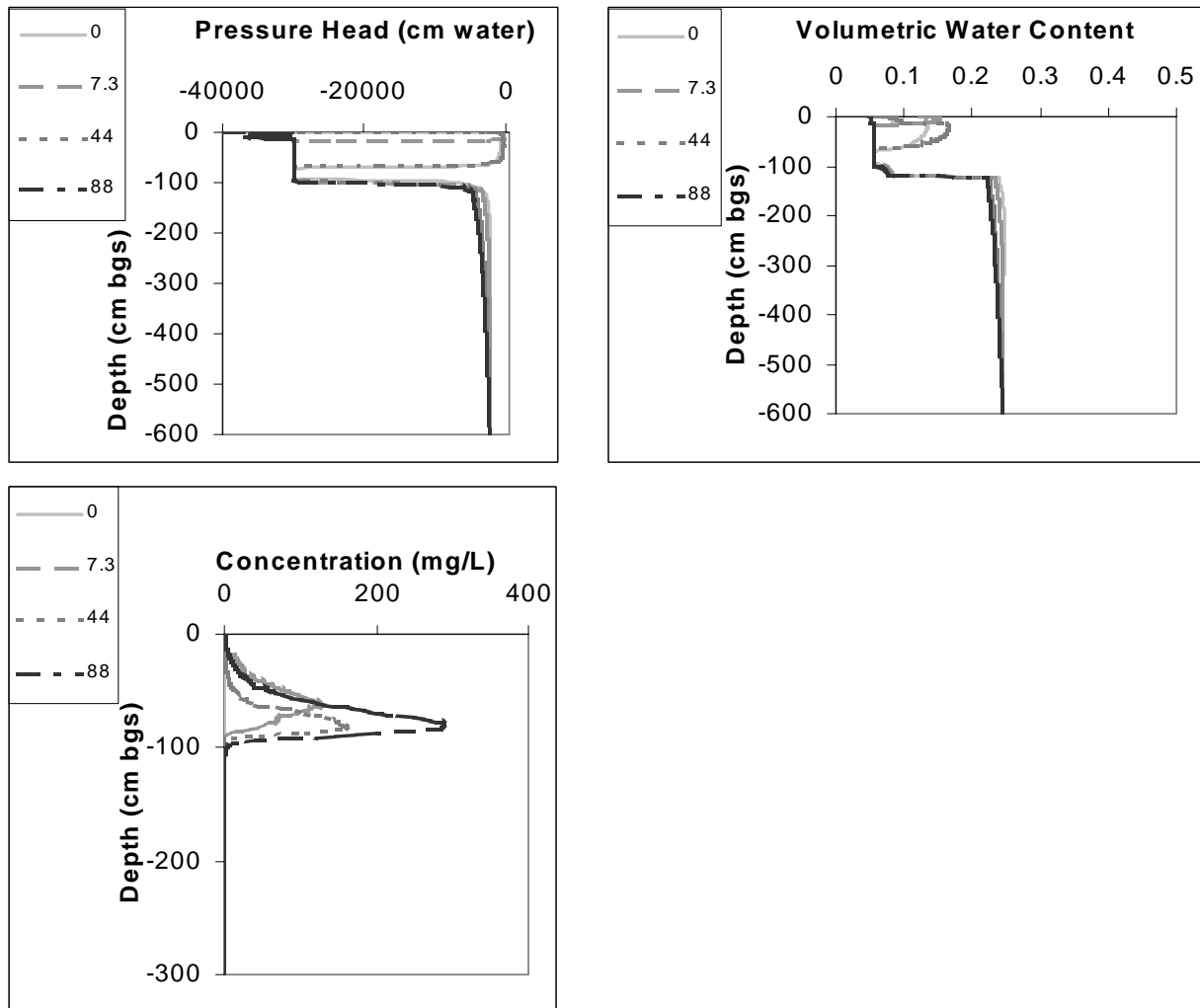


Figure B13. Plots of HYDRUS output from sensitivity analysis, design point #13.

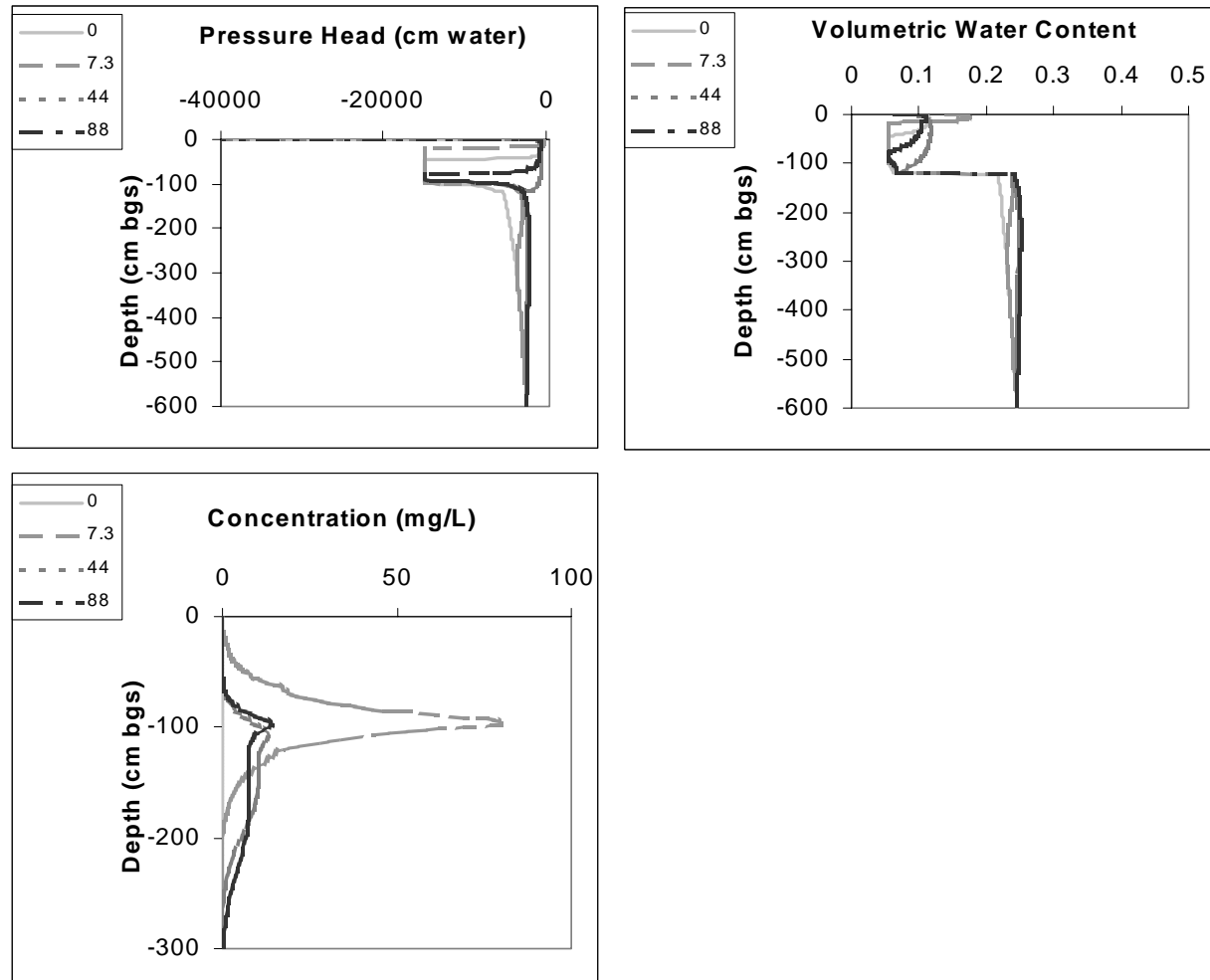


Figure B14. Plots of HYDRUS output from sensitivity analysis, design point #14.

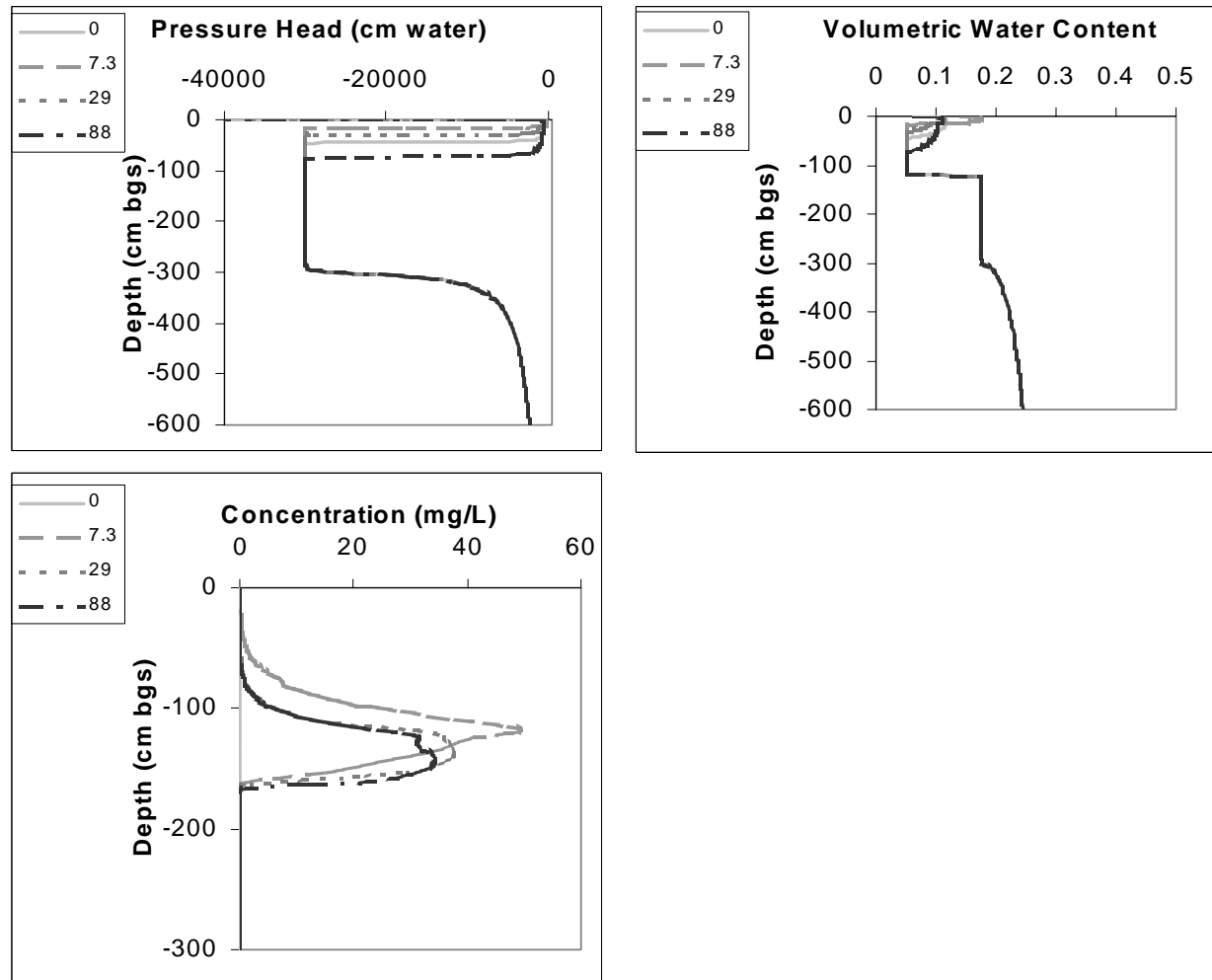


Figure B15. Plots of HYDRUS output from sensitivity analysis, design point #15.

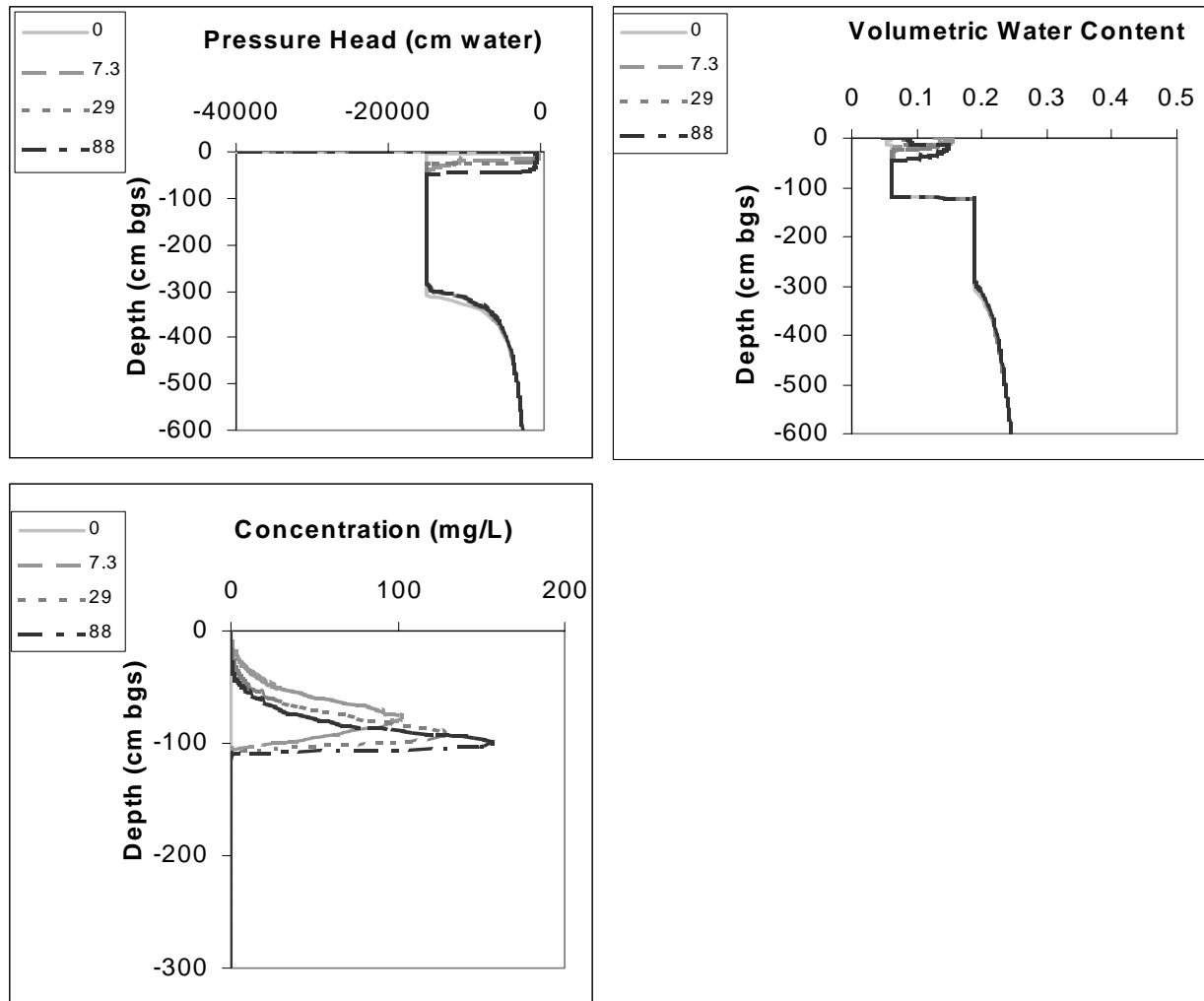


Figure B16. Plots of HYDRUS output from sensitivity analysis, design point #16.

APPENDIX C. TRENCH SOIL PROFILES AND FULL SOIL PROFILES.

H. Edward Bulloch, Jr., of the US Bureau of Indian Affairs was kind enough to come out to Fernandez Pueblo for a day's work with the author. This was during the time that the soil trenches were dug, in June of 1995 (refer to figure 2 in Chapter 2). He made soil profiles for seven rather arbitrarily-located sections along the trenches. Soil profiles based on his findings are shown as figures C1 through C7. The coordinates on these profiles are in the system local to the pueblo that was developed by the archeologists. Figure C8 is a copy of the site map made by the archaeologists of UNM-OCA, with the local coordinates system included [Doleman, 1995].

In addition, Mr. Bulloch performed particle size analyses on the cutting samples from the air rotary drilling of borehole 72. A soil profile based on these samples is shown as figure 9.

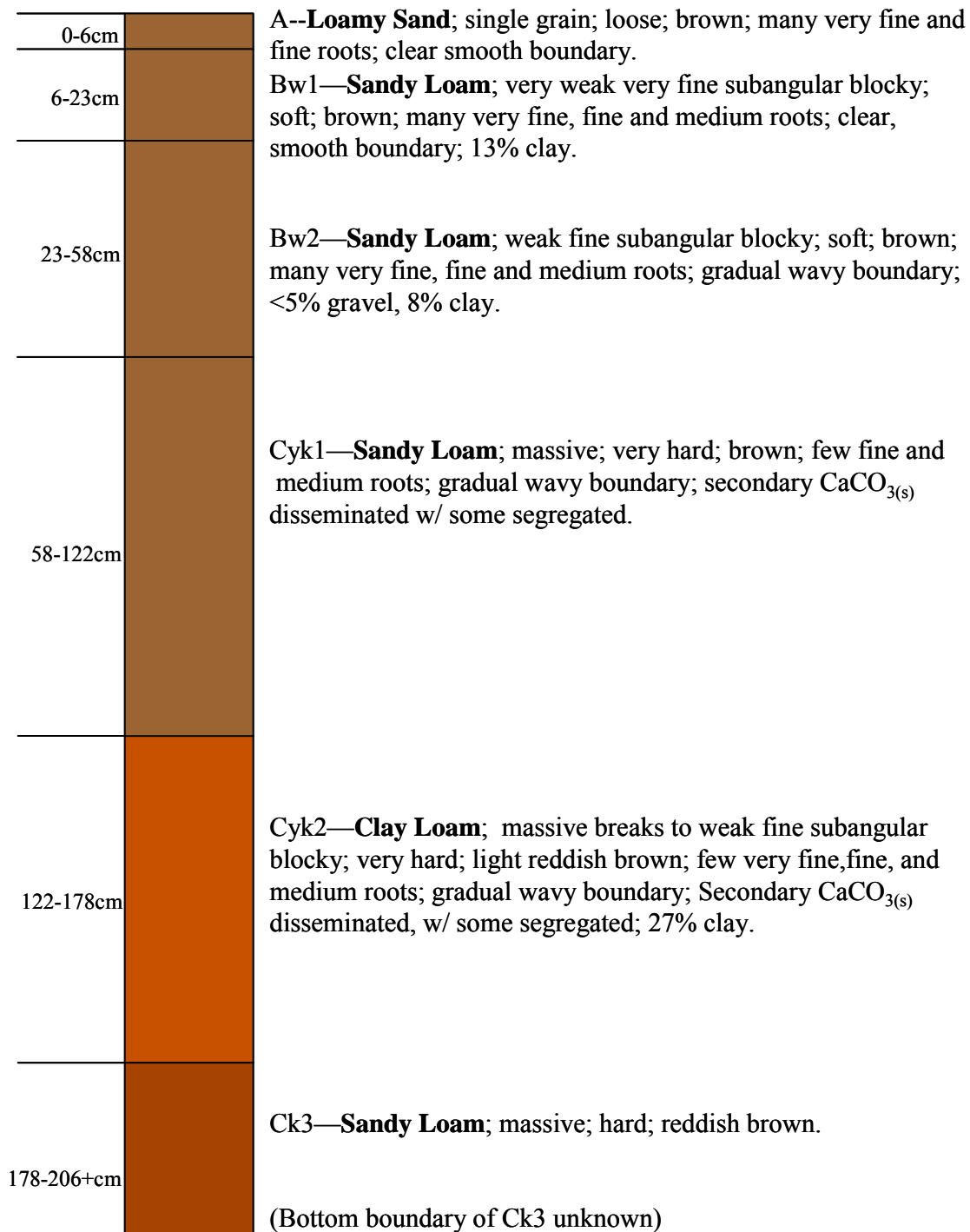


Figure C1. Soil profile at 544.5N : 581.7E.

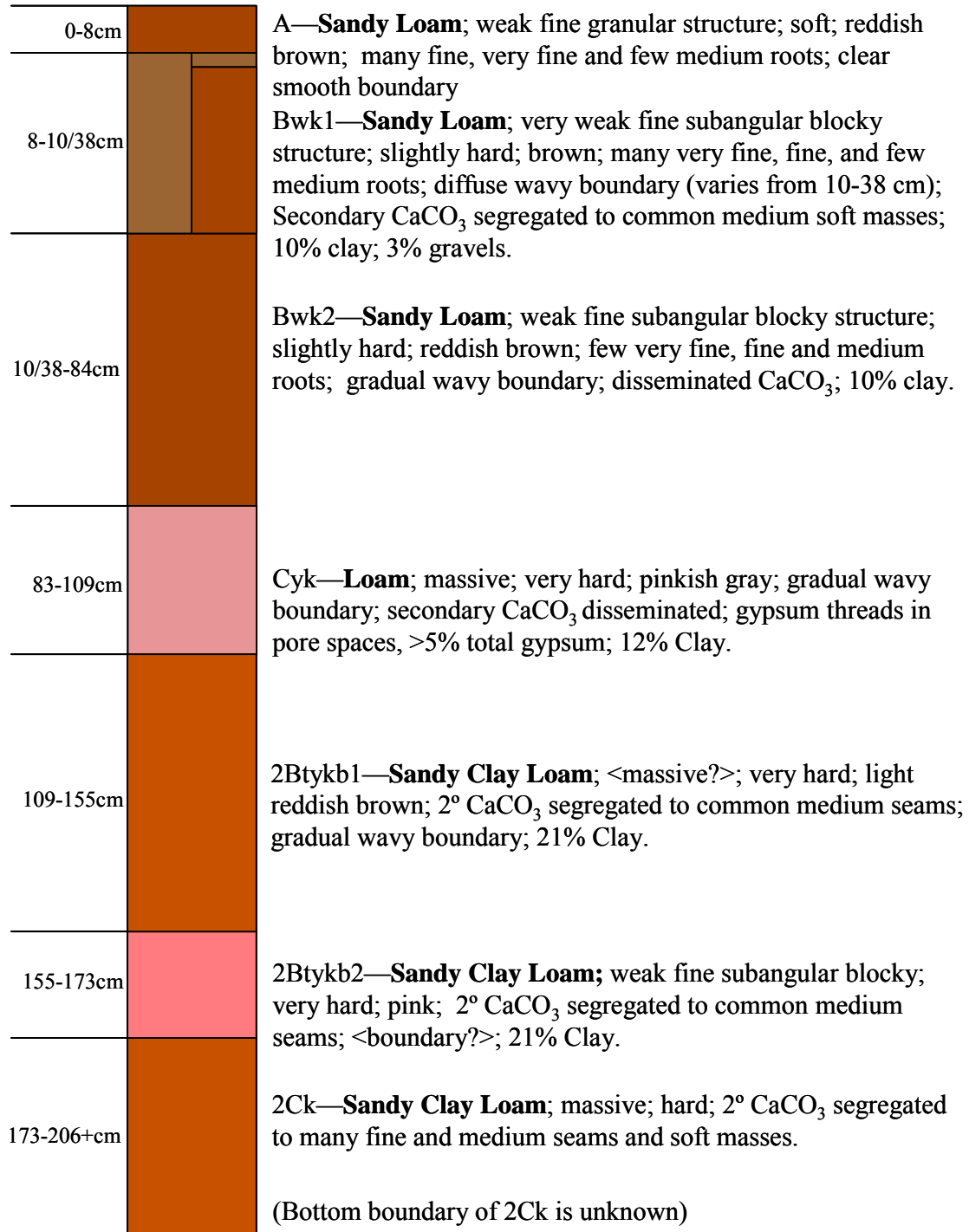


Figure C2. Soil profile at 544.5N : 594E

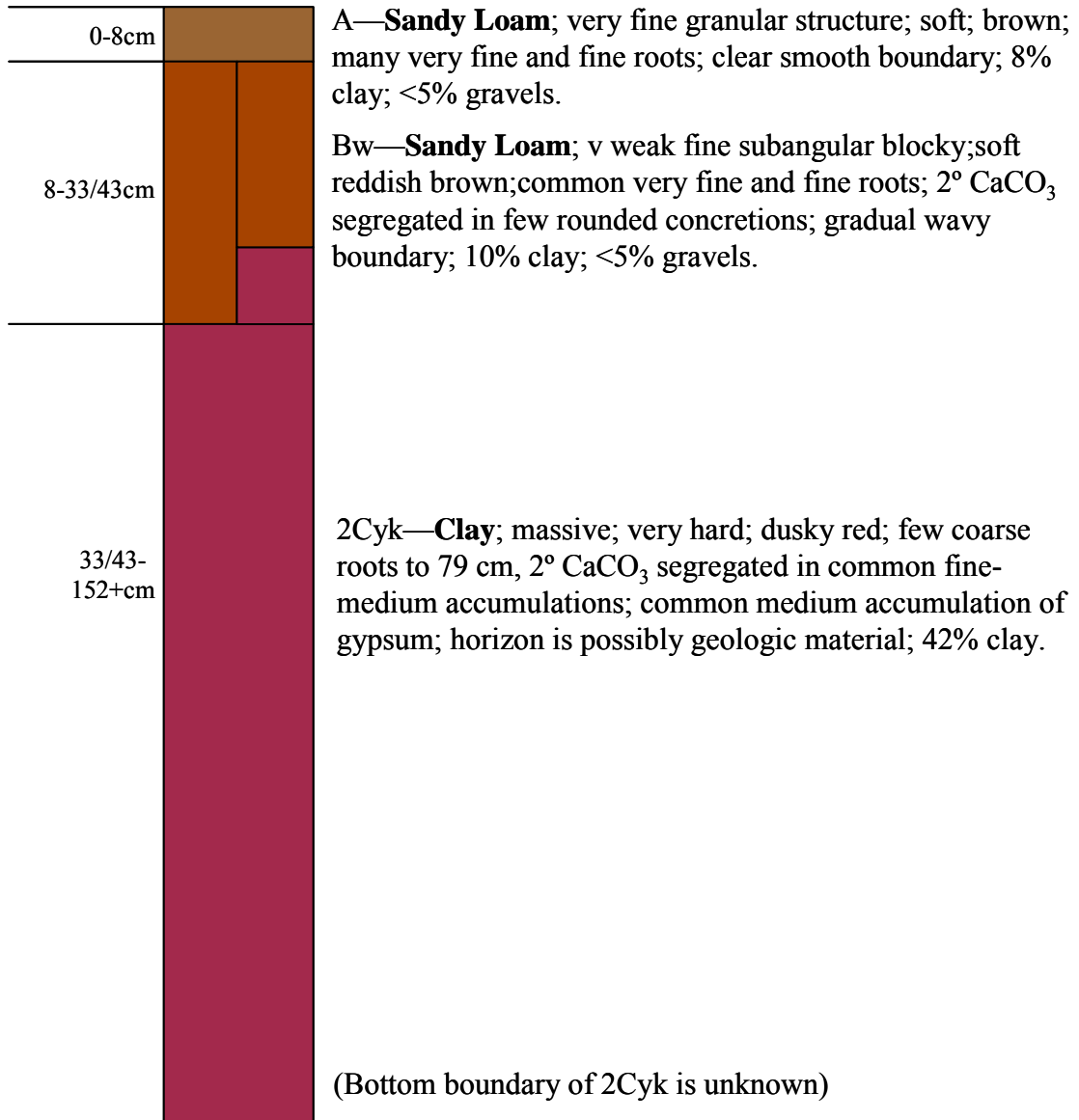


Figure C3. Soil profile at 544.5N : 571E.

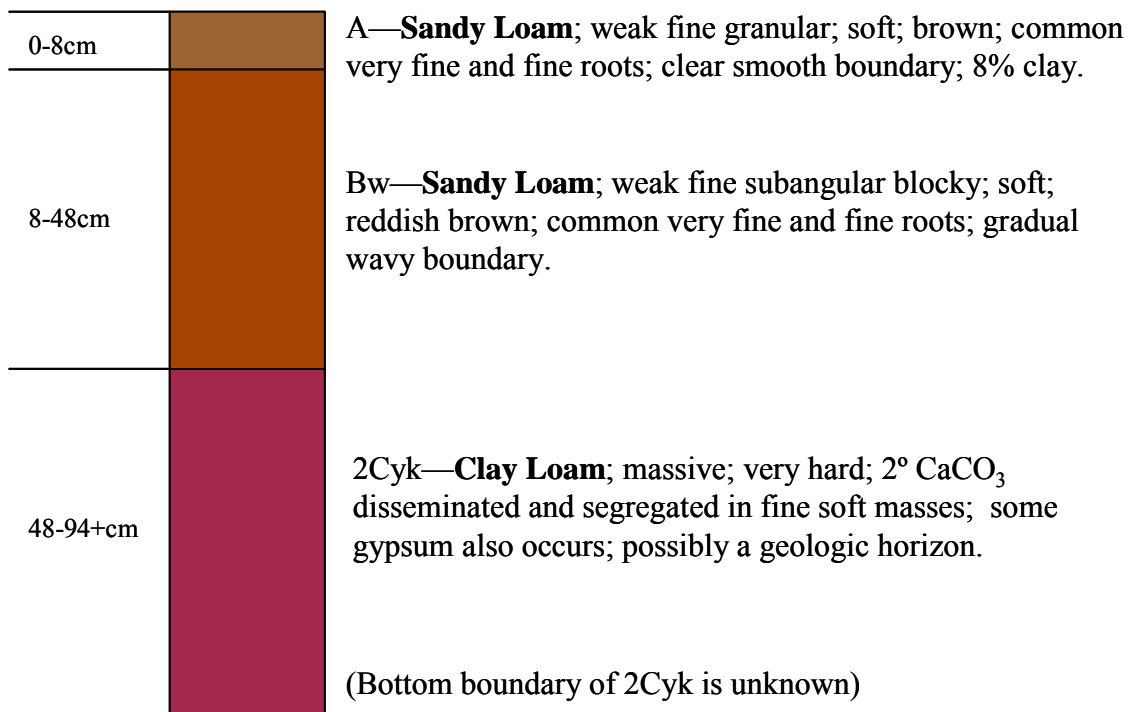


Figure C4. Soil profile at 544.5N : 565E.

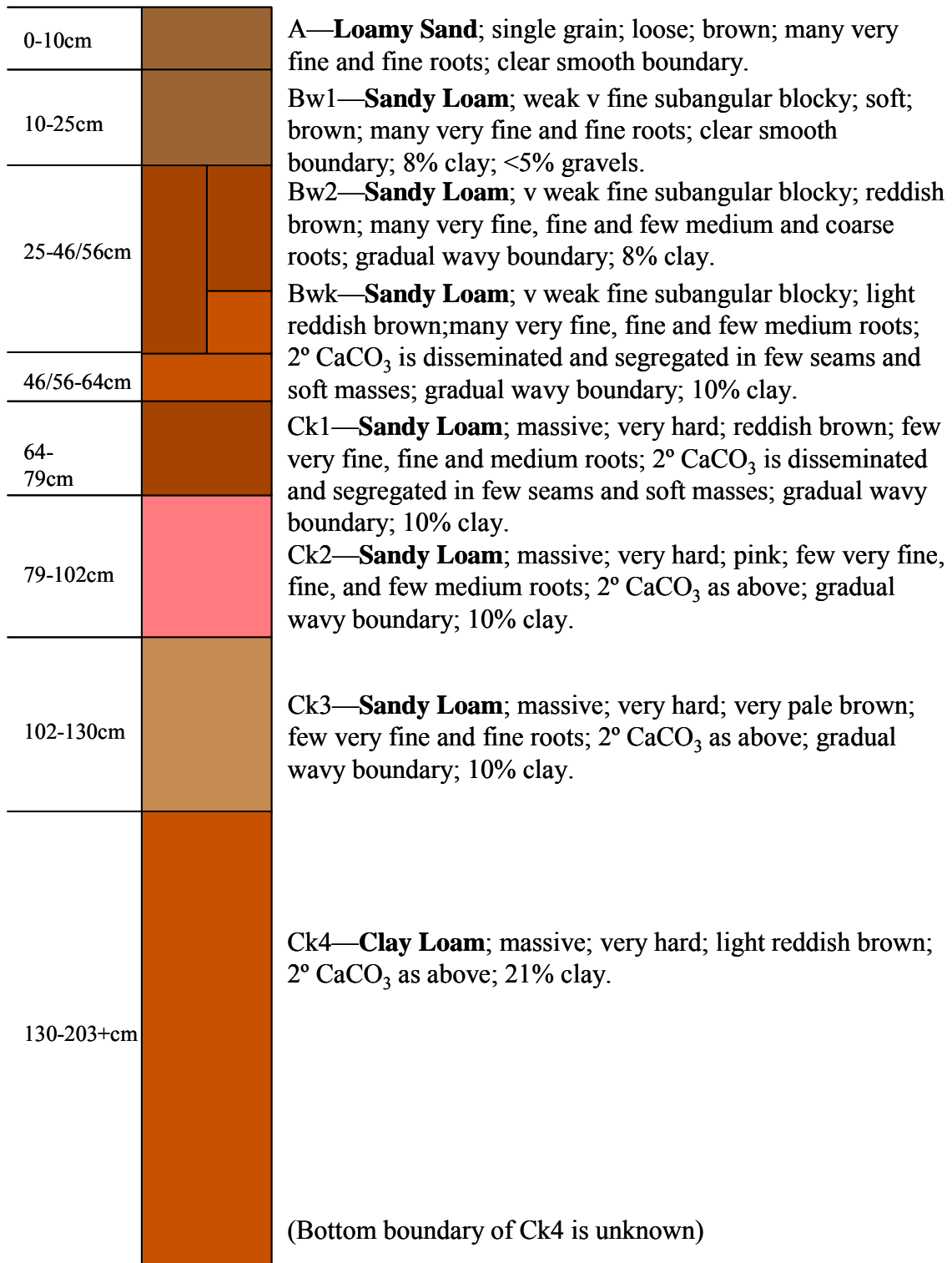


Figure C5. Soil profile at 580.5N : 577E.






0-10cm		A— Loamy Sand ; single grain; loose; brown; many very fine and fine roots; clear smooth boundary; <1% gravel.
10-33cm		Bwk1— Sandy Loam ; weak fine subangular blocky; soft; light reddish brown; common very fine, fine, and few medium roots; 2° CaCO ₃ disseminated and segregated in few medium seams and soft masses; gradual wavy boundary; 12% clay.
33-107cm		Bwk2— Sandy Loam ; weak fine subangular blocky; hard; light reddish brown; few very fine, fine, and medium roots; 2° CaCO ₃ as above; gradual wavy boundary.
107-142cm		2Cyk— Loam ; massive; hard; pinkish white; few very fine, fine and medium roots; 2° CaCO ₃ disseminated; diffuse irregular boundary.
142-203+cm		2Ck— Loamy Sand ; massive; soft; pink; 2° CaCO ₃ disseminated. (Bottom boundary of 2Ck is unknown)

Figure C6. Soil profile at 580.5N : 596.5E.

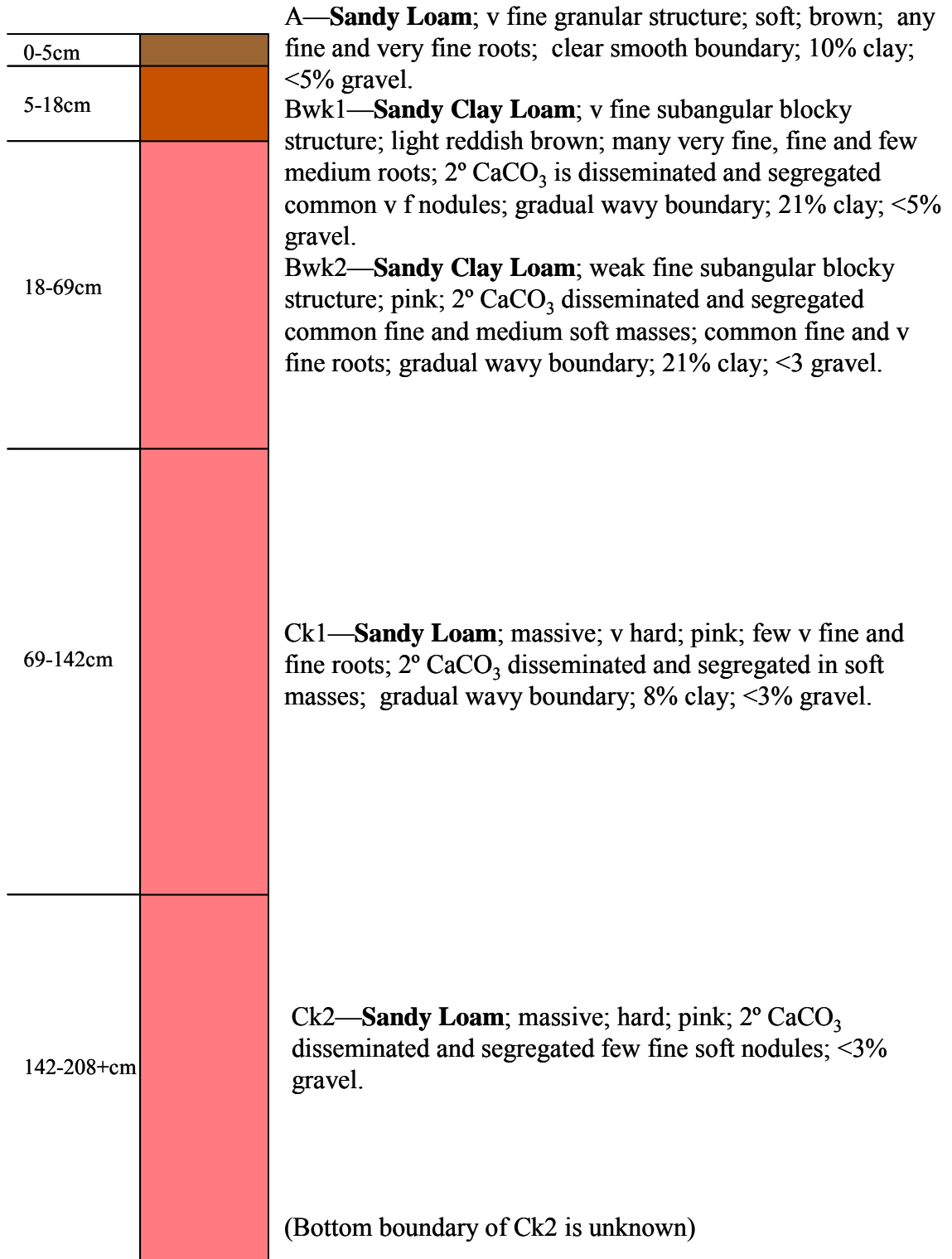


Figure C7. Soil profile at 580.5N: 622.5E

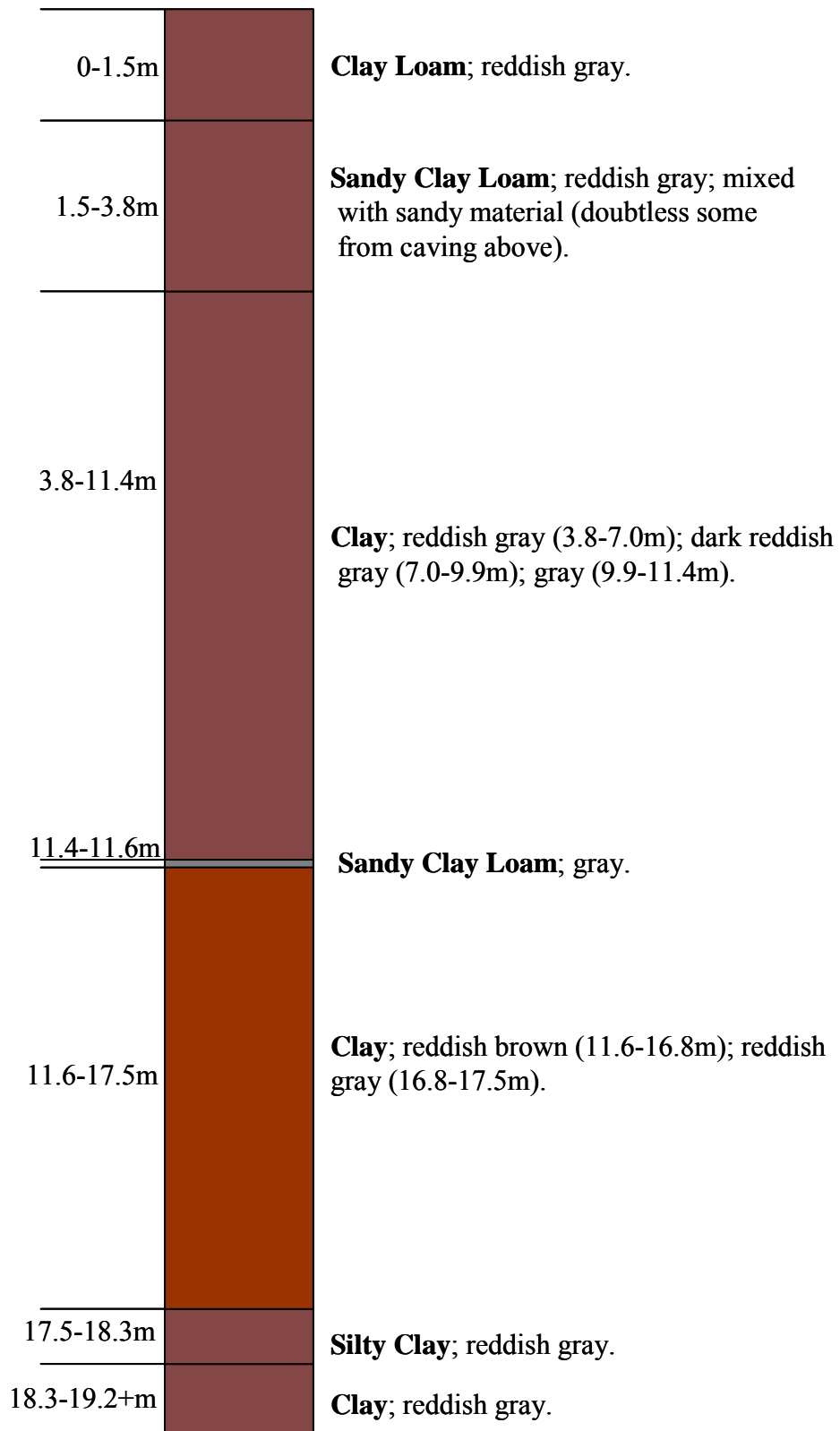


Figure C9: Soil profile inferred from grab samples taken during drilling of borehole 72 [605N:552E].

**APPENDIX D. A FEW COMMENTS ON OBSERVING AND MODELING A
RATIO OF SOLUTES.**

The advection-dispersion equation and its common variants are the standard models used for solute transport in subsurface hydrology. Within these models are the assumptions that actual solute transport is a combination of two separate but not independent processes, advection and dispersion. Advection moves a solute from its source in the direction of flow, as if it were a rigid body moving in the sense that all solute particles retain their spatial relationships with each other. Dispersion is a group of processes that all tend to thin the solute concentration, by causing the particles of solute (individual molecules and groups of molecules) to move apart from each other, to spread away from their mean position. But is this equation and the attendant model of solute transport appropriate, when one is concerned with tracking a ratio of solutes, such as the chloride/bromide ratio used in this Midden Project research? What follows is a derivation and some discussion that partly addresses this issue.

The following derivation is essentially identical to the one Wolff used in his independent study [1990], except that he assumed saturated conditions. Relaxing this assumption does change some important details in the final result.

The advection-dispersion equation for one-dimensional transport of an ideal, conservative solute in unsaturated media is:

$$\frac{\partial}{\partial x} \left(D\theta \frac{\partial C}{\partial x} \right) - \frac{\partial(Cq)}{\partial x} - \frac{\partial(C\theta)}{\partial t} = 0 \quad (\text{D1}).$$

Let C and S be two ideal conservative solutes. Assuming that the dispersion coefficients are the same, equations of transport like (D1) for these solutes may be added and rearranged as:

$$\frac{\partial}{\partial x} \left[\theta D \frac{\partial(C+S)}{\partial x} \right] - \frac{\partial(qC+qS)}{\partial x} - \frac{\partial(\theta C+\theta S)}{\partial t} = 0 \quad (\text{D2}).$$

We substitute for $(C+S)$ by noting that $\alpha(C+S) = \alpha S(C/S+1)$, where α is a generic coefficient. This substitution allows us the following transformations for the dispersion, advection, and storage terms in (D2):

$$\begin{aligned} & \frac{\partial}{\partial x} \left\{ \theta D \frac{\partial}{\partial x} [S(C/S+1)] \right\} = \\ & (C/S+1) \frac{\partial}{\partial x} \left[\theta D \frac{\partial S}{\partial x} \right] + S \frac{\partial}{\partial x} \left[\theta D \frac{\partial(C/S)}{\partial x} \right] + 2\theta D \frac{\partial S}{\partial x} \frac{\partial(C/S)}{\partial x} \end{aligned} \quad (\text{D3a}),$$

$$\frac{\partial}{\partial x} [qs(C/S+1)] = (C/S+1) \frac{\partial(qs)}{\partial x} + qS \frac{\partial(C/S)}{\partial x} \quad (\text{D3b}),$$

and

$$\frac{\partial}{\partial t} [\theta S(C/S+1)] = (C/S+1) \frac{\partial(\theta S)}{\partial t} + \theta S \frac{\partial(C/S)}{\partial t} \quad (\text{D3c}).$$

Substitution of (D3a-c) into (D2) gives, after rearrangement,

$$\begin{aligned} & S \left\{ \frac{\partial}{\partial x} \left[\theta D \frac{\partial(C/S)}{\partial x} \right] - q \frac{\partial(C/S)}{\partial x} - \theta \frac{\partial(C/S)}{\partial t} \right\} \\ & + (C/S+1) \left\{ \frac{\partial}{\partial x} \left[\theta D \frac{\partial S}{\partial x} \right] - \frac{\partial(qs)}{\partial x} - \frac{\partial(\theta S)}{\partial t} \right\} \\ & + 2\theta D \frac{\partial S}{\partial x} \frac{\partial(C/S)}{\partial x} = 0 \end{aligned} \quad (\text{D4}).$$

The part of the second term in (D4) that is in braces is collectively equal to 0, because it is identical to the left-hand-side of equation (D1) for the denominator species S . Dividing what is left of (D4) after this cancellation by S gives the final result:

$$\frac{\partial}{\partial x} \left[\theta D \frac{\partial(C/S)}{\partial x} \right] - \left[q - \frac{2\theta D}{S} \frac{\partial S}{\partial x} \right] \frac{\partial(C/S)}{\partial x} - \theta \frac{\partial(C/S)}{\partial t} = 0 \quad (\text{D5}).$$

This result has the same form as (D1) except for a couple of important differences. First, just like in Wolff's result, the advective part in (D5)—that part which includes the first-order space derivative, $\frac{\partial(C/S)}{\partial x}$ --includes a new term, when compared to the standard ADE in (D1). The apparent specific discharge based on the movement of a ratio of solutes will therefore be given by

$$q_{app} = q - \frac{2\theta D}{S} \frac{\partial S}{\partial x} \quad (\text{D6a}),$$

and the apparent groundwater velocity will be

$$v_{app} = v - \frac{2D}{S} \frac{\partial S}{\partial x} \quad (\text{D6b}).$$

This means that, in the presence of an increasing concentration of the denominator species in the ratio (Br^- in our case), the apparent specific discharge and velocity will underestimate the actual specific discharge and velocity. Curiously, this effect is independent of the slope of the numerator species concentration (Cl^- in our case). Apparently, the math turns out this way because the numerator species is in the “proper” position of a solute within the derivatives (D3a-c) that lead to the result (D5), unlike the denominator species.

With reference to the Midden Project data, it has been previously noted that the position of the Cl:Br ratio peak significantly “lagged behind” the $\text{NO}_3\text{-N}$ peak.

Moreover, these two anthropogenic peaks are on the rising leg of the environmental peaks of Cl and Br. The previous derivation allows us to explore the possibility that this lag in the Cl:Br peak might be primarily due to the apparent (negative) advection due to the dispersion of Br⁻. An analysis follows.

When one reads the position of the peak of a solute ratio off of a profile, compares it to its source location, and uses these to calculate velocity and specific discharge, one is implicitly assuming that a model like equation (D1) applies, absent any retardation due to sorption or like effects. But (D5) shows that the apparent advection (and peak position) of a ratio of solutes is dependent not only on the velocity, but also on the dispersion coefficient, and concentration of the denominator species, and concentration gradient of the denominator species.

Now *suppose* that the difference between the Cl:Br peak position and the NO₃-N position is entirely caused by the dispersion-induced advection effect outlined above, and assume that the dispersion coefficients for all three species are sufficiently alike. Then we can solve for an effective dispersion coefficient for the solutes from (D6b) above, and the data from borehole 71.

v_{app} = average apparent water velocity, based on the Cl:Br peak = 1.8 mm yr⁻¹,

v = actual water velocity, assuming that the NO₃ peak is reflective of it = 2.9 mm yr⁻¹,

S = average Br⁻ concentration in range between 1 to 3 m bgs (the approximate range of the Cl:Br ratio peak) = 17 mg l⁻¹, (see figure D1),

$\partial[Br^-]/\partial x$ between 1 and 3 m bgs \approx 10 mg l⁻¹ m⁻¹, (fig. D1).

Rearranging (D6b) for dispersion gives

$$D = \frac{v - v_{app}}{2} [Br^- \left(\frac{\partial [Br^-]}{\partial x} \right)^{-1}] = 3 \times 10^{-7} \text{ cm}^2 \text{ s}^{-1}.$$

The tabulated values for the *diffusion* coefficients of common Cl^- , Br^- , and NO_3^- salts in free water are all roughly $2 \times 10^{-5} \text{ cm}^2 \text{ s}^{-1}$ in the range 0.01 to 1 molar concentrations [Weast et al., 1986]. Thus, even allowing for a high tortuosity (>100), we can hypothesize that this dispersion-induced apparent advection (here, the only component of dispersion being considered is diffusion) might be responsible for the difference in position between the two anthropogenic solute signals. But this is almost pure speculation in the case of the Cl:Br ratio at Fernandez Pueblo, except that no other logical reason for the anthropogenic signal disparity has come to light. The main point of interest here is that ratios of solutes are commonly used in isotope tracer studies, and over long times in the case of studies of desert ground water recharge and waste interment. It may be interesting in future research to investigate whether this dispersion-induced apparent advection has had any impact on previously-performed $^{36}\text{Cl}/\text{Cl}$ studies.

A second difference between equations (D1) and (D5) is that the specific discharge, q , is outside the space derivative in the advective term of (D5) while it is inside the space derivative in (D1). Likewise, the volumetric water content, θ , is analogously outside the time derivative in the storage term in (D5) while it is inside the time derivative in (D1). This means that there might be a problem in modeling the movement (or assessing the meaning of actual transport) of a *ratio* of solutes in unsaturated flow using (D1), if either $\frac{\partial q}{\partial x}$ or $\frac{\partial \theta}{\partial t}$ are “sufficiently” large. In the particular solute transport studied here this would tend to be a problem at early time, because at early time is when the solute is nearest the surface, and hence most exposed to the abrupt changes in water content and specific discharge that come with precipitation.

But I will not try to assess the potential impact of these derivative terms here; again, this might be an interesting bit of research to do.

References for Appendix D

Weast, R.C., M.J. Astle, W.H. Beyer [editors]. 1986. CRC Handbook of Chemistry and Physics. CRC Press, Inc. Boca Raton, FL.

Wolff, M. 1990. Dispersion induced advection of an isotope ratio. Master's Thesis, Department of Earth and Environmental Science, New Mexico Tech. Socorro, New Mexico.

**APPENDIX E. TWO ADDITIONAL HYDRUS SIMULATIONS EXPLORING
THE EFFECT OF K_{SAT} ON SOLUTE MOVEMENT.**

It was desired to see whether a doubling of the saturated hydraulic conductivities of the loamy sand, sandy loam, and clay layers would by itself produce a significant effect on the solute transport in the HYDRUS model. The conductivities of these layers in design points 8 and 12 were doubled and the model was run as before, until the solute transport became slow enough that further simulation seemed unnecessary. The new simulations were named simply “8A” and “12A”, and are identical except that 8A has the wet scenario top boundary condition, while 12A has the dry scenario top boundary condition. The saturated hydraulic conductivities of these simulations were 1.12×10^3 cm day⁻¹ for the loamy sand, 1.04×10^3 cm day⁻¹ for the sandy loam, and 3.00×10^1 cm day⁻¹ for the clay.

The results of simulations 8A and 12A are shown on Figure F1. Recall that these simulations were the same as design points 8 and 12 of the sensitivity analysis, except that they had double the K_{sat} as was used in the sensitivity analysis simulations, and were allowed to run for longer than 88 years of simulation time. The final position of the solute center of mass in simulation 8A was -155 cm after 88 years, in contrast to the -145 cm that was reached in design point 8 after 88 years. Thus, the doubling of the hydraulic conductivities caused an approximate 7% increase in the ability in the simulated system’s

ability to transport the surface-applied solute. The position of the solute center of mass in simulation 12A was -122 cm after 88 years of simulation, while the final position in design point 12 was -102 cm. In this case, then, doubling the hydraulic conductivity caused an ~18% increase in downward solute movement over the first 88 years of simulation. The final solute center of mass position in simulation 8A was -159 cm at 248 years, while the final solute center of mass position in simulation 12A was -131.9 cm after 264 years.

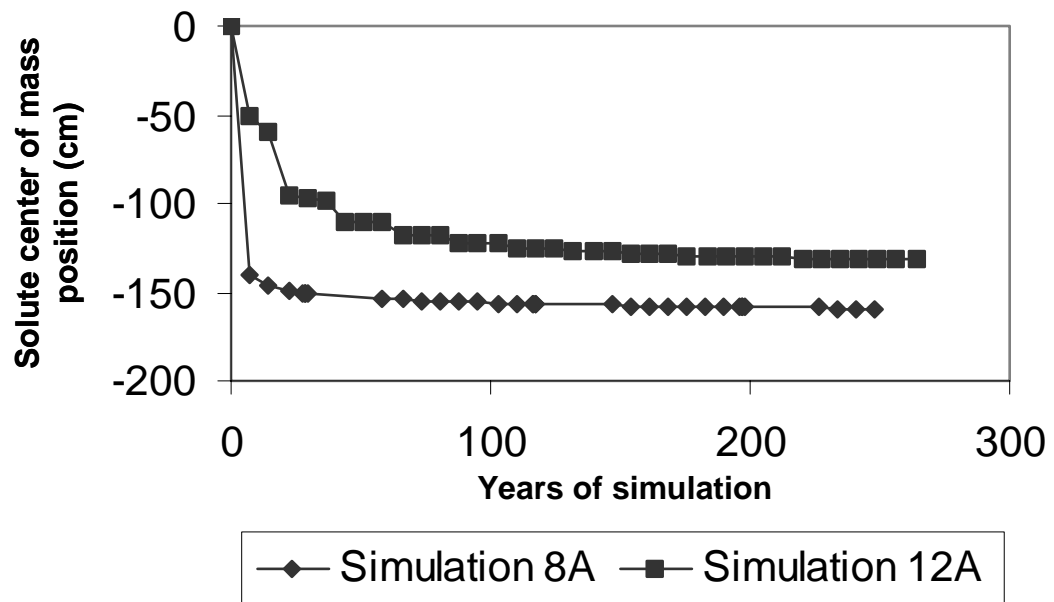


Figure E1. Results of the simulations 8A and 12A.

APPENDIX F. SAMPLE INPUT FILES FROM A HYDRUS SIMULATION.

The following are sample input files from the HYDRUS-1D simulations, that were described in detail in the body of this thesis. HYDRUS was prone to crash—either going divergent for no obvious reason, or simply not moving on to the next time step at some point—for very long simulations. All of the simulations in this work used *days* as the nominal time increment, and the boundary condition in the simulation was imposed for each day. The number of time steps used by HYDRUS usually ran into the tens of millions per hundred years of simulation time. To minimize the damage done when a simulation crashed, the long scenarios were broken into discrete chunks. For example, one simulation began the original wet scenario and ran for 80 years. The data at $t = 80$ years (29,220 days) was then used as the initial condition in the next simulation in the chain, and so on. This process was continued until the simulation was determined to be completed by near-zero movement of the anthropogenic solute, or the final time of the overall scenario or sensitivity design point was reached. These final times were 620 years for the dry and wet scenarios, and 88 years for the sensitivity analysis points. The particular files given here are for the years 273-368 of the wet scenario.

To easily distinguish the input files from regular text, they are in a different font (the regular text of this thesis is 12 point Times New Roman, while the input files are 12 point Courier New).

The file on this page is called "HYDRUS-1D.DAT". It mainly consists of logical switches that tell HYDRUS what processes are active for these simulations.

```
[Main]
HYDRUS_Version=2
WaterFlow=1
SoluteTransport=1
HeatTransport=0
EquilibriumAdsorption=1
RootWaterUptake=1
RootGrowth=0
MaterialNumbers=6
SubregionNumbers=1
SpaceUnit=cm
TimeUnit=days
PrintTimes=39
NumberOfSolutes=1
InitialCondition=0
;
[Profile]
NumberOfNodes=453
ProfileDepth=2.E+03
ObservationNodes=6
GridVisible=1
SnapToGrid=1
ProfileWidth=80
LeftMargin=40
GridOrgX=0
GridOrgY=0
GridDX=5.E+00
GridDY=5.E+00
```

The file on this page and the following two pages is called "Selector.in", and contains the basic water flow, solute transport , and root uptake information.

```

*** BLOCK A: BASIC INFORMATION *****
Heading
Re-start combo3 w/ all IC heads>-15000cm
LUnit  TUnit  MUnit  (indicated units are obligatory for all input data)
cm
days
mmol
lWat    lChem  lTemp  lSink  lRoot  lShort  lWDep  lScreen  lVariabBC  lEquil  lInverse
t       t      f      t      f      t      f      t      t          t      f
NMat    NLayer CosAlpha
6       1      1
*** BLOCK B: WATER FLOW INFORMATION *****
MaxIt   TolTh   TolH      (maximum number of iterations and tolerances)
80      0.001    1
TopInf  WLayer  KodTop  InitCond
t       t      -1      f
BotInf  qGWLf   Freed   SeepF   KodBot  DrainF
f       f      f      f      1      f
      hTab1   hTabN
      1e-006  10000
      Model  Hysteresis
      0      0
      thr   ths   Alfa   n      Ks      l
0.0485  0.3904  0.0347  1.7466  105.12  0.5
0.0387  0.387  0.0267  1.4484  38.25   0.5
0.0387  0.387  0.0267  1.4484  38.25   0.5
0.0982  0.4588  0.015  1.2529  14.75   0.5

```

```

0.09      0.11      0.015      1.2529      0.0001475      0.5
0.0633    0.3837    0.0211    1.3298      13.19          0.5
*** BLOCK C: TIME INFORMATION *****
      dt          dtMin          dtMax          DMul          DMul2          ItMin          ItMax          MPL
      0.1          1e-005          5            1.3            0.7            3             7             39
      tInit          tMax
      0.0001          227916
TPrint(1),TPrint(2),...,TPrint(MPL)
      5844          11688          17532          23376          29220          35064
      40908          46752          52596          58440          64284          70128
      75972          81816          87660          93504          99348          105192
      111036          116880          122724          128568          134412          140256
      146100          151944          157788          163632          169476          175320
      181164          187008          192852          198696          204540          210384
      216228          222072          227916
*** BLOCK F: SOLUTE TRANSPORT INFORMATION *****
Epsi  lUpW  lArtD  lTDep  cTolA  cTolR  MaxItC  PeCr  No.Solutes  lTort
0.5    f      f      f      0      0      1      2      1      t
      Bulk.d.      DisperL.      Frac      Mobile WC (1..NMat)
      1.5          10          1          0
      1.5          10          1          0
      1.5          10          1          0
      1.5          10          1          0
      1.5          10          1          0
      1.5          10          1          0
      DifW          DifG          n-th solute
      0            0
      Ks          Nu          Beta          Henry          SnkL1          SnkS1          SnkG1
SnkL1'          SnkS1'          SnkG1'          SnkL0          SnkS0          SnkG0          Alfa

```

```

0      0      0      1      0      0      0      0
0      0      0      0      0      0      0      0
0      0      0      1      0      0      0      0
0      0      0      0      0      0      0      0
0      0      0      1      0      0      0      0
0      0      0      0      0      0      0      0
0      0      0      1      0      0      0      0
0      0      0      0      0      0      0      0
0      0      0      1      0      0      0      0
0      0      0      0      0      0      0      0
0      0      0      1      0      0      0      0
0      0      0      0      0      0      0      0

```

```

kTopSolute  SolTop  kBotSolute  SolBot
-1          0        -1          0

```

```
tPulse
```

```
227916
```

```
*** BLOCK G: ROOT WATER UPTAKE INFORMATION *****
```

```
Model (0 - Feddes, 1 - S shape) cRootMax
```

```
0 1.41433e-038
```

```

P0      P2H      P2L      P3      r2H      r2L
-10     -200     -800     -15000  0.5     0.1

```

```
POptm(1),POptm(2),...,POptm(NMat)
```

```
-25     -25     -25     -25     -25     -25
```

```
Solute Reduction
```

```
f
```

```
*** END OF INPUT FILE 'SELECTOR.IN' *****
```

The following two pages contain an abbreviated version of the file "PROFILE.DAT". The complete file has all of the geometric information and the layer information for all of the finite difference/finite element nodes of the profile, as well as the initial conditions of matric potential and concentration.

```

3
  1  0.000000e+000  1.000000e+000  1.000000e+000
  2 -5.000000e+000  1.000000e+000  1.000000e+000
  3 -2.000000e+003  1.000000e+000  1.000000e+000
453   1   1   1 x           h           Mat   Lay           Beta           Axz
Bxz           Dxz           Temp           Conc           SConc
  1  0.000000e+000 -3.000000e+004           1           1  1.000000e+000  1.000000e+000
1.000000e+000  1.000000e+000  2.000000e+001  3.070000e+000
  2 -1.000000e-001 -4.773740e+003           1           1  1.000000e+000  1.000000e+000
1.000000e+000  1.000000e+000  2.000000e+001  3.040000e+000
  3 -2.000000e-001 -2.508570e+003           1           1  1.000000e+000  1.000000e+000
1.000000e+000  1.000000e+000  2.000000e+001  3.010000e+000
  4 -3.000000e-001 -1.885190e+003           1           1  1.000000e+000  1.000000e+000
1.000000e+000  1.000000e+000  2.000000e+001  2.980000e+000
  5 -4.000000e-001 -1.595390e+003           1           1  1.000000e+000  1.000000e+000
1.000000e+000  1.000000e+000  2.000000e+001  2.950000e+000
  6 -5.000000e-001 -1.427800e+003           1           1  1.000000e+000  1.000000e+000
1.000000e+000  1.000000e+000  2.000000e+001  2.920000e+000
  7 -6.000000e-001 -1.313340e+003           1           1  1.000000e+000  1.000000e+000
1.000000e+000  1.000000e+000  2.000000e+001  2.900000e+000
.
.
.

```

441	-1.994000e+003	4.852900e+002	5	1	0.000000e+000	1.000000e+000
1.000000e+000	1.000000e+000	2.000000e+001	0.000000e+000			
442	-1.994500e+003	4.865100e+002	5	1	0.000000e+000	1.000000e+000
1.000000e+000	1.000000e+000	2.000000e+001	0.000000e+000			
443	-1.995000e+003	4.877400e+002	5	1	0.000000e+000	1.000000e+000
1.000000e+000	1.000000e+000	2.000000e+001	0.000000e+000			
444	-1.995500e+003	4.889600e+002	5	1	0.000000e+000	1.000000e+000
1.000000e+000	1.000000e+000	2.000000e+001	0.000000e+000			
445	-1.996000e+003	4.901900e+002	5	1	0.000000e+000	1.000000e+000
1.000000e+000	1.000000e+000	2.000000e+001	0.000000e+000			
446	-1.996500e+003	4.914200e+002	5	1	0.000000e+000	1.000000e+000
1.000000e+000	1.000000e+000	2.000000e+001	0.000000e+000			
447	-1.997000e+003	4.926400e+002	5	1	0.000000e+000	1.000000e+000
1.000000e+000	1.000000e+000	2.000000e+001	0.000000e+000			
448	-1.997500e+003	4.938700e+002	5	1	0.000000e+000	1.000000e+000
1.000000e+000	1.000000e+000	2.000000e+001	0.000000e+000			
449	-1.998000e+003	4.951000e+002	5	1	0.000000e+000	1.000000e+000
1.000000e+000	1.000000e+000	2.000000e+001	0.000000e+000			
450	-1.998500e+003	4.963200e+002	5	1	0.000000e+000	1.000000e+000
1.000000e+000	1.000000e+000	2.000000e+001	0.000000e+000			
451	-1.999000e+003	4.975500e+002	5	1	0.000000e+000	1.000000e+000
1.000000e+000	1.000000e+000	2.000000e+001	0.000000e+000			
452	-1.999500e+003	4.987700e+002	5	1	0.000000e+000	1.000000e+000
1.000000e+000	1.000000e+000	2.000000e+001	0.000000e+000			
453	-2.000000e+003	5.000000e+002	5	1	0.000000e+000	1.000000e+000
1.000000e+000	1.000000e+000	2.000000e+001	0.000000e+000			

6

59 127 172 221 241 331

The following two pages contain an abbreviation of “ATMOSPH.IN”, which in its complete form contains the the entire top boundary condition record, including precipitation, potential evaporation and transpiration, and the input solute concentration coming in with the precipitation. Below are shown the input records for the first 21 days; the actual input file for this simulation contained records for 227,916 days.

```

*** BLOCK I: ATMOSPHERIC INFORMATION *****
  MaxAL                      (MaxAL = number of atmospheric data-records)
 227916
  hCritS                      (max. allowed pressure head at the soil surface)
    0
    tAtm                      Prec          rSoil          rRoot          hCritA          rB          hB
  ht      tTop              tBot          Ampl          cTop          cBot
0         1                0          0.196          0            30000          0            0
0         0                0          0            0            0            0            0
         2                0          0.174          0            30000          0            0
0         0                0          0            0            0            0            0
         3                0          0.161          0            30000          0            0
0         0                0          0            0            0            0            0
         4                0          0.161          0            30000          0            0
0         0                0          0            0            0            0            0
         5                0          0.181          0            30000          0            0
0         0                0          0            0            0            0            0
         6                0          0.176          0            30000          0            0
0         0                0          0            0            0            0            0
         7                0          0.199          0            30000          0            0
0         0                0          0            0            0            0            0

```


0	8	0	0.196	0	30000	0	0
0	0	0	0	0	0	0	0
0	9	0	0.215	0	30000	0	0
0	0	0	0	0	0	0	0
0	10	0	0.202	0	30000	0	0
0	0	0	0	0	0	0	0
0	11	0	0.231	0	30000	0	0
0	0	0	0	0	0	0	0
0	12	0	0.197	0	30000	0	0
0	0	0	0	0	0	0	0
0	13	0	0.188	0	30000	0	0
0	0	0	0	0	0	0	0
0	14	0	0.2	0	30000	0	0
0	0	0	0	0	0	0	0
0	15	0	0.188	0	30000	0	0
0	0	0	0	0	0	0	0
0	16	0	0.177	0	30000	0	0
0	0	0	0	0	0	0	0
0	17	0.127	0.082	0	30000	0	0
0	0	0	0	0	0	0	0
0	18	0.5842	0.097	0	30000	0	0
0	0	0	0	0	0	0	0
0	19	0	0.226	0	30000	0	0
0	0	0	0	0	0	0	0
0	20	1.5748	0.095	0	30000	0	0
0	0	0	0	0	0	0	0
0	21	0.0762	0.096	0	30000	0	0
0	0	0	0	0	0	0	0